OCS STUDY
MMS 85-0047

GEOTECHNICAL PROPERTIES

OF MISSISSIPPI RIVER DELTA SEDIMENTS

UTILIZING IN SITU

PRESSURE SAMPLING TECHNIQUES

1985

A.2

U.S. DEPARTMENT OF THE INTERIOR/MINERALS MANAGEMENT SERVICE

This report has not been edited for conformity with MMS editorial standards.

MMS 85-0047

GEOTECHNICAL PROPERTIES OF MISSISSIPPI RIVER DELTA SEDIMENTS UTILIZING IN SITU PRESSURE SAMPLING TECHNIQUES

by

Mark W. Johns
Oceanography Department

William R. Bryant
Oceanography Department

Wayne A. Dunlap
Civil Engineering Department

Texas A&M University
College Station, Texas 77843

Prepared under Contract 14-12-0001-G-709

for

Minerals Management Service
Gulf of Mexico OCS Regional Office
Department of the Interior
Metairie, Louisiana 70010

July 1985

REPORT AVAILABILITY

Preparation of this report was conducted under Contract between the Minerals Management Service and Texas A&M Research Foundation. Extra copies of the report may be obtained from the Public Information Section (Mail Stop OPS-3-4) at the following address:

Minerals Management Service
Gulf of Mexico OCS Regional Office
U.S. Department of the Interior
P.O. Box 7944
Metairie, Louisiana 70010
Attn: Public Information Section
Phone: (504) 838-0519

DISCLAIMER

This volume should be cited as:

Johns, M.W., W.R. Bryant, and W.A. Dunlap. 1985. Geotechnical Properties of Mississippi River Delta Sediments Utilizing *in situ* Pressure Sampling Techniques. (Final Report by Texas A&M University submitted to Minerals Management Service, Metairie, LA. Contract No. 14-08-0001-G-709). 101p.

ABSTRACT

Rapid accumulation of silts and clays in the Mississippi Delta has led to the presence of thick layers of very soft, underconsolidated sediments. These sediments are also organic-rich, and the subsequent anaerobic, biogenic decomposition of the organic material has produced substantial quantities of biogenic methane gas in the pro-delta surficial sediments (0-50 m subsurface). The methane gas is believed to play a major role in the shallow sediment instability which is prominent in the region. In addition, the presence of biogenic gas in bubble form is thought to cause the acoustic attenuation of high resolution seismic signals which results in acoustic "wipeout" commonly observed over large areas of pro-delta sediments.

When standard offshore geotechnical sampling techniques are used in the gas-charged sediments, the samples are significantly disturbed by gas expansion during decompression. The lack of undisturbed samples has hampered the study of the physical properties of the sediment.

New techniques are described for geotechnical sampling using both a pressure core barrel and pressurized Shelby tube samples. Sample testing procedures require the use of a manned hyperbaric chamber, pressurized to in situ sample pressure. These procedures provide insight into the effects of methane solubility and the resultant physical characteristics of samples collected and tested at in situ pressures versus those tested at ambient pressures. Test results indicate that samples containing high methane concentrations show marked reduction in

strength characteristics resulting from evolution of methane gas in bubble form upon release of *in situ* pressures. Gas bubble formation is directly evidenced as increased sample void ratio and porosity. Consolidation test results indicate that this process can be correlated to increased coefficients of consolidation and compressibility.

TABLE OF CONTENTS

TABLE OF CONTENTS (Continued)

LIST OF TABLES

LIST OF FIGURES

LIST OF FIGURES (Continued)

INTRODUCTION

General

In 1974, the United States Geological Survey, Office of Marine Geology, Corpus Christi, Texas, initiated a broad study of the geohazards associated with the Mississippi delta complex. It was quickly recognized that the shallow pro-delta sediments contained large quantities of methane gas, and that gas could contribute to the complex behavior of the sediments. The study reported herein, the investigation of the role of methane on sediment consolidation behavior, is one portion of the larger geohazard study.

Objectives

The primary objective of this study is to describe the consolidation characteristics and geotechnical properties of the sediment recovered from seven foundation borings on the Mississippi delta complex utilizing new techniques for maintaining samples under in situ pressure conditions. Two new methods were utilized to recover samples of this type. Pressurized core barrel and repressurized Shelby tube samples were obtained at these borings (Denk et al, 1981; Johns et al, 1982). The geotechnical properties studied herein include the following: 1) consolidation characteristics; 2) water content; 3) porosity; 4) void ratio; 5) bulk density; 6) specific gravity of solids; 7) clay mineralogy; 8) particle size distribution; and 9) undrained shear strength. Particular emphasis is placed on the evaluation of the consolidation characteristics obtained by three testing procedures on identical samples. These procedures include testing samples at in situ

and ambient pressures, using remolded samples as a control test procedure.

Review of Pertinent Literature

The continental shelf deposits of offshore Louisiana are predominately clayey sediments of late Quaternary age. The nature, distribution and thickness of these deposits reflect the effects of sea level fluctuation during this time and the proximity to the Mississippi River. Near the end of Pleistocene time, sea level stood about 140 meters below its present level and what is now the Mississippi delta complex began forming seaward of its present position. As sea level rose at the end of the last glacial epoch, deltaic sedimentation could not keep pace with the rise in sea level; the shoreline receded and a series of retreatal deltas was constructed (Fisk and McClelland, 1959).

Kolb and Van Lopik (1958) depicted the frontal outlines of these deltas which were formed in response to course changes of the river (Figure 1). The dates shown indicate the duration of significant flow that occurred at each delta. The geologic history and sedimentary patterns of the deltas have been extensively studied (Russell and Russell, 1939; Fisk et al, 1954; Fisk and McFarlan, 1955; Scruton, 1960; Shepard, 1960; Coleman and Gagliano, 1964; Gould, 1965; Morgan, 1965; Kolb and Van Lopik, 1966; Kolb and Kaufman, 1967; Coleman et al, 1974; Coleman, 1976; Roberts et al, 1976; Prior and Coleman, 1981).

The modern Mississippi River has an approximate discharge rate of 15,631 cubic meters per second with associated high sediment input to the delta of approximately 2.7×10^7 tons per year (2.4×10^{11}kg) (Coleman, 1981). Preservation of sedimentary organic matter is a common

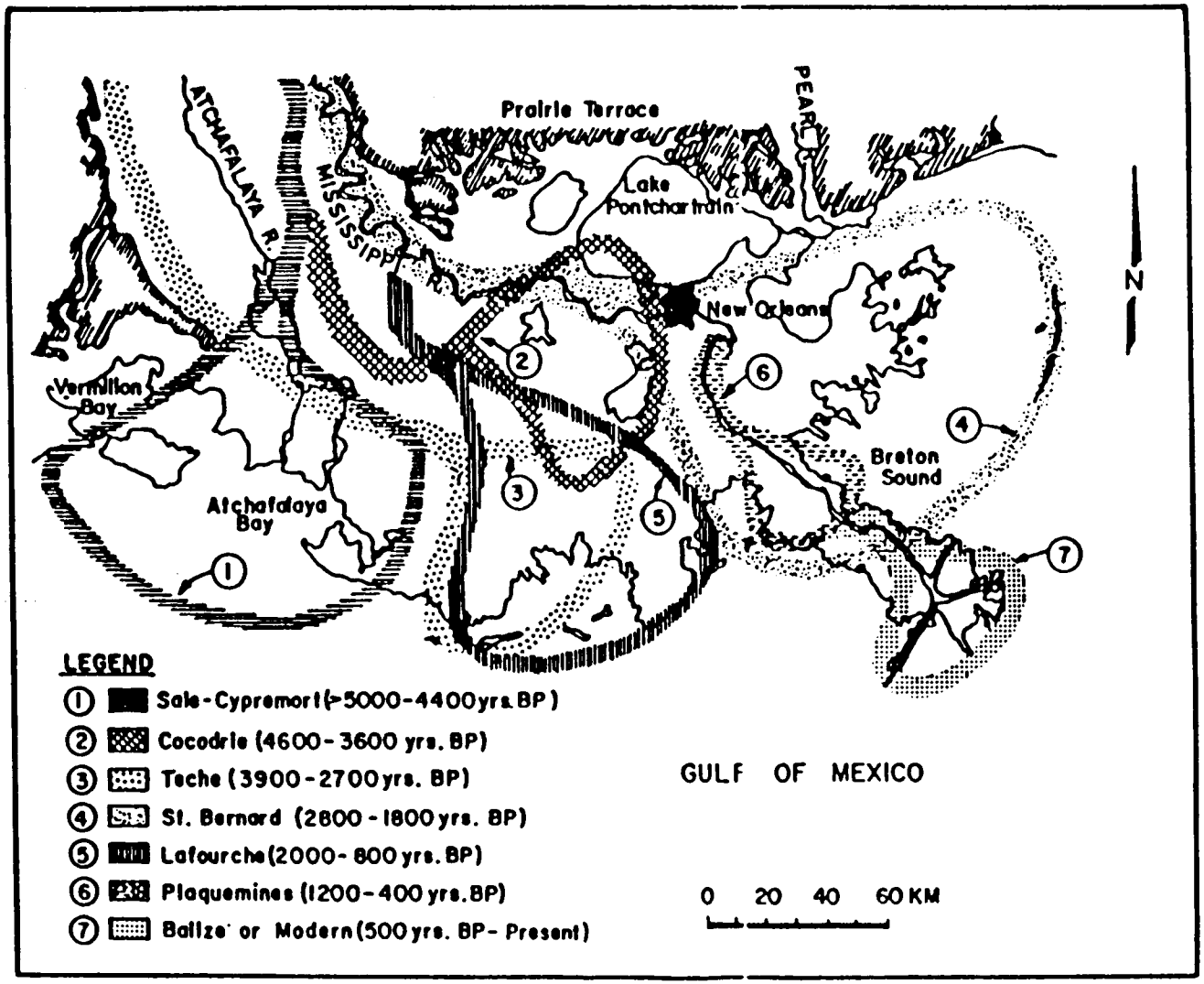

Figure 1. Mississippi River deltas (after Kolb and Van Lopik, 1958).

occurrence near river mouths with high depositional rates and is a necessary requirement for the generation of gas (Whelan et al, 1976). The Mississippi river-mouth depositional patterns have been modified by sediment-deforming processes. Several types of deformation resulting from sediment degassing are present, among which, mass wasting and flowage induced by wave motion are important processes.

Much time and effort has been spent investigating the results of mass wasting processes and their effects on bottom-supported structures. A more detailed discussion of processes and the resultant features may be found in Shepard (1955), Morgan et al (1963), Henkel (1970), Bea (1971), Coleman et al (1972), Bea and Arnold (1973), Coleman and Wright (1974), Garrison (1974), and Yamamoto (1982). The occurrence of methane gas in recent sediments and its effect on soil stability has been studied to a much lesser degree. Whelan et al (1975, 1976) found that a noteable reduction in undrained shear strength occurs in sediments with high methane concentrations.

The formation of near-surface biogenic gas by bacterial activity occurs as the early stages of diagenesis. Methane is the primary hydrocarbon produced in measureable quantity, but trace quantities of C2-C6 hydrocarbons may also be present (Waples, 1980). Methane production in anoxic sediments occurs only after dissolved sulfate has been depleted by way of biochemical reactions generating sulfide and bicarbonate (Nissenbaum et al, 1972). The presence of sedimentary gas bubbles, primarily methane, distorts acoustical quality (Jones et al, 1958, 1964; Hampton, 1966; Anderson, 1974; Schubel, 1974). Similarly, an apparent reduction in undrained shear strength results from sedimentary gas ebullition (Whelan et al, 1975, 1976; Denk et al, 1981).

Two practical means exist to evaluate the geotechnical strength characteristics of gas charged sediments as they actually exist under *in situ* conditions: 1) remote *in situ* measurements performed through a borehole with the sediment in place, and 2) measurements performed under controlled pressure conditions (hyperbaric chamber) after collection at *in situ* pressures. Standard *in situ* devices include pressuremeter, remote vane, and remote cone (Doyle et al, 1971). This type of testing has proved useful, but lacks the basic advantage of the latter technique, i.e. the ability to actually perform a basic strength test under variable pressure conditions on samples collected by the same means. Consolidation testing cannot be performed under *in situ* conditions. However, pressurized sampling techniques combined with a pressure controlled hyperbaric environment and slightly modified consolidometer equipment does allow testing at *in situ* pressure conditions. By this means, consolidation tests can be performed on gas-charged sediments without the release of pressure and the subsequent deleterious effects of gas bubble evolution on the soil structure.

Chiou (1980) performed soil microfabric studies on pressurized and degassed samples collected with the pressure core barrel and found that samples collected and maintained under *in situ* pressures exhibit highly oriented soil microstructure, while degassed samples are typically highly disrupted. Disruption of the microstructure appears to be time dependent (Chiou, 1981). Similarly, observations of the methane gas concentration studies of pressurized core barrel samples show that at least 98% of the methane is released from the sediment matrix within 3-5 hours after pressure reduction to ambient (Whelan et al, 1981).

THEORY

Consolidation Theory

The conventional theory of consolidation for saturated soils was solved by Terzaghi (1925). This equation is governed by the equations of equilibrium of soil, the stress-strain relations for the mineral skeleton, and the continuity equation for the pore fluid (Lambe and Whitman, 1969). The differential equation governing consolidation is:

$$k_z \frac{\partial^2 h}{\partial z^2} + k_x \frac{\partial^2 h}{\partial x^2} = \frac{1}{1+e}\left(e \frac{\partial S}{\partial t} + S \frac{\partial e}{\partial t}\right) \qquad (1)$$

where,

z = coordinate in vertical direction

x = coordinate in horizontal direction

k_z, k_x = permeabilities in respective directions

e = void ratio

h = total head

S = degree of saturation

t = time.

Considering solely the case of one-dimensional consolidation in the vertical direction, the above equation reduces to:

$$k \frac{\partial^2 h}{\partial z^2} = \frac{1}{1+e}\left(e \frac{\partial S}{\partial t} + S \frac{\partial e}{\partial t}\right) \qquad (2)$$

With the advent of back pressure consolidation, assuming $S = 1$, then $\partial S/\partial t = 0$ (Lowe et al, 1964). The governing equation reduces to:

$$k \frac{\partial^2 h}{\partial z^2} = \frac{1}{1+e}\left(\frac{\partial e}{\partial t}\right) \qquad (3)$$

For simple conditions, the stress-strain equation governing consolidation is:

$$-a_v = \frac{\partial e}{\partial \sigma_{vo}'}, \tag{4}$$

where a_v is the coefficient of compressibility and σ_{vo}' is the effective overburden stress. Combining the two above equations yields:

$$\frac{k(1 + e)}{a_v} \frac{\partial^2 h}{\partial z^2} = \frac{-\partial \sigma_{vo}'}{\partial t} \tag{5}$$

Assuming no excess pore pressure, u, exists:

$$h = \frac{u}{\gamma_w} \tag{6}$$

where γ_w is equal to the unit weight of seawater. Substitution of the above two equations into the governing equation yields

$$\frac{k(1 + e)}{\gamma_w a_v} \frac{\partial^2 u}{\partial z^2} = \frac{-\partial \sigma_{vo}'}{\partial t} \tag{7}$$

The coefficient in this equation is defined as the coefficient of consolidation, C_v:

$$C_v = \frac{k(1 + e)}{\gamma_w a_v} = \frac{k}{\gamma_w m_v} \tag{8}$$

where m_v is the coefficient of volume compressibility.

Effective overburden stress can be expressed in terms of total overburden stress and pore pressure:

$$\sigma_{vo}' = \sigma_{vo} - u \tag{9}$$

where σ_{vo} is the total overburden stress. Thus, the time rate of change of effective overburden stress is:

$$\frac{\partial \sigma_{vo}'}{\partial t} = \frac{\partial \sigma_{vo}}{\partial t} - \frac{\partial u}{\partial t} \tag{10}$$

and assuming the total overburden stress does not change with time then:

$$\frac{\partial \sigma_{vo}'}{\partial t} = \frac{-\partial u}{\partial t} \tag{11}$$

The governing equation can thus be expressed as:

$$C_v \frac{\partial^2 u}{\partial z^2} = \frac{\partial u}{\partial t} \tag{12}$$

It must be recalled that the evaluation of Terzaghi's governing equation of consolidation has limitations. Among the most important assumptions included in the equation are:

1) The soil is saturated.
2) Fluid flow obeys Darcy's Law.
3) Fluid flow is one dimensional in the z-direction.
4) The principle of effective stress is obeyed, thus the rate of volume change depends on the rate at which effective stress changes.
5) Conservation of mass exists, thus the net rate of volume inflow is equal to the net rate of volume change.
6) Small strains exist.

DEVELOPMENT OF TEST EQUIPMENT

Design Requirements of the Pressure Core Barrel (PCB)

The basic objective in the design of the pressure core barrel (PCB) was to develop a device capable of collecting and maintaining sediment at *in situ* downhole pressures. Significant difficulties were encountered in the design and construction of the apparatus. The following criteria were considered to be the most important:

A. Compatibility with existing offshore drilling equipment and techniques. The most important factor was that the pressure core barrel be compatible with existing offshore geotechnical boring equipment and techniques. Sampling in the Gulf of Mexico is routinely performed using wire line techniques from drill ships, thus the pressure core barrel was designed as a wire line tool. The maximum exterior diameter of the core barrel was set at 2.63 in because bore holes are commonly drilled with 3-1/2 in. I.F. casing (2.98 in. I.D.).

B. Obtain good quality core samples. Core barrel design followed good practice design regarding area ratios, and other factors which have become established requirements for undisturbed sampling (Horslev, 1948).

C. Capable of obtaining samples to 400 ft (122 m) of combined water and sediment depth. Most gas-associated features occur at combined depths of less than 400 ft. Thus, the design criteria for sampling and sealing at a minimum of 200 psi (1379 kPa) was established. However, the core barrel was designed to work to 500 psi (3447 kPa), allowing deployment to greater depths if future studies of geohazards so

required.

D. Capable of obtaining multiple sealing chambers at a single location. Pressure sealing chambers are utilized to transfer cores after collection with the pressure core barrel, thus permitting multiple sampling at a given site.

Further discussion of the PCB design can be found in Denk et al. (1981). Since publication of the initial design, modifications have been made to the lower ball valve assembly. Modifications to the original core barrel were performed to improve field operation and repair. Prior to these alterations, field repair or replacement of the pressure sealing ball valve and surrounding seals was virtually impossible.

Modifications to the Pressure Core Barrel (PCB)

During the initial operation and testing of the pressure core barrel a significant problem was encountered with opening and closing the ball valve. Investigation of the problem has shown that drilling mud under pressure at the bottom of a bore hole works its way into the interior of the core barrel forcing particles of fine, sand-sized barite around the yoke controlling the ball valve. This produced significant friction to prevent free movement of the ball valve. The problem was partially solved by increasing tolerances and packing the open spaces with teflon impregnated grease.

Increased tolerances and drilling without barite mud improved the core barrel operations, however, a complete remedy was sought. The design criteria were reviewed and modifications to the lower ball valve and yoke assembly were considered. Modifications included:

A. The outer barrel was cut and an easily removable lower section was threaded and emplaced in the lower ball sealing end. This allows for easy, quick, field cleaning, repairs and/or replacement of the ball valve and seals (Figure 2).

B. Teflon seals were replaced with nylon seals. The slight increase in rigidity with the nylon seals allows more precise adjustments of seal pressure without loss of sealing characteristics.

Design Requirements of the Mini-Hyperbaric Chamber (MHC)

Use of the pressure core barrel has been limited to sediments collected from less than 225 ft (69 m) of combined sediment plus water depth imposed by the hyperbaric chamber operations. A small, unmanned pressure chamber has been designed and constructed that allows vane-shear strength measurements and gas sample acquisition. This new chamber attaches to the pressure core barrel in the same manner as the present transportation chambers. Although quite simple in principle, significant difficulties were encountered in the design and construction of the apparatus. In the design, the following criteria were deemed most important:

A. The chamber must be capable of significantly higher pressure environments than limited by manned hyperbaric operations. The external pressure case was designed to withstand pressures to 400 psi (2758 kPa) allowing for sampling depths to 800 ft (244 m) of combined sediment plus water depth.

B. A convenient method of sample placement in the pressurized chamber was required. This was accomplished by utilizing the existing design criteria for the pressure sealing ball valve system developed for

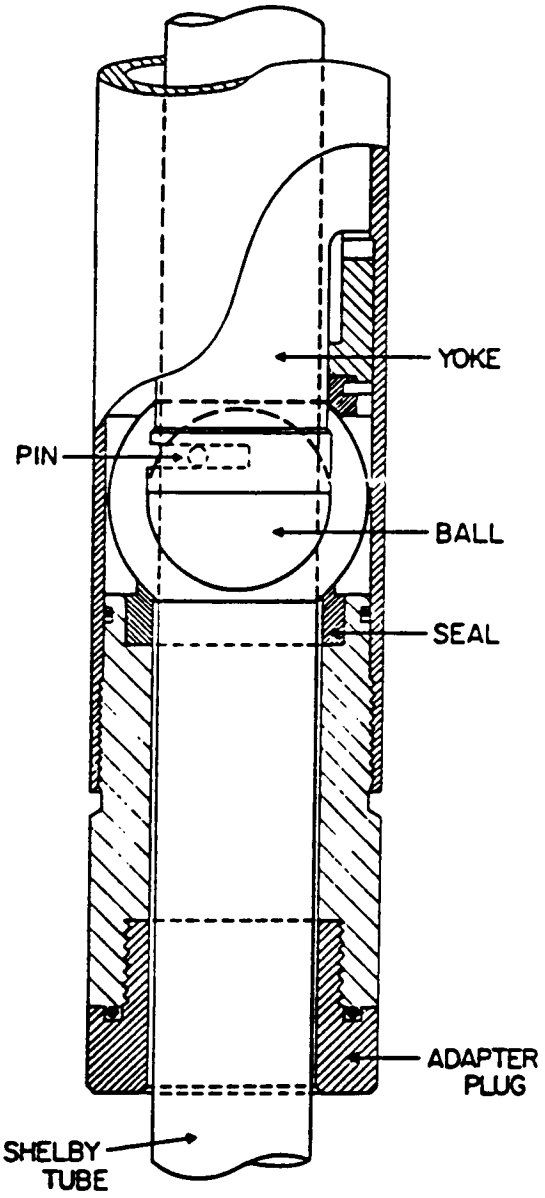

Figure 2. Pressure core barrel ball valve assembly with Shelby tube extended.

the pressure core barrel transportation chambers.

C. Transfer and removal of the core sample from the pressure core barrel must be accomplished by a mechanical system. Electrical servo motors were initially planned for this portion of the chamber. However, this idea was abandoned in favor of a simpler mechanical system, operated by a hand crank mechanism.

D. Placement of mechanical, remote cutters to allow 2 to 4 cm sample sub-sections to be removed in pressure sealing cannisters. These sub-samples could then be tested for gas content and bulk physical properties.

E. Placement of an interior-mounted vane shear blade. A sensitive vane shear device was designed to allow placement of a fresh, cut surface of a core sample into the vane for undrained shear strength measurements at in situ pressure conditions.

Description of the Mini-Hyperbaric Chamber (MHC)

The mini-hyperbaric chamber is constructed of 3/4 inch (1.91 cm) stainless steel plate, capable of withstanding working pressures to 400 psi (2758 kPa), having been tested to 600 psi (4137 kPa). For ease of understanding, the working parts are diagrammatically detailed in Figure 3. After attachment of the pressure core barrel (A), the MHC is sealed and pressurized to sample pressure, with the external helium supply (B). The ball valve (C) is open to ensure pressurization between the ball valve and the pressure core barrel (A), and checked against a sensitive pressure gauge (D). At this time the lower sealing ball valve on the PCB can be opened and the core tube can be extended into the MHC.

The Shelby core tube (E) is then mechanically detached from the PCB

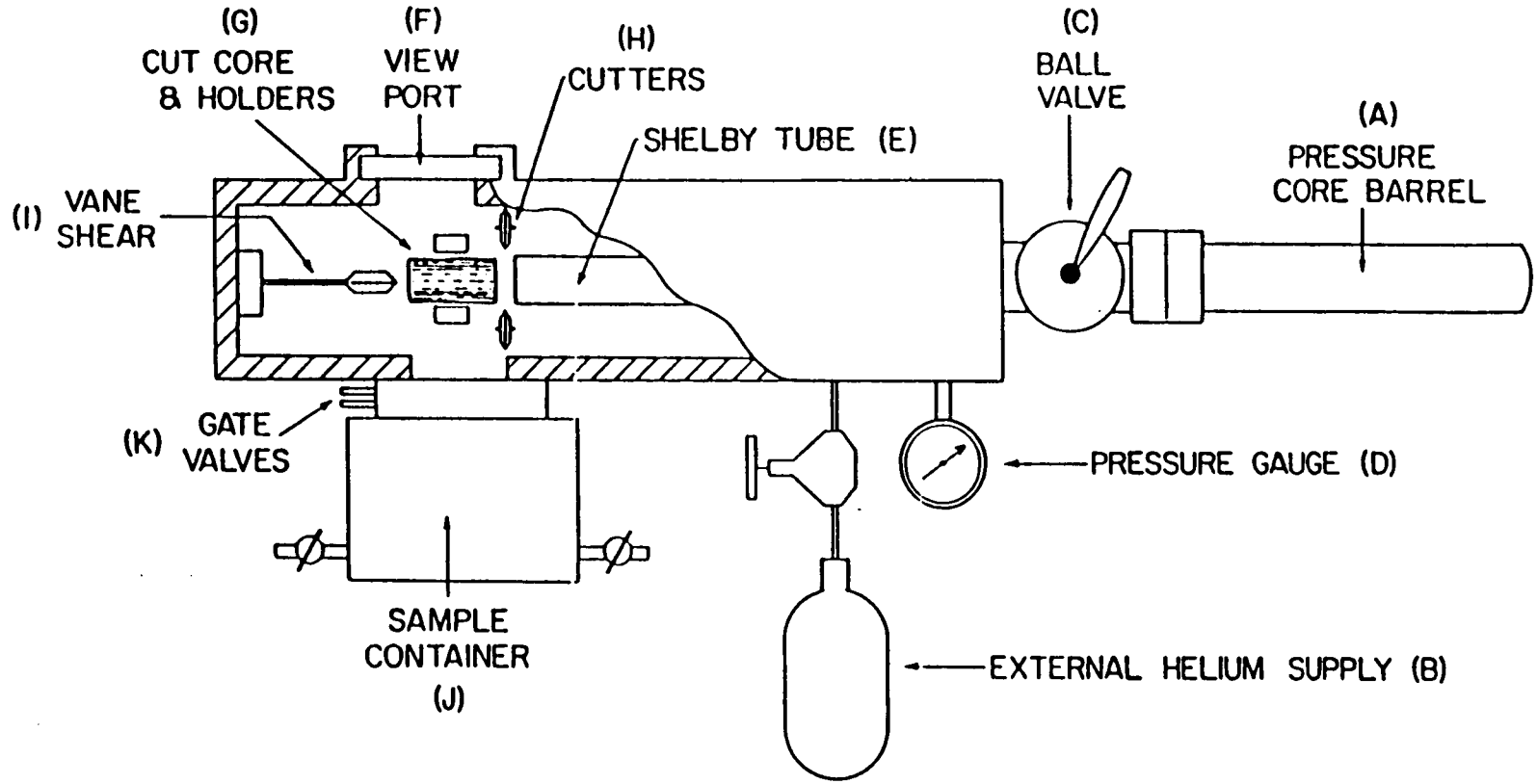

Figure 3. Cross section side view of mini-hyperbaric chamber.

by a gripper and crank mechanism (not shown). Forward translation of the core tube is accomplished by the same mechanism after mechanically changing the gearing mode from rotational to translational. Once the core tube reaches the view port (F) it can be engaged by the forward core holders (G). With an additional change of gearing mode, translational motion can be changed back to the rotational mode and the core tube and sample can be cut and trimmed (H) in preparation to be inserted in the vane shear (I).

Once the sample has been inserted in the vane shear, it is held in position by the core holders against rotation of the vane blade. The vane shear device is externally operated utilizing an external motor drive (not shown) at a rotation rate of 60° per minute (1.05 radians per minute) and the undrained shear strength record is graphically displayed on an external x-y plotter. Multiple vane shear measurements can be performed by simply retracting the core tube and cutting a fresh surface. In addition, subsamples may be collected in the sample container (J) (Figure 4) which can be detached from the MHC after the pressure sealing gate valves are closed. Two bleed valves connected to the sample container allowed an independent pressure supply to be attached and head space gas samples collected.

Design Requirements of the Pressurized Shelby Tube (PST) Chambers

Design and construction of the pressure Shelby tube (PST) chambers is quite simple. The primary objective in the design is the capability to withstand and maintain pressures to 100 psi (689 kPa). Secondary considerations included the ability to quickly seal and pressurize the chamber after sample recovery and maintain that pressure until the

A

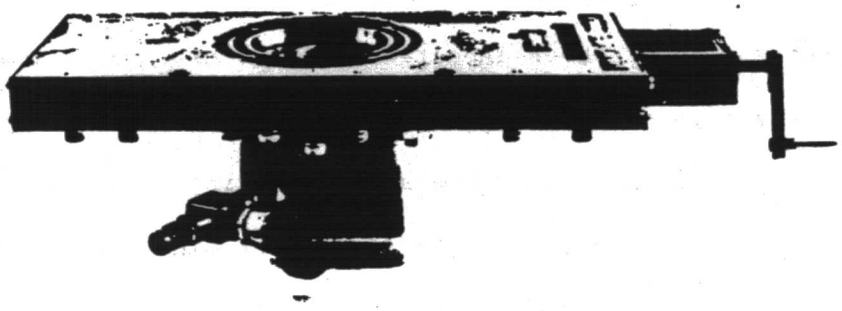

B

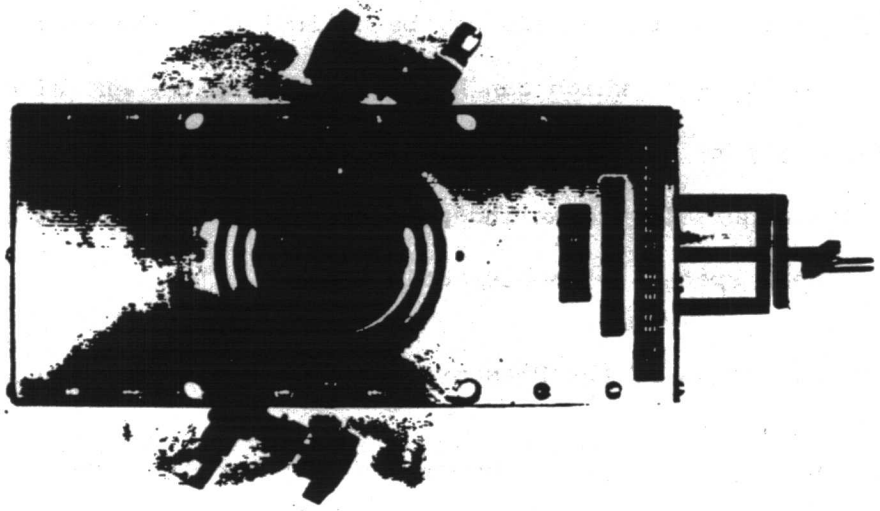

Figure 4. Photographs of gas sample collection chamber that attaches to mini-hyperbaric chamber: a) side view, and b) top view.

samples could be tested.

Two types of pressure Shelby tube chambers were produced. Both welded stainless steel and thick-walled PVC chambers adequately performed the desired tasks. The thick-walled PVC chambers were significantly less expensive to produce and were therefore, preferred to the expensive and heavier stainless steel models.

Description of the Pressurized Shelby Tube (PST) Chambers

The PST chamber consists of a 0 to 100 psi (689 kPa) pressure gauge, a quick connect port for the helium supply, a hyperbaric chamber connection port for the in-line pressure transducer and external pressure supply, and two valves to completely seal the chamber (Figure 5). Samples are placed in the chamber and pressure sealed with an o-ring seal by tightening six Allen head screws set in the end cap.

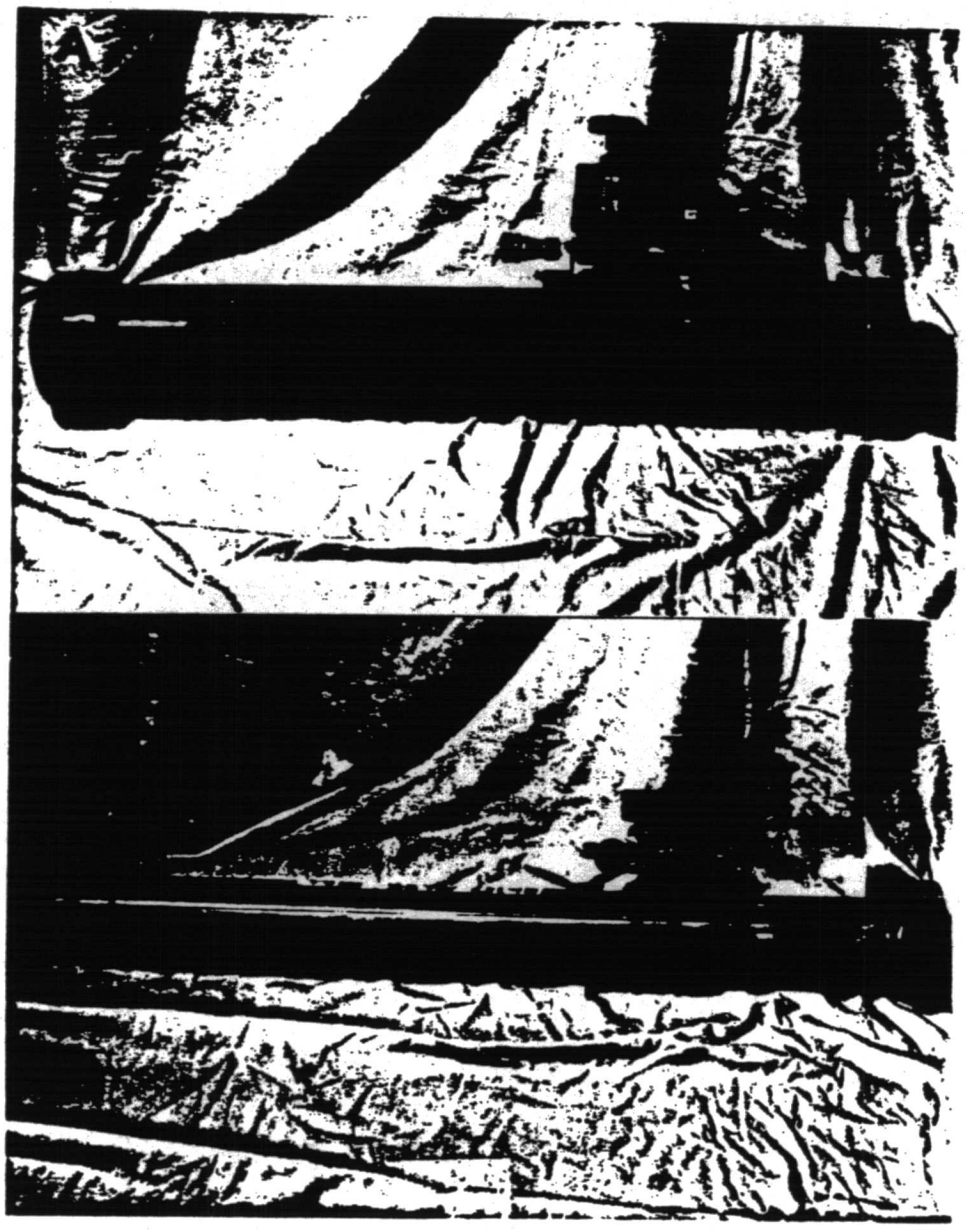

Figure 5. The two types of pressurized Shelby tube transportation chambers: a) PVC model, and b) stainless steel model.

EXPERIMENTAL PROGRAM

Borehole Locations

Core samples were obtained from several sediment borings located in three different regions of the outer continental shelf lease area of the Mississippi River delta. Locations and water depths of the seven sediment borings are as follows (Figure 6):

1) Boring 1, West Delta, OCS, Block 85, Water Depth 21.0 m, Latitude 28°52.891'N, Longitude 89°28.643'W
2) Boring 1A, West Delta, OCS, Block 85, Water Depth 21.0 m, Latitude 28°52.895'N, Longitude 89°28.650'W
3) Boring 2, West Delta, OCS, Block 85, Water Depth 38.1 m, Latitude 28°54.196'N, Longitude 89°30.133'W
4) Boring 2A, West Delta, OCS, Block 85, Water Depth 45.2 m, Latitude 28°54.214'N, Longitude 89°31.160'W
5) Boring 5, South Pass, OCS, Block 43, Water Depth 39.0 m, Latitude 28°53.057'N, Longitude 89°20.991'W
6) Boring 7, South Pass, OCS, Block 43, Water Depth 45.1 m, Latitude 28°54.115'N, Longitude 89°20.103'W
7) Boring 1, Main Pass, OCS, Block 74, Water Depth 44.2 m, Latitude 29°13.884'N, Longitude 89°54.407'W

Sample Acquisition Techniques

The samples were obtained on three separate cruises at the sites previously listed. Thirteen pressure core barrel samples were obtained at three drill sites in August of 1979 with McClelland Engineers under

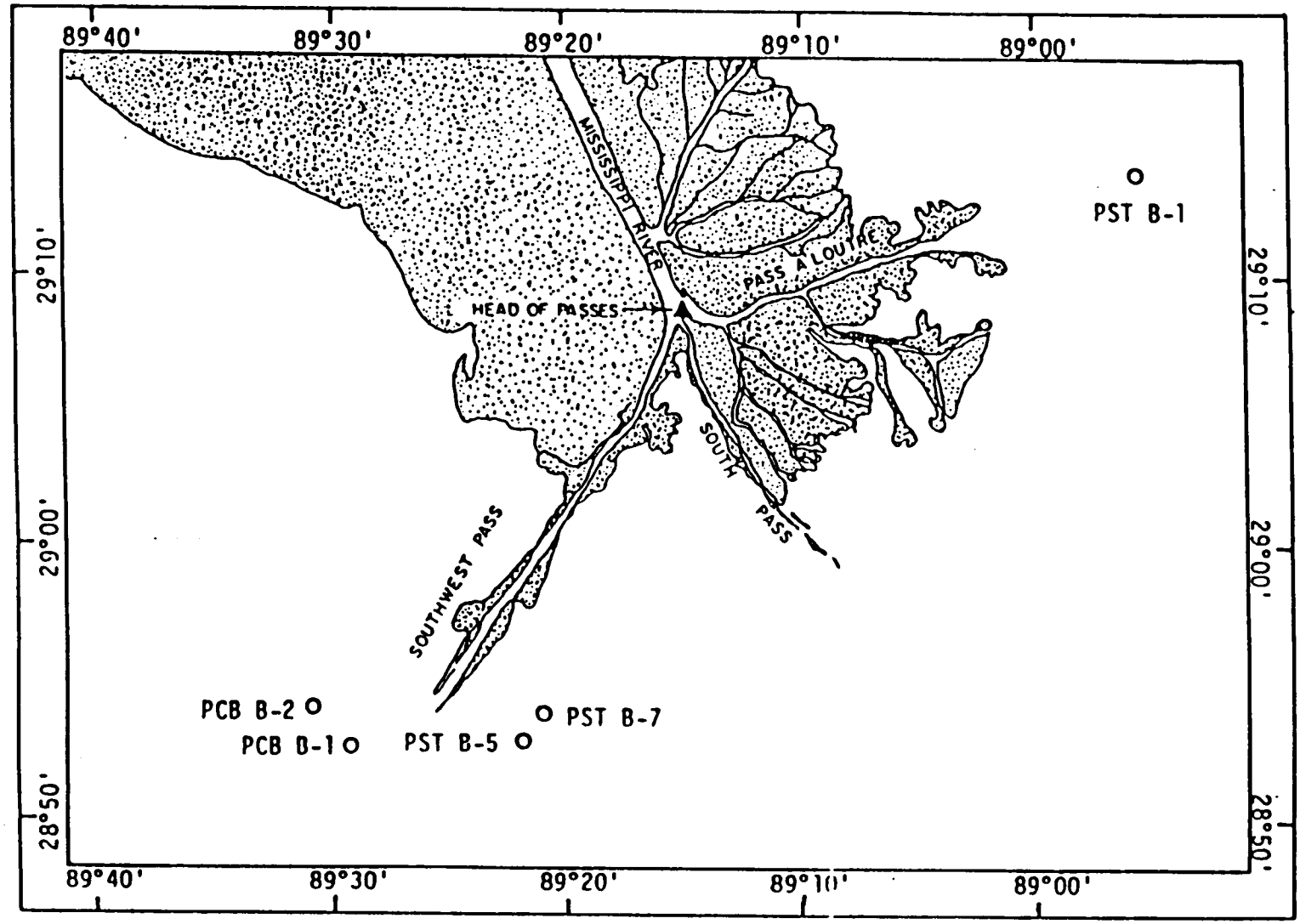

Figure 6. Locations of the pressure core barrel (PCB) and pressure Shelby tube (PST) sediment borings.

contract to Marathon Oil Company aboard the M/V "R. L. Perkins." Nine pressurized Shelby tube samples were obtained at two drill sites in October of 1980 with Woodward-Clyde Engineers under contract to Mobil Oil Company aboard the M/V "Sea Level #21." An additional nine pressurized Shelby tube samples were obtained at one drill site in March of 1981 aboard the M/V "Four-by-IV" with Geotest Engineering, Inc. under contract to Occidental Oil Company.

All sediment borings were drilled with 8.9 cm internal flush drill pipe by skid-mounted rotary rigs through wells installed in the decks. Pressurized Shelby tube samples were obtained using 5.72 and 6.35 cm outside diameter Shelby tubes operated on a wireline sampler through the drill pipe. The sampler was driven with a 79.5 kg weight, dropped from a height of approximately 150 cm a sufficient number of times to obtain 60 cm of penetration.

Immediately after recovery, the sample and Shelby tube are measured, capped and placed in a pressure transportation chamber (Figure 5). The transportation chamber is pressurized with helium gas to calculated *in situ* pressure of the sample, assuming a hydrostatic head of seawater, then placed in a refrigeration unit at 12.8 C in a horizontal attitude. The samples were returned to Texas A&M University and placed in a high humidity refrigeration chamber where pressures were maintained until their geotechnical properties were investigated.

Shelby tube sampling is routinely performed by offshore engineering firms. Immediate repressurization of the sample to *in situ* pressures minimizes the amount of degassing of saturated porewater gases and, thus, reduces the amount of sample disturbance. Recovery and repressurization of each sample requires less than two minutes.

Thirteen samples were recovered utilizing the pressure core barrel. The sampling procedure and design parameters employed were described by Denk et al (1981); only a brief outline of the pressure core barrel use will be described here.

The pressure core barrel is lowered by wireline to the bottom of a cleaned borehole through the drill pipe. The pressure sealing ball valve on the lower end of the tool is left open with the sampling tube retracted, allowing drilling fluid to enter the core barrel. This procedure for lowering the core barrel is utilized to prevent overdriving in soft sediments that may be encountered.

When the core barrel reaches the base of the borehole, two side-mounted inflatable rubber packers are actuated to provide a reaction force for driving the sampling tube. The sampling tube is then hydraulically driven into the sediment. Downhole pressure is measured by applying regulated gas (helium) pressure through a tube that exists from the interior of the core barrel immediately above the sampling tube. Pressure is increased until a no-flow condition exists as measured by an in-line flow meter. Maintaining this pressure, the sample tube is retracted, the pressure sealing lower ball valve closed, the rubber packers deflated, and the core barrel withdrawn from the drill pipe.

On deck, a transportation chamber is mated to the core barrel and pressurized with helium gas to match the core barrel pressure. Transfer of the sediment sample to the transportation chamber is accomplished after the ball valve on the transportation chamber and the pressure sealing ball valve on the core barrel are opened. The transportation chamber ball valve is then closed and the whole assembly disconnected

from the core barrel. Thus, these samples were always maintained at *in situ* pressures. The transportation chamber is then placed in a refrigeration unit at 12.8°C in a horizontal attitude. The samples were returned to Texas A&M University and placed in a high humidity chamber at 5°C where pressures could be maintained until their geotechnical properties could be analyzed.

Geotechnical Properties

The geotechnical properties investigated in this study include; 1) consolidation characteristics; 2) water content; 3) porosity; 4) void ratio; 5) bulk density (wet unit weight); 6) specific gravity of solids; 7) clay mineralogy; 8) particle size distribution; and 9) cohesive shear strength. Sub-sampling of the pressure core barrel and pressurized Shelby tube samples was undertaken in a manned hyperbaric chamber at the *in situ* pressure of the given sample. All of the above properties with the exception of cohesive shear strength were determined from sediment subsamples taken before and after the removal of the consolidation sample. Hand-held Torvane shear tests were performed on the open sediment cores within the hyperbaric chamber at *in situ* pressures.

Consolidation Testing

Consolidation tests were performed on 14 samples from the four foundation borings. These samples were selected by visual inspection at *in situ* pressures in the hyperbaric chamber. Standard X-radiography could not be performed in this situation due to the small size and restrictive environment of the manned hyperbaric chamber.

Pressure core barrel samples showed little, if any, evidence of gas

expansion as they were always maintained at in situ pressures. The pressure Shelby tube samples often showed signs of degassing within a few centimeters of the sample ends. This characteristically "frothy" or "cottage cheese" void filled texture was unmistakable (Denk et al, 1981). The use of a hand-held Torvane helped to delineate this degassed section. The consolidation sample was trimmed from the core immediately after the degassed section was delineated and discarded.

Evidence of subaqueous deformation was impossible to determine. Drilling disturbance was visualized in a core as mud intrusions, if present, generally found at the top or bottom of a core. Sampling disturbance was believed to have been held to a minimum. The pressure core barrel sampling tubes have area ratios less than 9% (Denk et al, 1981). Pressure Shelby tube samplers have area ratios between 13.1% and 14.8% (Horslev, 1948).

The collection of truly undisturbed sediment samples is impossible. The basic aim of standard sampling techniques is to minimize mechanical disturbance and changes in water content and void ratio of the soil structure. When utilizing standard sediment sampling techniques in regions of high pore water methane concentrations, sample recovery to ambient pressure releases this gas in bubble form (Whelan et al, 1975, 1976). This causes disruption of the soil structure, an increase in void ratio and a decrease in the percent saturation of the sample. Pressurized sampling techniques, additionally, reduce or eliminate the effects of changes in the hydrostatic pressure conditions, thus eliminating or minimizing disturbance to the sediment structure.

Terzaghi's theory of one-dimensional consolidation assumes complete sample saturation. The validity of coefficients derived from standard

consolidation testing of gas charged sediments must be questioned. Lowe et al (1964) found that gas bubbles within the sediment are highly compressible as compared to the relatively incompressible water. These gas bubbles impede the flow of water in the voids and thus reduce the soil permeability (Bjerrum and Huder, 1957).

Specially modified Anteus back pressure consolidometers were used for testing of all samples. The advantages of using the back pressure apparatus is outlined by Lowe et al (1964), Bryant et al (1967), and Shephard et al (1979). Only modifications to the above mentioned testing procedures necessary for testing the pressurized samples will be discussed herein.

Each sample was released in a manned hyperbaric chamber which had been pressurized to the sample pressure. The maximum allowable dive depth was 102 psi (225 ft of seawater). When preparing for a dive the transfer chamber, consolidometer and the necessary equipment for loading the sample were placed in the hyperbaric chamber. The pressurized transfer chamber and consolidometer were connected through a port to an external gas (helium) supply with an in-line pressure transducer.

At this time, the hyperbaric chamber was manned and pressurized to sample pressure. When sample pressure had been reached, as indicated by the pressure transducer, the transfer chamber was opened and the sample tube removed. Preliminary visual inspection included a sample description and search for evidence of any disturbance caused by degassing or mud intrusion. A hand-held extruder was used to remove the sample from the Shelby tube in approximately one centimeter intervals. Hand-held Torvane measurements were taken between extrusions to delineate any disturbed zones. Generally, a small amount of degassing

was found to occur near the ends of the pressurized Shelby tube samples. These gas disturbed zones were easily distinguished from undisturbed sections as mentioned previously. Sub-samples were bagged and labelled for later use in laboratory testing of index properties and for remolded consolidation testing.

If no degassing was present at this point and a consistent undrained shear strength had been maintained for 3 or 4 centimeters, the consolidation sample was trimmed. The consolidation sample was slowly extruded and trimmed with a stainless steel cutting ring. The pressurized Shelby samples and pressure core barrel samples were trimmed to 4.45 cm and 3.18 cm diameters, respectively. The upper and lower surfaces were then trimmed to plane surfaces using the top and bottom of the ring as a guide. A spacer disc was inserted in the sample, up from the bottom of the ring, after trimming the lower surface and before trimming the upper surface. This permits trimming a sample to a height of approximately 2.54 cm for the pressure Shelby tube samples and approximately 1.91 cm for the pressure core barrel samples.

The sample was then loaded into a teflon lined confining ring with filter papers and saturated porous stones on top and bottom. Once the sample was in place in the confining ring, the lucite chamber and loading dome were placed in position. The saturating water was added to the water reservoir and the lucite chamber. The oil reservoir was then lowered to the neutral position and the load valve was opened. The loading plate was slowly lowered under its own weight until contact with the upper porous stone was evidenced by lack of movement of the extensiometer. The external gas supply was then regulated to the consolidometer at the sample pressure. The Shelby tube was then

resealed in the transfer chamber for later use and hyperbaric chamber decompression was initiated.

During decompression of the hyperbaric chamber, the load valve of the consolidometer was left in the open position with the oil reservoir in a neutral position. Decompression of the divers takes place in stages with rapid pressure reductions occurring at each stage. Decompression of the sample does not occur, as the external gas supply to the consolidometer is maintained at the *in situ* hydrostatic pressure of the sample. Any deflections of the dial gauge due to rapid hyperbaric chamber pressure changes were noted and recorded. When decompression of the divers was complete, the consolidometer was transferred to the laboratory with an external pressure supply, where it was connected to the laboratory air pressure system. Consolidation testing began immediately.

The consolidation test loading sequence began at 3.125 or 6.250 kPa, depending on the soil strength, and continued to 50 kPa at double load increments by raising a sliding reservoir to calibrated heights on a standpipe. Load increments of 100, 200, 400, 800, 1600, and 3200 kPa were applied using the load regulator to control the sliding reservoir pressure. Each load was applied, utilizing double drainage, for a minimum of 24 hours or until linear secondary consolidation was confirmed. Sample height was indicated by an extensiometer which measured the movement of a dial pin resting on the top of the loading plate.

A hysteresis loop was generally performed between 10% and 15% strain. Unloading was accomplished in increments of one fourth the previous load. The final unloading sequence continued to zero load,

where the sample was allowed to swell with no vertical load for 24 hours. A final dial reading was taken and the back pressure was released. The sample was unloaded from the confining ring, oven dried at 105°C for 24 hours, and weighed.

The response of consolidation (rate of compression) was determined for each load increment and represented by the coefficient of consolidation, C_v. For each load increment (decrement), compression (swell) versus logarithm of time was plotted. The end of primary consolidation was determined using the method described by Casagrande (1936). Coefficients of 50% primary consolidation were then determined graphically from these plots.

Compression versus the square root of time was plotted for each load. The coefficient at 90% primary consolidation was graphically determined for each load using the method outlined by Taylor (1948).

The initial void ratio, e_o, defined as the volume of voids divided by the volume of solids, was calculated for each sample. Decompression of methane charged sediments to ambient pressures results in degassing and an increase in the void ratio. The cross-sectional area, A, of a consolidation sample remained constant throughout the test, therefore, the initial void ratio can be defined as the height of voids, $2H_o - h_s$, divided by the height of solids, h_s, where H_o is equal to the height of the drainage path. The initial void ratio equation becomes:

$$e_o = \frac{(2H_o - h_s)}{h_s} \tag{13}$$

The height of solids is calculated at the end of the consolidation test. The height of solids, h_s, is calculated from:

$$h_s = \frac{W_s}{A G \gamma_w} \tag{14}$$

where W_s is the weight of dried solids (gm) in the consolidation sample, A is the cross-sectional area (cm^2) of the sample, G is the specific gravity of the solids, and γ_w is the unit weight of water (g/cm^3). The void ratio, e_i, at the end of each load was calculated from:

$$e_i = e_o - \frac{\Delta h}{h_s} \tag{15}$$

where Δh is the incremental compression or swell of the sample.

The results of the consolidation test were plotted as void ratio versus logarithm of vertical effective stress curves on semi-log paper. At 100% primary consolidation for a given load no excess pore pressure exists within the sample; the pore pressure, u, is equal to the back pressure and the vertical effective stress, σ_v', equals the applied pressure.

The effective preconsolidation stress, σ_{vc}', represents the maximum pressure to which the sample had been loaded in nature. The Casagrande method (Casagrande, 1936) was used to graphically determine this stress from the e-log σ_v' curves.

The <u>in situ</u> effective overburden stress, σ_{vo}', acting at any given sample depth is the difference between the stress exerted by the overlying sediments and the pore water pressure at that depth. As stated previously, no pore pressure measurements were obtained, therefore, a hydrostatic head of sea water was assumed for the given sample depths. For underconsolidated sediments, the pore pressure exceeds the hydrostatic condition, thus for the sediments studied herein the effective overburden stress is actually an "apparent" effective overburden stress.

The equation utilized for calculation of effective overburden

stress, σ_{vo}' in kPa, was presented by Helwick (1977) for a given interval of known bulk (wet) density, γ_b (kg/m^3). The intervals were then summed to the appropriate sample depth. The equation is:

$$\sigma_{vo}' = 9.8065[z_1(\gamma_b) - z_1(1025)] \tag{16}$$

where z_1 (m) is the interval depth and 1025 is the unit weight of seawater (kg/m^3).

It is necessary to consider the stress history of the soil to rationally interpret the e-log σ_v' curve. The slope of the e-log σ_v' curve, plotted on semi-log paper is nearly a straight line whose slope can be denoted by the compression index, C_c. The compression index is equal to the change in void ratio for a given change in logarithm vertical effective stress. The compression index was calculated for each sample in the region of the virgin slope of the e-log σ_v' curve and can be computed according to the relationship:

$$C_c = \frac{\Delta e}{\Delta \log \sigma_v'} \tag{17}$$

where Δe and $\Delta\sigma_v'$ are the change in void ratio and effective overburden stress over the region of the maximum slope. Standard soil mechanics procedure assumes a positive value for the compression index.

The coefficient of consolidation, C_v, is calculated for each load increment for the compression versus logarithm of time and square root of time curves. The governing equation is:

$$C_v = \frac{T_v H_o^2}{t} \tag{18}$$

where T_v is the dimensionless time factor, equal to 0.197 for 50% consolidation and 0.848 for 90% consolidation, H_o is the height of

drainage path (cm) and t is the time (seconds).

Terzaghi's (1943) equation for the theoretical coefficient of permeability:

$$k = C_v m_v \gamma_w \tag{19}$$

derived from the theory of consolidation, was used to calculate permeabilities using the C_v obtained from the square root of time technique derived by Taylor (1948). The coefficient of volume change, m_v, can be calculated from:

$$m_v = \frac{a_v}{1 + e} \tag{20}$$

The coefficient of compressibility, a_v, equals:

$$a_v = \frac{-\Delta e}{\Delta \sigma_v'} \tag{21}$$

where Δe is the change in void ratio and $\Delta \sigma_v'$ is the change in vertical effective stress (kPa).

Shear Strength

Calculation of shear strength may be obtained from:

$$\tau = C + \sigma_n \tan \phi \tag{22}$$

where τ is the shear strength, C is the cohesion, σ_n is the normal stress, and ϕ is the angle of internal friction. The shear strength tests were performed directly below that portion of the sediment sample utilized for consolidation, with a Soiltest, Inc. hand-held Torvane. Saturated clayey sediments stressed with no water loss, as these samples were tested, act as purely cohesive materials with ϕ equal to zero.

Thus, the undrained shear strength, C_u, is equal to the cohesion of the soil (Moore, 1961), or:

$$\tau = C = C_u \tag{23}$$

Index Properties

Index properties investigated include: 1) water content; 2) bulk density (wet unit weight) and specific gravity; 3) grain size; 4) clay mineralogy; and 5) gas concentration. The procedures for determinations of these index properties are similar to those outlined by Lambe (1951) and modified by Cernock (1967).

Bulk Density and Specific Gravity

A Beckman air comparison pycnometer with an accuracy of 0.02 cm was utilized to obtain wet and dry volumes of the sediment samples. No direct measurements of pore water salinity were available. However, a salt correction was made assuming a salinity of 35 o/oo (Hamilton, 1971). The correction for pore water salinity affects the computations for water content, specific gravity, void ratio, porosity, and degree of pore water saturation.

Grain Size

Approximately 10 gram (dry weight) portion of sample was wet sieved through a 62 micron mesh (40) to determine the coarse fraction present. Pipette analysis was run on the less than 62 micron (greater than 40) portion to determine the relative amounts of fine fraction, using the technique described by Krumbein and Pettijohn (1938). This method

assumes a specific gravity of 2.65 for spherical particles using Stokes' law for calculation of settling velocities.

Clay Mineralogy

Sample preparation techniques for x-ray diffraction of the less than 2 micron clay fraction followed those outlined by Jackson (1956) and modified by Hottman (1975). The Bradley form factor technique described by Scafe and Kunze (1971) was used to obtain relative percentages of clay mineral abundances. The peak height method for estimating relative percentages was chosen for this study to maintain the consistency with previous studies in the Gulf of Mexico.

Gas Concentrations

Sections of selected core samples were quickly canned in degassed water on board ship. The canning procedure requires a consistent, rapid transfer (to minimize gas loss) of a sediment section into a 500 ml can filled with 400 ml of degassed water. Sediment is added until the water level is directly at the top of the can, allowing a 100 ml volume of sample to be consistently sealed in the can. This canned sample is subsequently analyzed in the laboratory for methane and other pertinent gasses using gas chromatography (Whelan et al, 1975, 1976).

RESULTS

Comparative testing was performed on one pressure core barrel (PCB) sample and thirteen pressure Shelby tube (PST) samples. Pressurized, degassed, and remolded specimens were sub-sampled from a given core at intervals of less than 14 cm. All pressurized test specimens were back pressured to *in situ* pressures while degassed and remolded samples were tested with no back pressures by standard methods. The remold test for sample B5S28R was performed with a back pressure of 100 psi (689 kPa). Insufficient sample was collected to perform a degassed test on sample B1S2. Therefore, only pressurized and remold test results are available for this specimen.

Index Property Test Results

The index properties for all samples can be found in Table 1. Sample designators contain boring number, sample number, and consolidation test treatment type. Consolidation treatment types are:

I for *in situ* or pressurized test

D for degassed test

R for remold test

Specific Gravity and Wet Bulk Density

Values for wet bulk density (salt corrected) range between 1.55 and 1.76 Mg/m^3 with a mean value of 1.63 Mg/m^3 and a standard deviation of 0.06 Mg/m^3. Specific gravity of solids varies between 2.54 and 2.77 with a mean value and standard deviation of 2.69 and 0.07, respectively. Bulk density increases while water content and porosity decrease with

Table 1. Index properties for all samples.

Core-Section	Test Type	Depth, z (m)	Water content, w (%)	Initial void ratio, e_o	Initial porosity, n (%)	Wet bulk density, γ_b (Mg/m^3)	Specific gravity	Undrained shear strength, C_u (kPa)	Liquid limit, w_l (%)	Plastic limit, w_p	Weight percent $CaCO_3$ (%)	Grain Size Sand (%)	Silt (%)	Clay (%)
B2 S10	I	11.76				2.69								
	D	11.76				2.67								
B1 S2	I	6.72	63	1.626	61.92	1.69	2.68	14.82	77	40	1.21	1.74	41.85	56.41
	R		63	1.630	61.98	1.69	2.68		77	40	2.61			
B1 S4	I	12.41	61	1.511	60.18	1.68	2.60	6.75	74	37	7.05	1.37	47.32	51.31
	D	12.37	61	1.778	64.00	1.66	2.71		74	37	2.66	3.37	44.80	51.83
	R		60	1.628	61.95	1.66	2.71		74	37	2.87			
B1 S6	I	18.78	74	1.995	66.61	1.61	2.71	9.39	97	63	7.44	0.32	33.08	66.60
	D	18.72	75	2.279	69.50	1.61	2.77		97	63	2.64	0.82	34.62	64.56
	R		72	2.163	68.38	1.61	2.77		97	63	2.86			
B1 S8	I	24.32	85	2.283	69.54	1.55	2.75	14.82	103	50	5.37	1.16	46.73	52.11
	D	24.18	89	2.451	71.02	1.55	2.75	14.66	103	50	3.37	0.85	26.82	72.33
	R		85	2.292	69.62	1.55	2.75		103	50	3.31			
B7 S9	I	10.24	62	1.650	62.26	1.69	2.59	15.32	84	48	2.64	0.01	53.49	46.50
	D	10.20	81	2.246	69.19	1.60	2.69	14.33	84	48	2.64	0.03	34.82	65.15
	R		73	1.969	66.32	1.60	2.69		84	48	2.59			
B7 S15	I	16.37	78	2.018	66.87	1.58	2.61	14.89	84	44	2.96	0.00	34.00	66.00
	D	16.31	66	1.823	64.58	1.58	2.61	16.54	84	44	2.96	0.00	34.00	66.00
	R		68	1.708	63.07	1.58	2.61		84	44	3.53	0.06	42.05	57.89
B5 S10	I	13.29	65	1.526	60.41	1.66	2.54	17.48	86	51	4.28	0.00	40.38	59.62
	D	13.21	57	1.414	58.57	1.66	2.54	19.76	86	51	3.26	0.35	44.96	54.69
	R		56	1.325	65.99	1.66	2.54		86	51	2.74	0.35	44.96	54.69
B5 S15	I	19.42	50	1.230	55.16	1.76	2.68	19.15	68	39	3.00	1.42	54.23	44.35
	D	19.47	49	1.395	58.25	1.76	2.68	19.65	68	39	3.84	1.80	52.07	46.13
	R		49	1.283	56.20	1.76	2.68		68	39	3.60	1.80	52.07	46.13

Table 1 continued.

Core-Section	Test Type	Depth, z (m)	Water content, w (%)	Initial void ratio, e_o	Initial porosity, n (%)	Wet bulk density, γ_b (Mg/m^3)	Specific gravity	Undrained shear strength, C_u (kPa)	Liquid limit, w_l (%)	Plastic limit, w_p	Weight percent $CaCO_3$ (%)	Grain Size Sand (%)	Silt (%)	Clay (%)
B5 S23	I	36.49	62	1.504	60.06	1.69	2.57	16.47	90	47	3.39	3.66	32.08	64.24
	D	36.44	62	1.728	63.34	1.70	2.68		90	47	3.06	0.43	34.87	64.70
	R		67	1.837	64.75	1.65	2.70		90	47	3.41	0.36	29.65	69.99
B5 S26	I	42.47	85	2.022	66.91	1.56	2.77	21.69	103	52	2.79	0.04	24.39	75.57
	D	42.50	77	2.393	70.53	1.56	2.77	18.94	103	52	2.84	0.82	33.72	65.46
	R		75	2.139	68.14	1.56	2.77		103	52	4.10			
B5 S28	I	45.54	69	1.777	63.99	1.65	2.71	19.77	95	45	4.27	0.10	25.06	74.84
	D	45.49	71	1.941	66.00	1.65	2.71	19.93	95	45	4.72	0.10	25.63	74.27
	R		70	1.821	64.55	1.65	2.71		95	45	4.59	0.10	25.63	74.27
B5 S30	I	51.76	80	2.243	69.16	1.58	2.76	29.69	87	44	2.42	0.03	16.10	83.87
	D	51.80	74	2.245	69.18	1.62	2.76	21.91	87	44	3.72	0.03	19.05	80.92
	R		70	2.128	68.03	1.62	2.76		87	44	4.04	0.12	23.06	76.82
B5 S32	I	57.80	75	2.122	67.97	1.62	2.75	33.52	107	54	11.65	0.57	13.16	86.27
	D	57.74	73	2.091	67.65	1.62	2.75	28.16	107	54	5.56	0.58	15.78	83.64
	R		72	2.050	67.21	1.62	2.75		107	54	4.69	0.58	15.78	83.64

depth (correlation coefficient r^2 = 0.90 and 0.86, respectively).

Grain Size

Sand content is low for all samples and ranges between 0% and 3.7%. Silt and clay contents are considerably more variable, however, silt and clay contents show opposite trends with depth. The silt content decreases with depth (r^2 = 0.86), while clay content tends to increase with depth (r^2 = 0.85). Variation between comparative samples is low, except for samples B7S9 and B5S26, which have variations of 20% and 10% between comparative samples for the silt and clay contents. All samples can be classified as clayey silts, except for B5S15 (all samples) and B7S9I which contain slightly higher silt contents, and are classified as silty clays (Folk, 1974).

Water Content and Atterberg Limits

As mentioned previously, all water content determinations include a salt correction of 35 o/oo (Hamilton, 1971). Water contents for all samples vary between 49% and 89%. Comparative samples from Boring 1 are quite similar, variations being 0 to 4%. Boring 5 and 7 samples do not exhibit as close a correlation between comparative samples. Variations between comparative samples range from 0 to 19%, with the samples tested at *in situ* pressure generally having higher values. These samples were tested prior to those for the degassed or remold consolidation tests and, therefore, indicate either partial drying of the samples prior to testing, or a loss of porewater resulting from degassing of porewater gasses.

Initial water contents for all samples fall between the liquid

limit, w_l, and the plastic limit, w_p. The liquid limits for all samples range between 68% and 107%, while the plastic limits range between 37% and 63%. The mean value for the liquid limit is 89% with a standard deviation of 12%, while the respective values for the plastic limits are 47% and 7%. Based on the Unified Soil Classification System, these soils can be classified as clays of high plasticity or organic clays of high to medium plasticity.

Calcium Carbonate Content

Analytical determinations of weight percent calcium carbonate content were made using a modified carbonate bomb technique (Schink et al, 1979). Values for all samples are low and range between 1.21% and 11.65%. Test results indicate only minor variations exist between comparative samples. Variation appears to be within the standard error (±0.3%) for the test procedure. The mean value is 3.83% with a standard deviation of 1.79%.

Clay Mineralogy

One sediment sample was utilized for x-ray diffraction analysis for each set of consolidation samples. These samples were collected from an interval between consolidation samples and therefore, are assumed to be representative of the relative type of clay minerals present in the sediments of a given consolidation test group. The results of clay mineral analyses indicate a fairly uniform distribution of clay minerals in the sediments studied for pressurized Shelby tube Borings 1, 5, and 7 (Table 2).

The semi-quantitative nature of estimating mineralogical

Table 2. Semi-quantitative analysis (relative %) of clay minerals in sediments of Borings 1, 5, and 7.

Sample	Smectite (%)	Illite (%)	Kaolinite (%)	Chlorite (%)
B1S2	22	58	14	6
B1S4	27	58	11	4
B1S6	33	52	13	2
B1S8	33	58	7	2
B7S9	20	65	11	4
B7S15	20	71	7	2
B5S10	25	65	8	2
B5S15	28	63	7	2
B5S23	29	64	4	3
B5S26	27	64	8	1
B5S28	28	63	7	2
B5S30	18	70	10	2
B5S32	21	64	13	2

composition and the fact that all calculations are based on 100 percent clay should be kept in mind. In this study of the less than 2 micron fraction, illite is the dominant mineral (52 - 71%) with smectite (18 - 33%), kaolinite (4 - 14%), and chlorite (1 - 6%) constituting far lesser portions.

Gas Concentrations

Methane concentrations for the sampled sections of Boring 1, Main Pass are quite high (to 47,412 ppm) (Table 3). In addition to the shipboard canned profile, three samples were collected in the manned hyperbaric chamber while consolidation samples were being loaded (Figure 7). These samples were collected as near to the consolidation samples as possible, and more closely reflect the sample methane content. However, it must be noted that these values were not measured from the actual consolidation sample. Micro-scale methane variability within a core was not evaluated for this study. The values represent the total gas content including the decompressed or head space gas and matrix values extracted from the pore water and sediment particles at ambient pressure.

Borings 5 and 7 contain relatively lower values of methane concentrations (Table 1). The values plotted in Figure 8 were collected in the hyperbaric chamber, adjacent to the consolidation samples. These values again represent total methane concentration. Three samples contain significant values of methane: B7S9, B5S26, and B5S30. The remainder of the sediments tested have less than 566 ppm.

The interpreted methane concentration versus depth profile for Boring 2 indicates that sample B2S10 (11.76 m), collected with the

Table 3. Primary consolidation characteristics for all samples.

Core-Section	Test Type	Depth, z (m)	Initial void ratio, e_o	Initial porosity, n (%)	Undrained shear strength, C_u (kPa)	Effective overburden stress, σ'_{vo} (kPa)	Effective preconsolidation stress, σ'_c (kPa)	Compression indices, C_c High	Low	Methane content (ppm)	Overconsolidation ratio, OCR
B2 S10	I	11.76	1.701	62.97			23	0.493	0.493	~ 60,000	
	D	11.76	1.896	65.47			32	0.429	0.429		
B1 S2	I	6.72	1.626	61.92	14.82	43.56	37	0.656	0.656		0.849
	R		1.630	61.98				0.445	0.445		
B1 S4	I	12.41	1.511	60.18	6.75	79.17	16	0.397	0.397	41,500	0.202
	D	12.37	1.778	64.00		78.91	13	0.518	0.518		0.165
	R		1.628	61.95				0.436	0.436		
B1 S6	I	18.78	1.995	66.61	9.39	115.84	96	0.948	0.640	47,412	0.829
	D	18.72	2.279	69.50		115.49	22	0.806	0.565		0.190
	R		2.163	68.38				1.440	0.497		
B1 S8	I	24.32	2.283	69.54	14.82	154.86	32	0.928	0.589	3,309	0.207
	D	24.18	2.451	71.02	14.66	154.02	37	1.161	0.709		0.240
	R		2.292	69.62				0.765	0.542		
B7 S9	I	10.24	1.650	62.26	15.32	66.48	48	0.824	0.518	16,840	0.722
	D	10.20	2.246	69.19	14.33	66.22	34	0.869	0.585		0.513
	R		1.969	66.32				0.528	0.528		
B7 S15	I	16.37	2.018	66.87	14.89	99.90	41	1.210	0.601	203	0.410
	D	16.31	1.823	64.58	16.54	99.58	35	0.760	0.445		0.351
	R		1.708	63.07				0.474	0.474		
B5 S10	I	13.29	1.526	60.41	17.48	82.37	43	0.468	0.468	566	0.522
	D	13.21	1.414	58.57	19.76	81.87	65	0.518	0.518		0.794
	R		1.325	65.99				0.424	0.424		
B5 S15	I	19.42	1.230	55.16	19.15	126.31	89	0.405	0.405	485	0.705
	D	19.47	1.395	58.25	15.65	126.67	54	0.449	0.369		0.268
	R		1.283	56.20				0.353	0.353		

Table 3 continued.

Core-Section	Test Type	Depth, z (m)	Initial void ratio, e_o	Initial porosity, n (%)	Undrained shear strength, C_u (kPa)	Effective overburden stress, σ'_{vo} (kPa)	Effective preconsolidation stress, σ'_c (kPa)	Compression indices, C_c High	Low	Methane content (ppm)	Overconsolidation ratio, OCR
B5 S23	I	36.49	1.504	60.06	16.47	238.64	51	0.555	0.366	210	0.214
	D	36.44	1.728	63.34		238.31	38	0.581	0.422		0.159
	R		1.837	64.75				0.730	0.730		
B5 S26	I	42.47	2.022	66.91	21.69	270.13	90	0.844	0.844	4,516	0.333
	D	42.50	2.393	70.53	18.94	270.92	60	0.900	0.900		0.222
	R		2.139	68.14				0.604	0.604		
B5 S28	I	45.54	1.777	63.99	19.77	288.83	110	0.956	0.521	120	0.381
	D	45.49	1.941	66.00	19.93	287.72	54	0.732	0.732		0.188
	R		1.821	64.55				0.495	0.495		
B5 S30	I	51.76	2.243	69.16	29.69	322.86	69	0.941	0.702	1,370	0.214
	D	51.80	2.245	69.18	21.91	323.02	74	1.036	0.798		0.229
	R		2.128	68.03				0.605	0.605		
B5 S32	I	57.80	2.122	67.97	33.52	357.87	64	0.717	0.717	170	0.179
	D	57.74	2.091	67.65	28.16	357.52	60	0.741	0.741		0.169
	R		2.050	67.21				0.623	0.623		

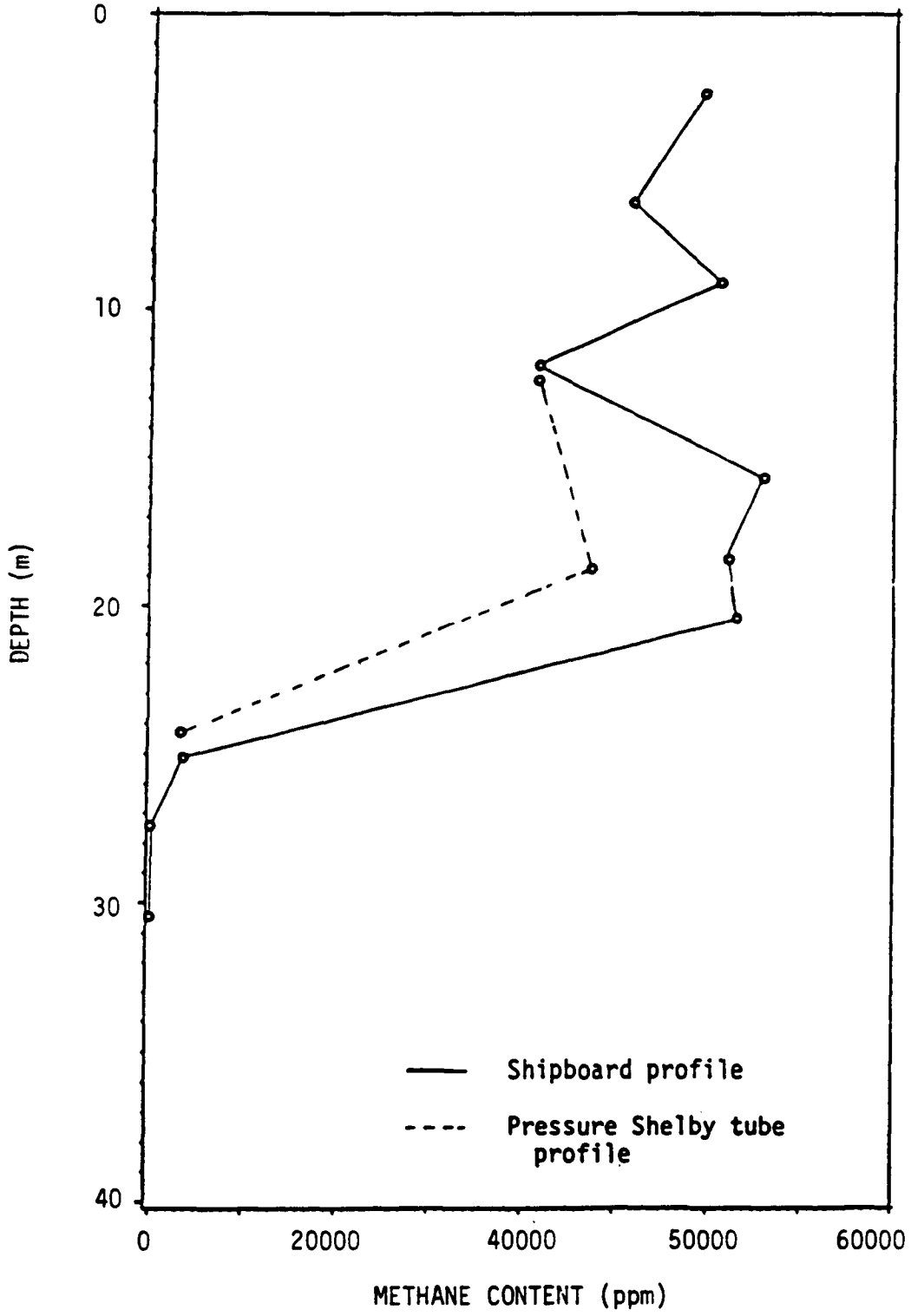

Figure 7. Methane concentration versus depth for PST Boring 1, Main Pass, Block 74.

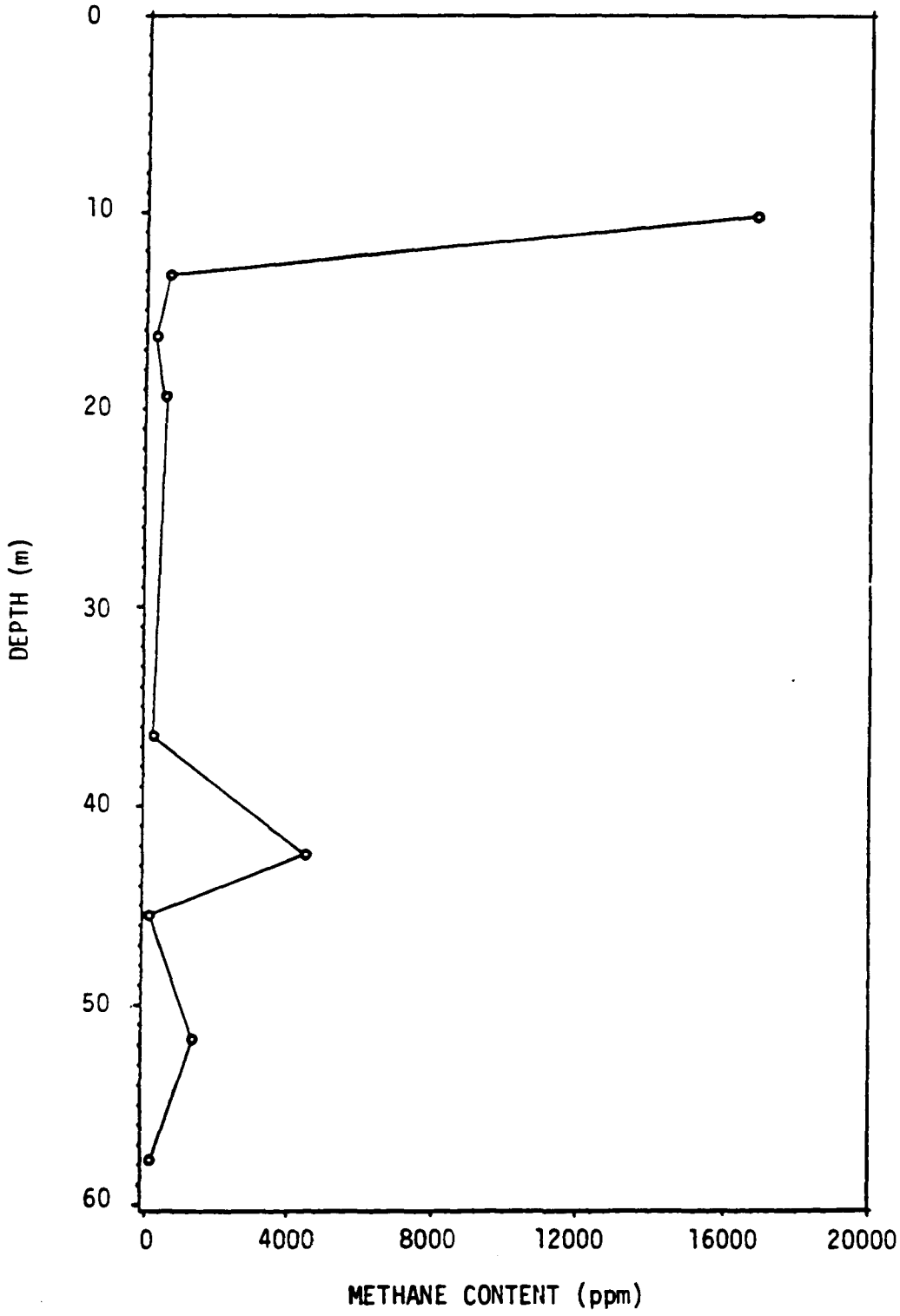

Figure 8. Methane concentration versus depth for PST samples from PST Borings 5 and 7, South Pass, Block 43.

pressure core barrel, contains approximately 60,000 ppm (Figure 9). Methane concentrations were analyzed shipboard.

Consolidation Test Results

The primary consolidation characteristics for all the samples can be found in Table 3. The results of comparative consolidation testing are graphically displayed as e-log σ_v' curves (Figures 10 through 23). The coefficients of consolidation, C_v, for the respective e-log σ_v' curves are plotted against logarithm of vertical effective stress, C_v-log σ_v' , on the same scale as the e-log σ_v' curves to aid in comparison. Because the initial structure of a clay depends on many factors, and the volume changes under pressure are a function of structure, a clay does not have a unique consolidation curve (Mitchell, 1976). It must be noted that sample variability could not be analyzed due to the lack of multiple consolidation analyses for each test procedure.

Sample B7S9 clearly shows the effects of degassing on the soil structure as evidenced in the void ratio and coefficient of consolidation curves versus logarithm of vertical effective stress (Figure 11). The degassed sample exhibits a drastically different e-log σ_v' curve, clearly indicating greater amounts of compression for a given load than for the *in situ* or remold test results. This is not within the expected normal range of variation for test specimens of the same sample. The compression indices, C_c, for the three specimens are much different (Table 3).

The primary difference between the *in situ* and degassed test results is shown by the time rate of compression curves of Figure 24.

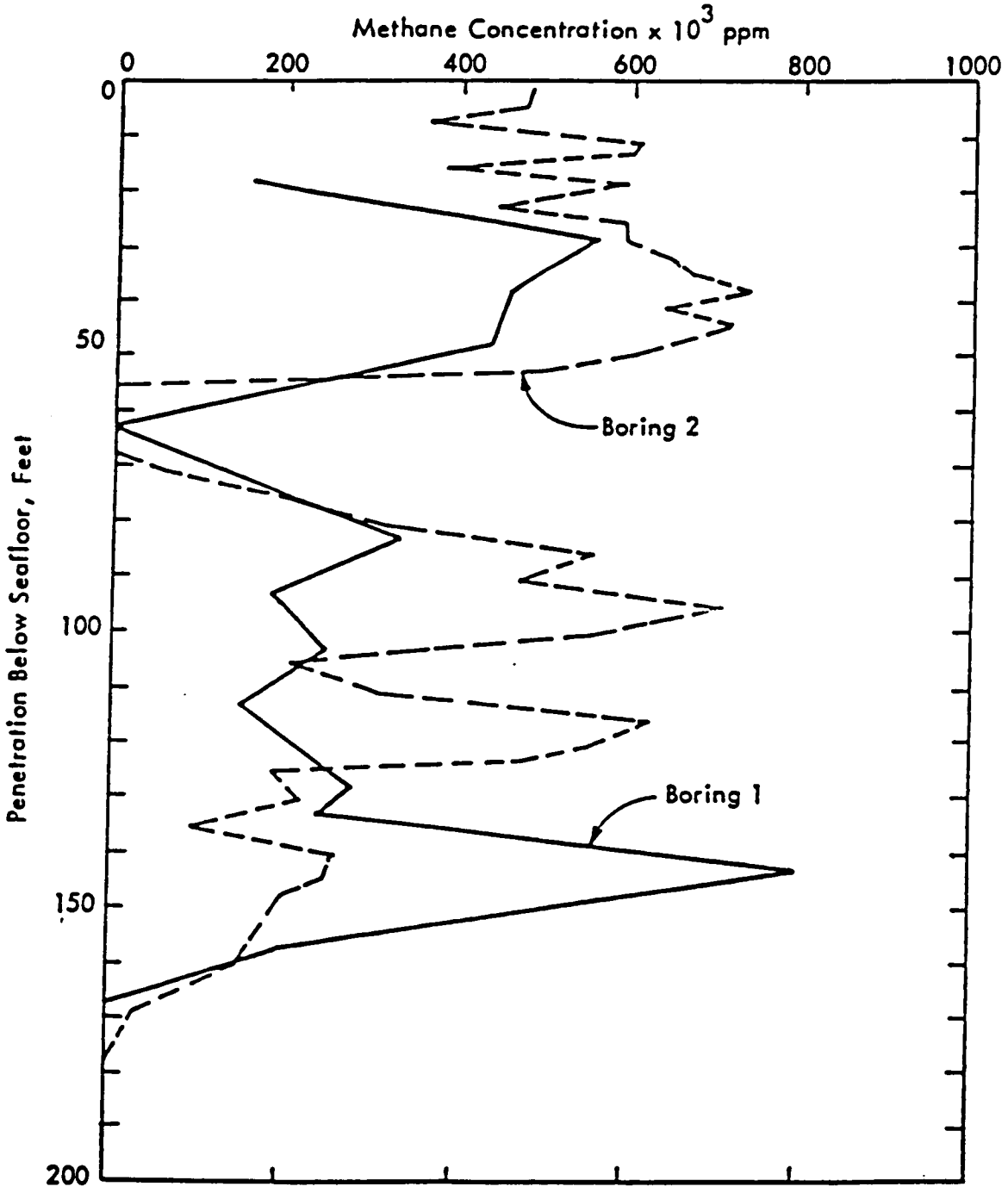

Figure 9. Methane concentration versus depth for PST Boring 2, West Delta, Block 85.

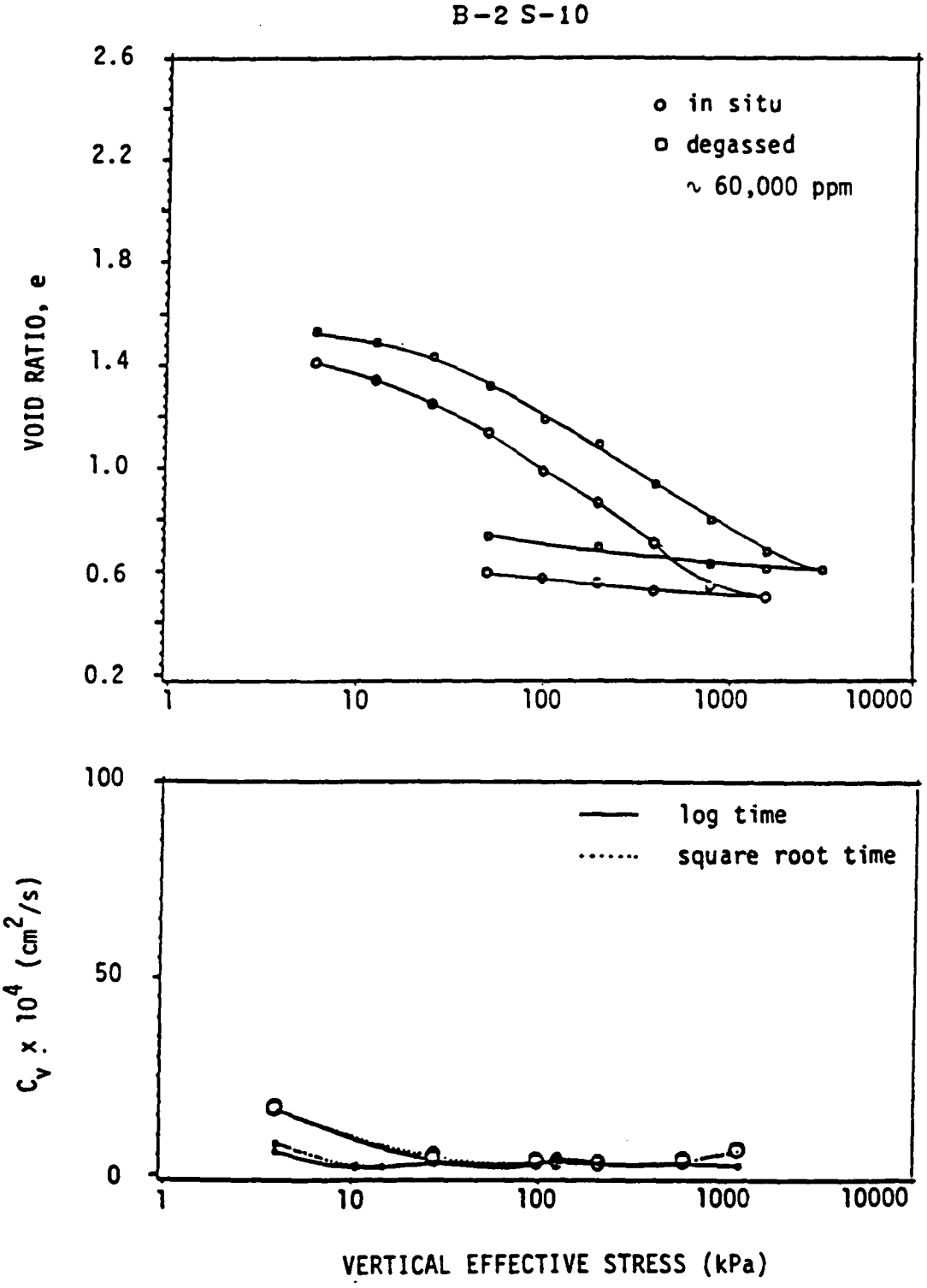

Figure 10. Comparative test results for Sample B2S10.

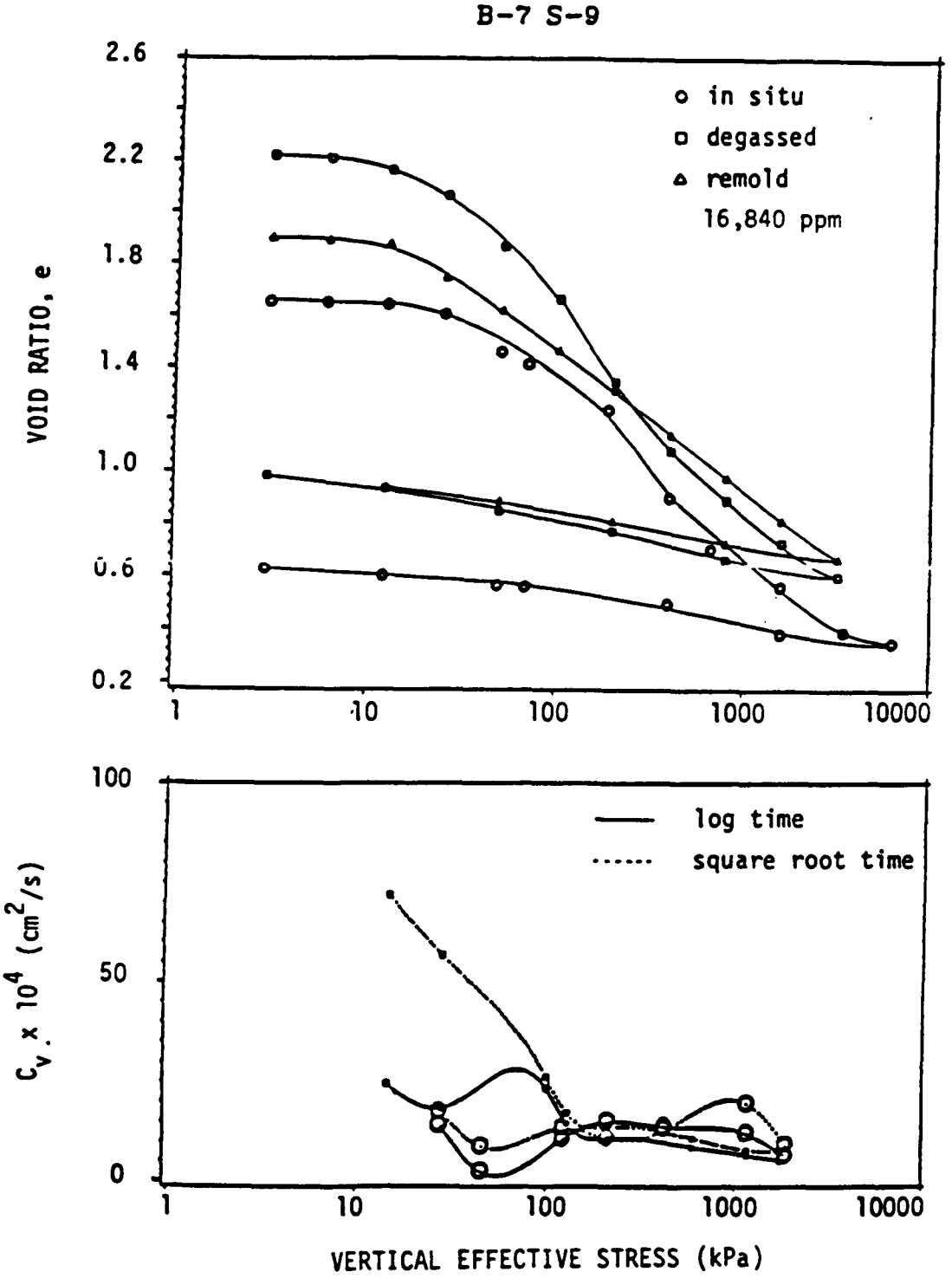

Figure 11. Comparative test results for Sample B7S9.

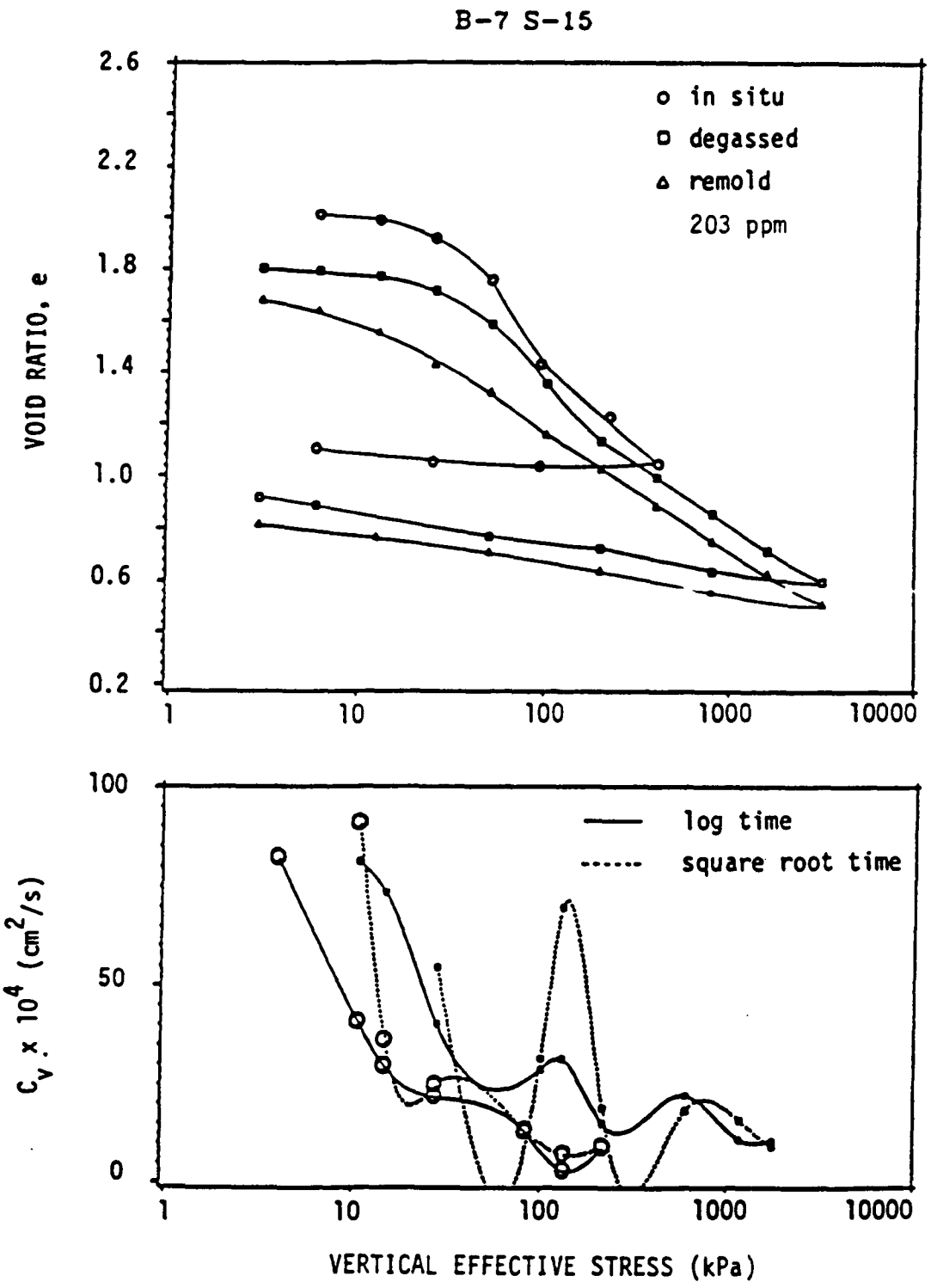

Figure 12. Comparative test results for Sample B7S15.

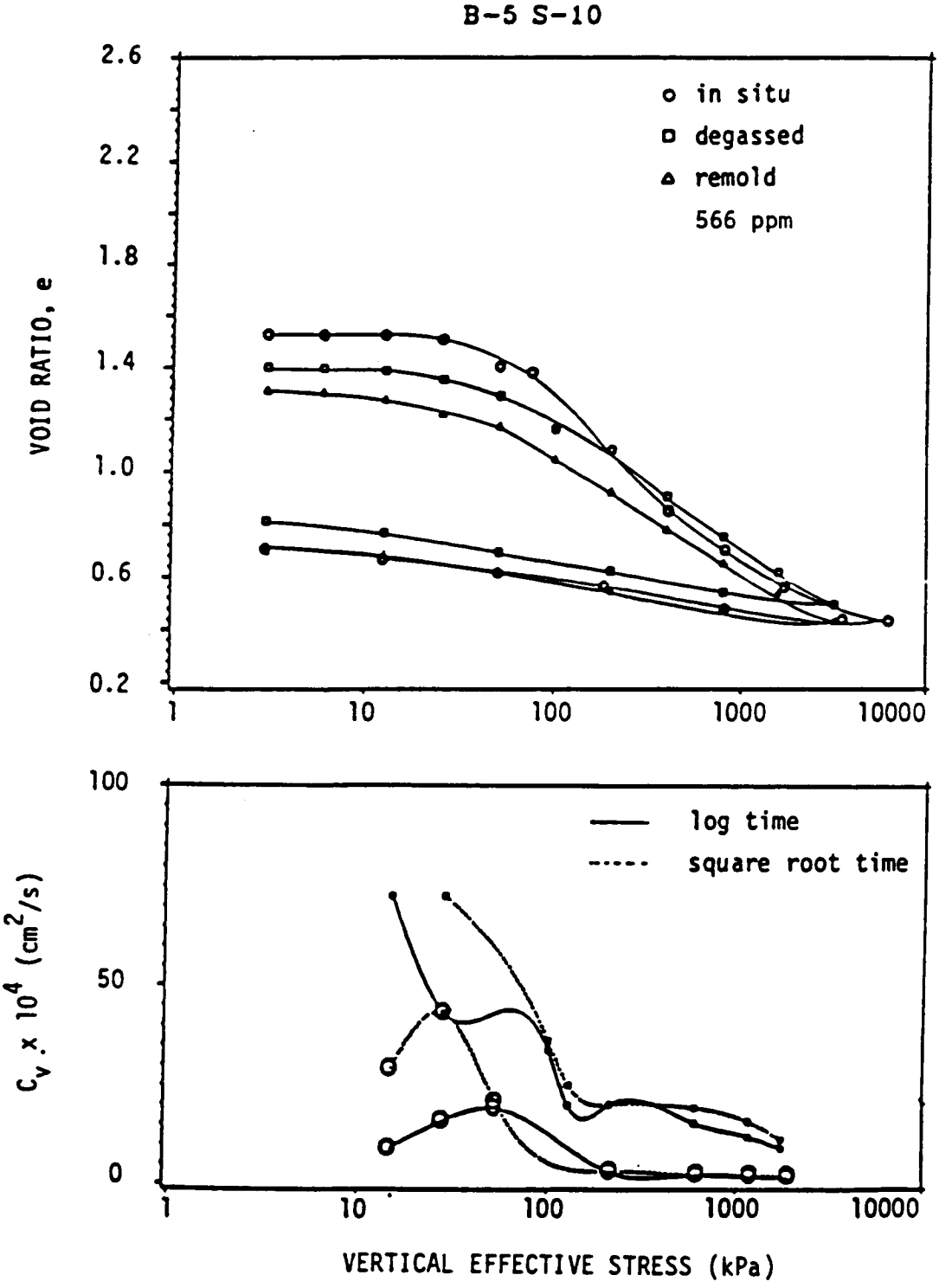

Figure 13. Comparative test results for Sample B5S10.

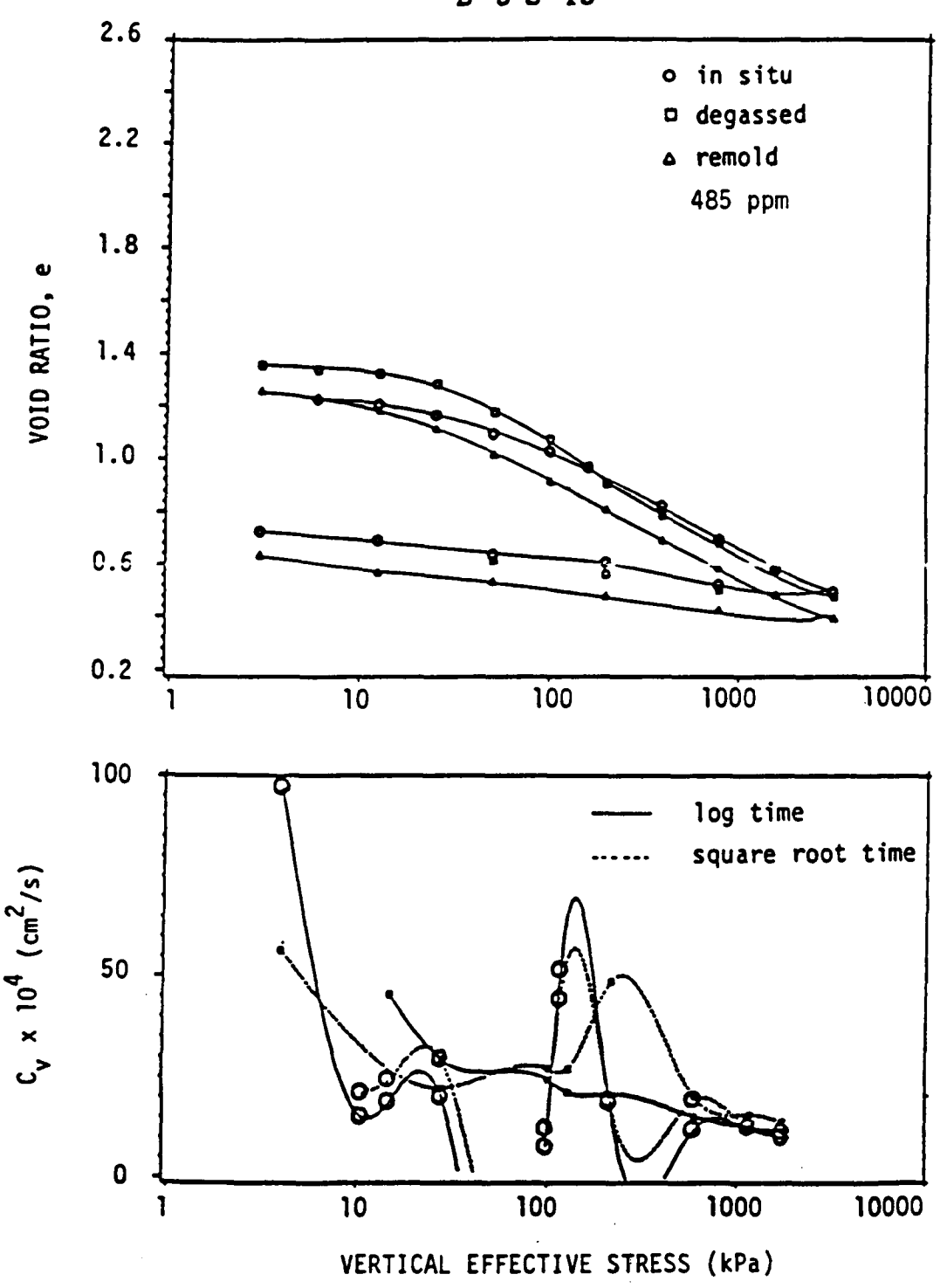

Figure 14. Comparative test results for Sample B5S15.

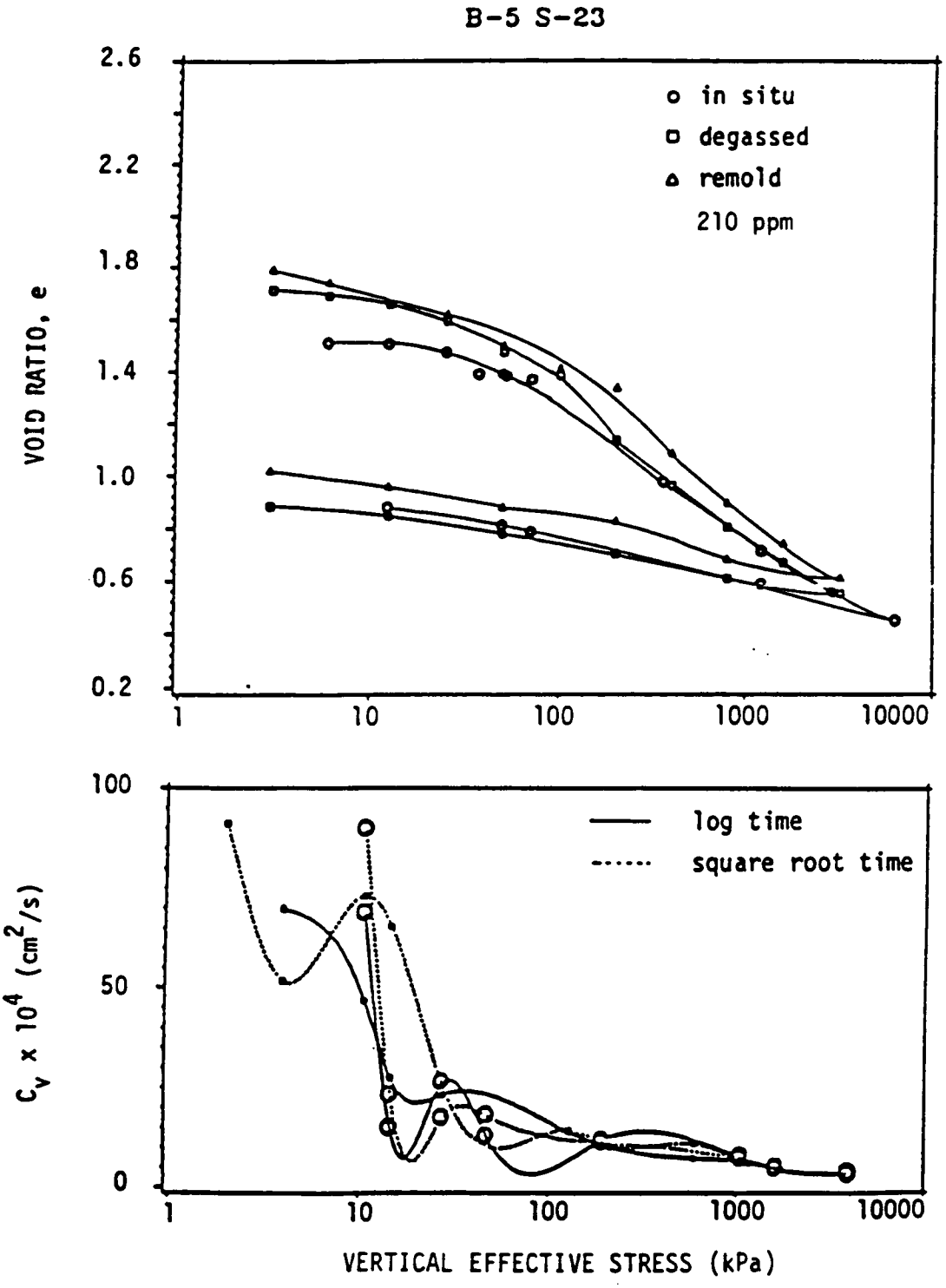

Figure 15. Comparative test results for Sample B5S23.

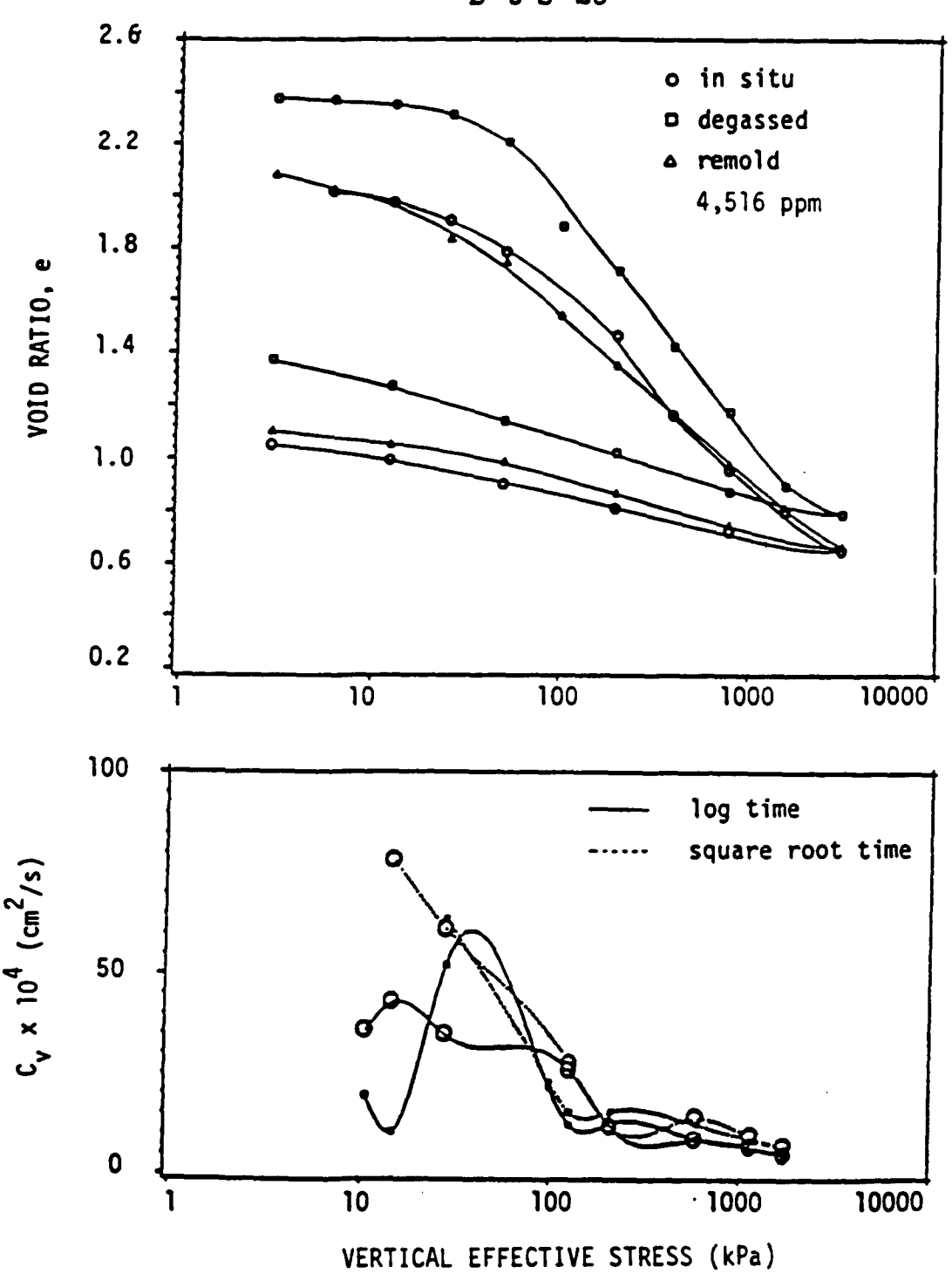

Figure 16. Comparative test results for Sample B5S26.

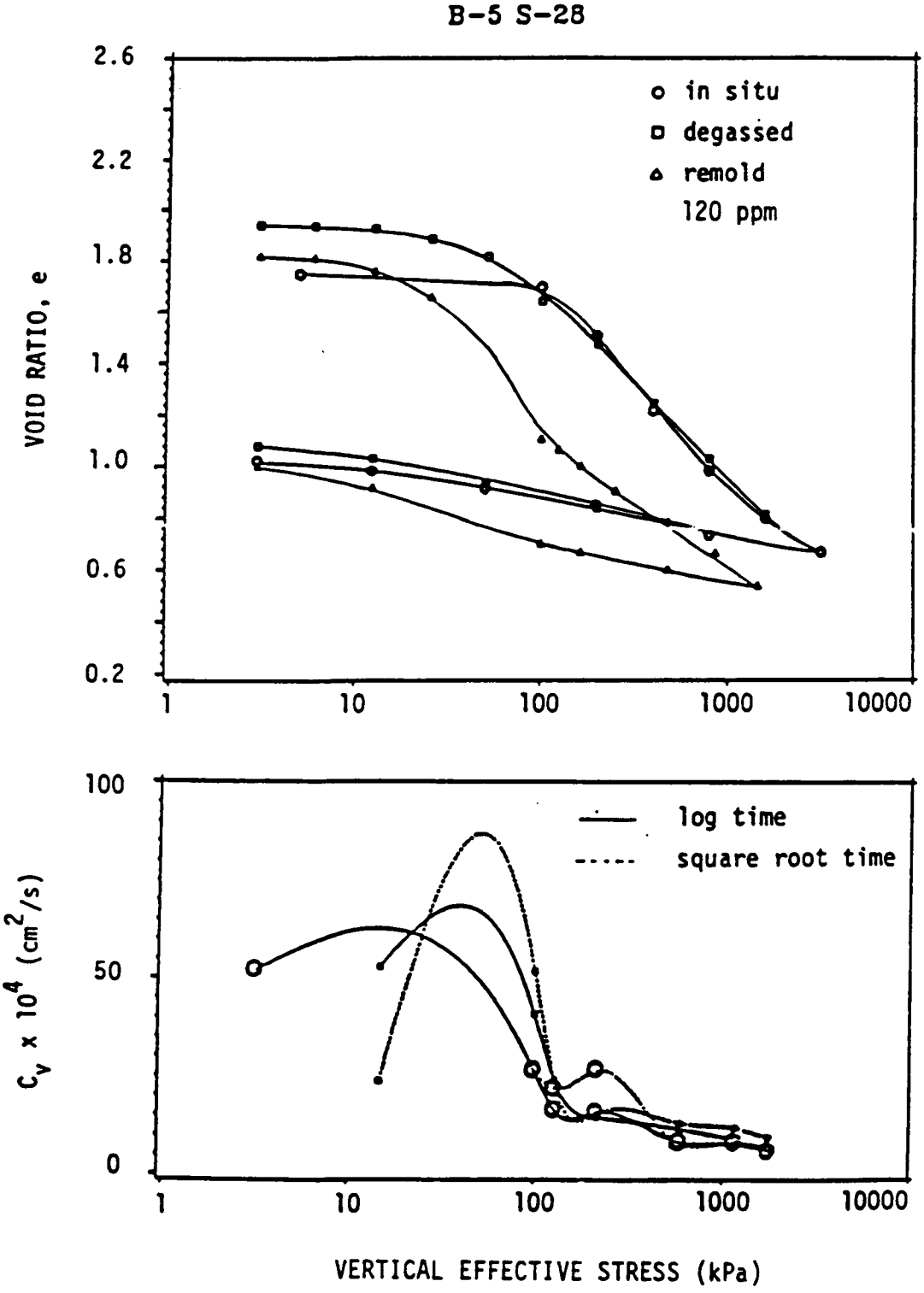

Figure 17. Comparative test results for Sample B5S28.

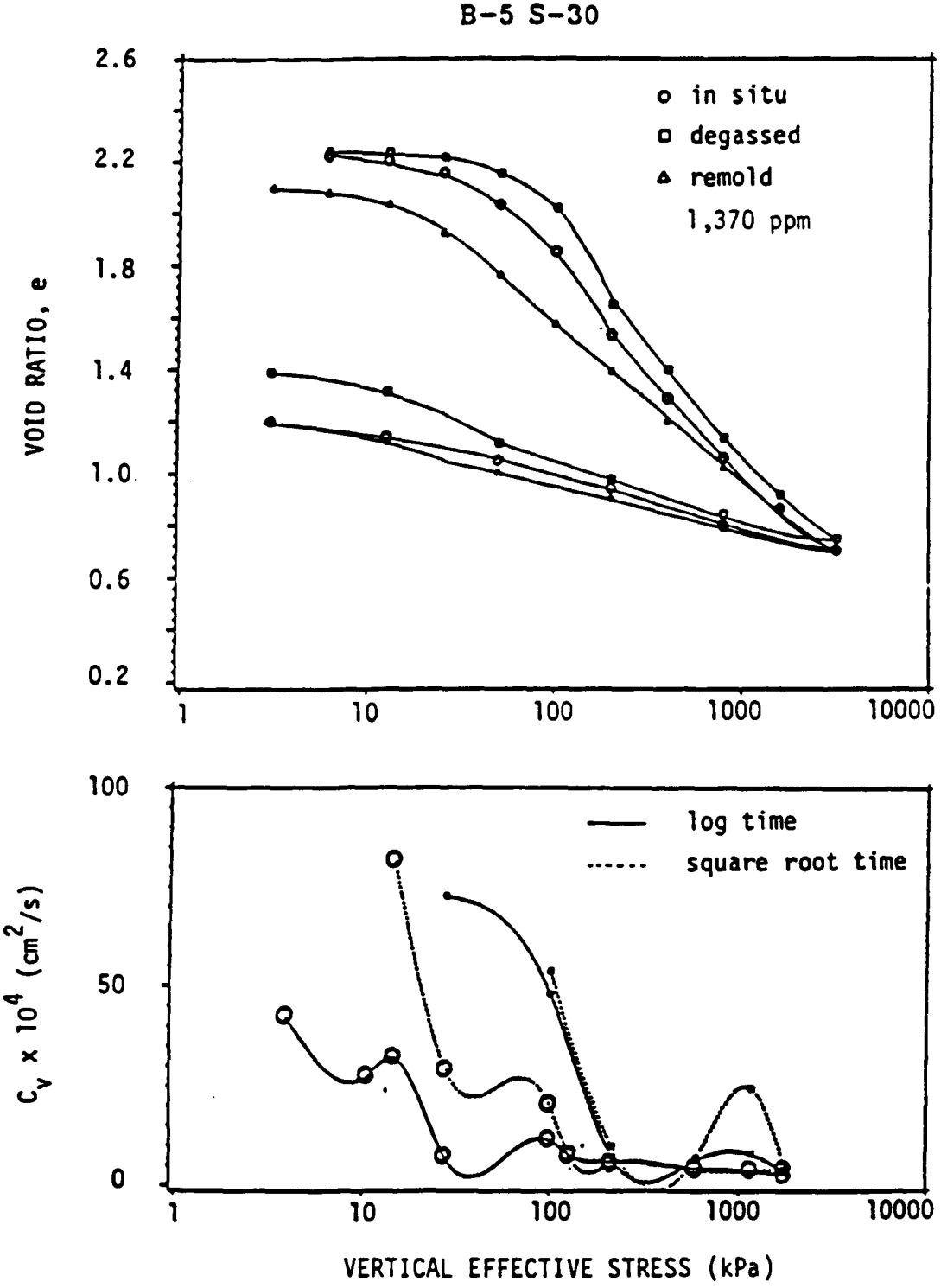

Figure 18. Comparative test results for Sample B5S30.

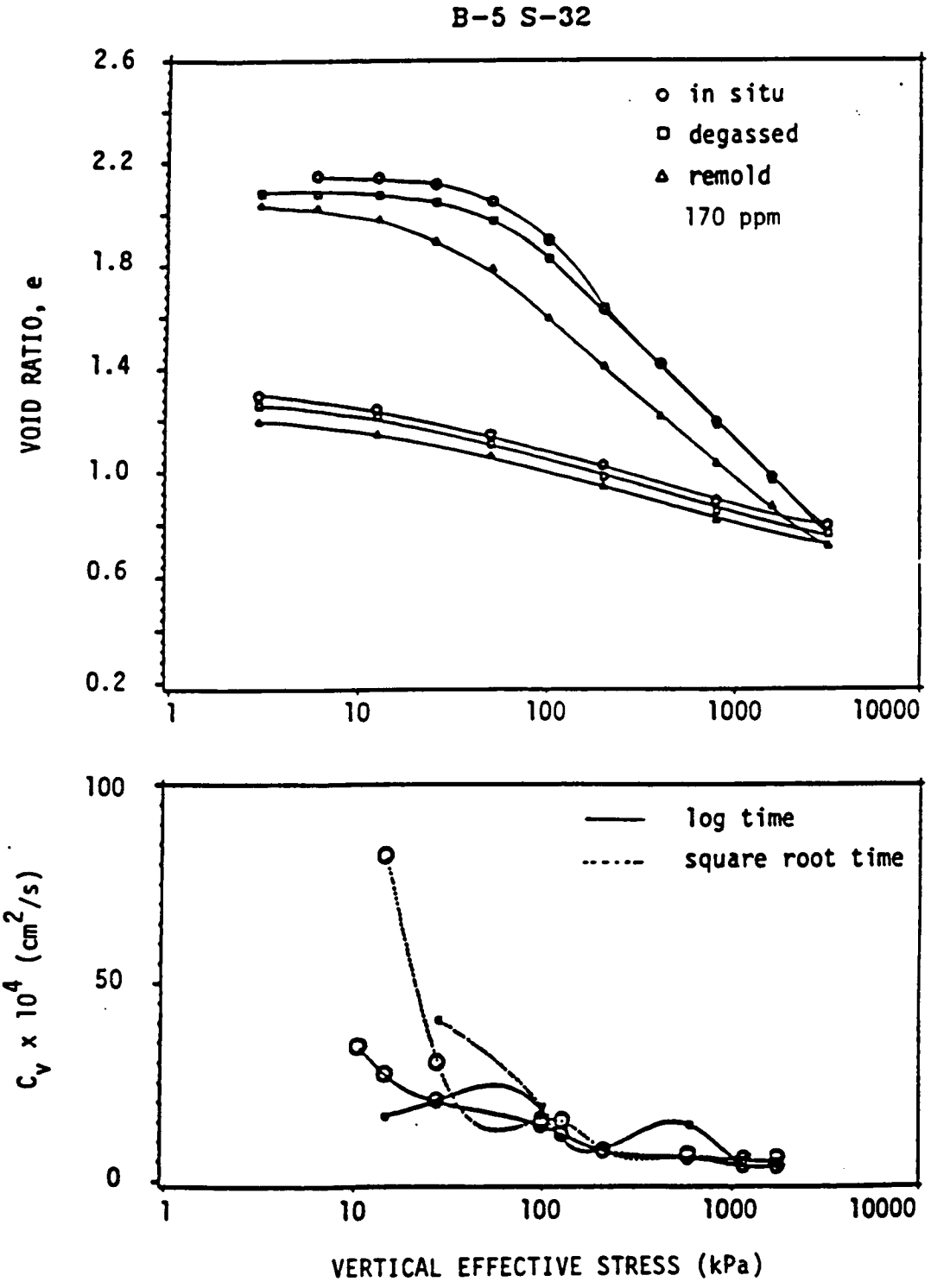

Figure 19. Comparative test results for Sample B5S32.

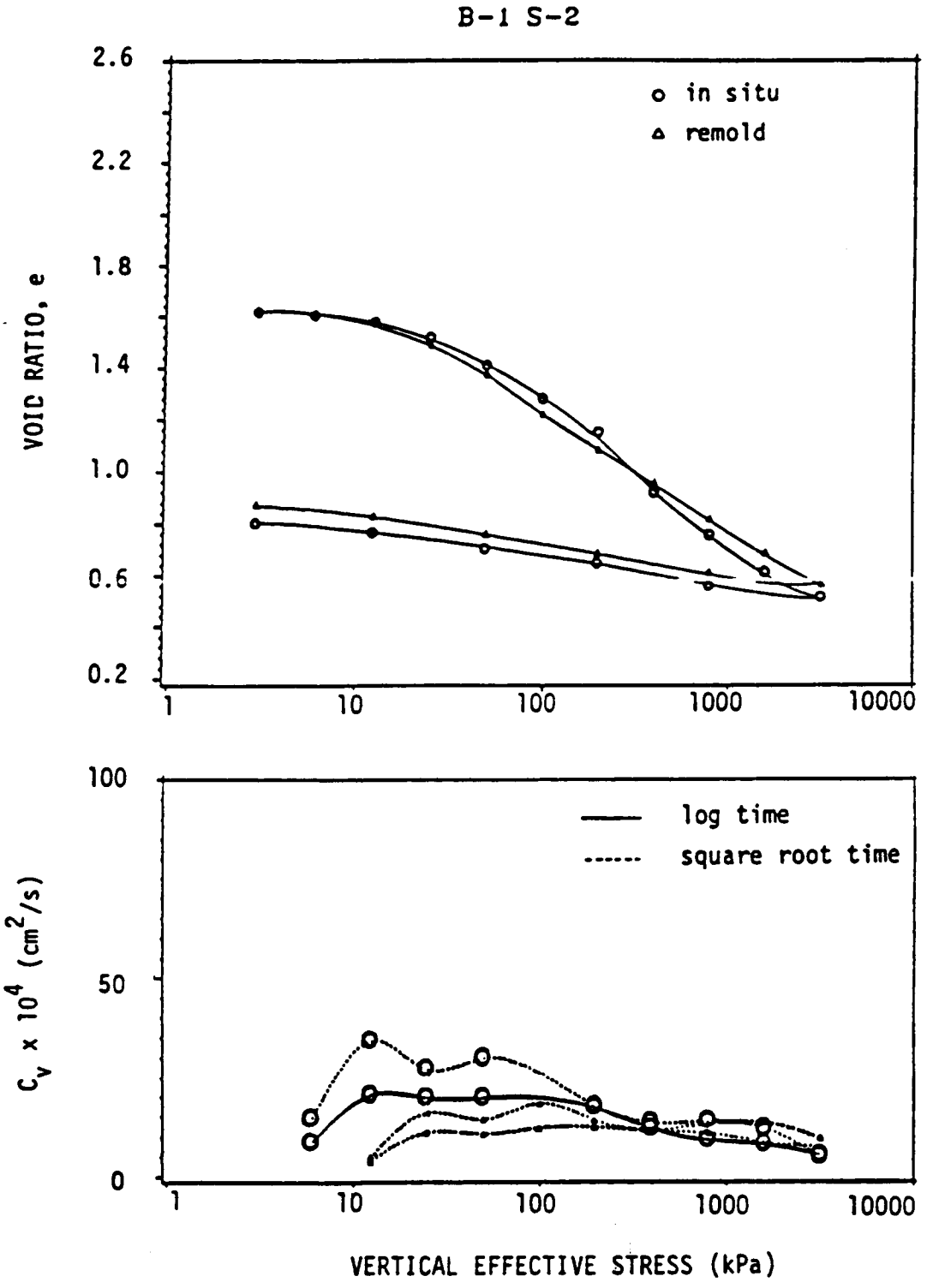

Figure 20. Comparative test results for Sample B1S2.

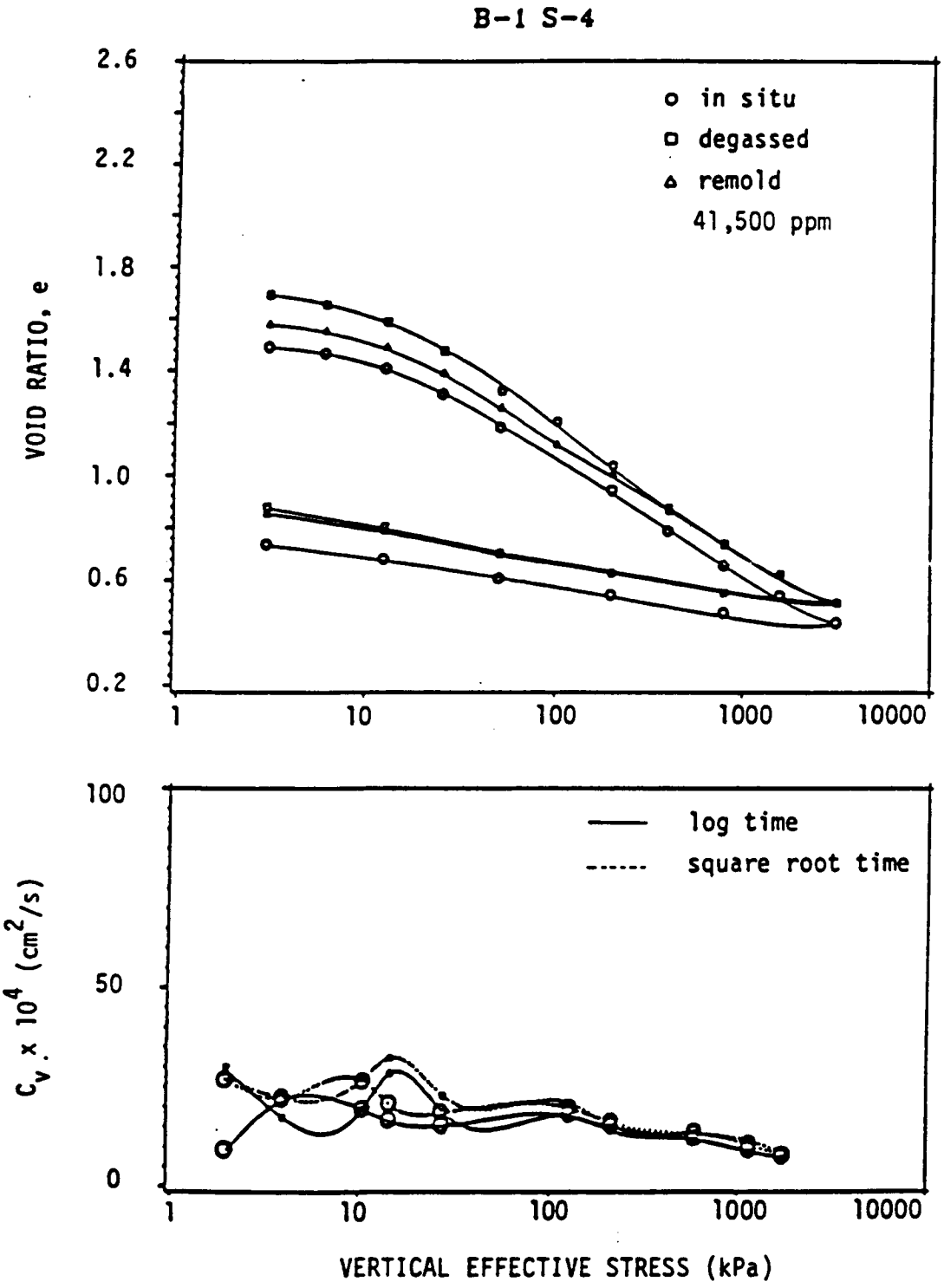

Figure 21. Comparative test results for Sample B1S4.

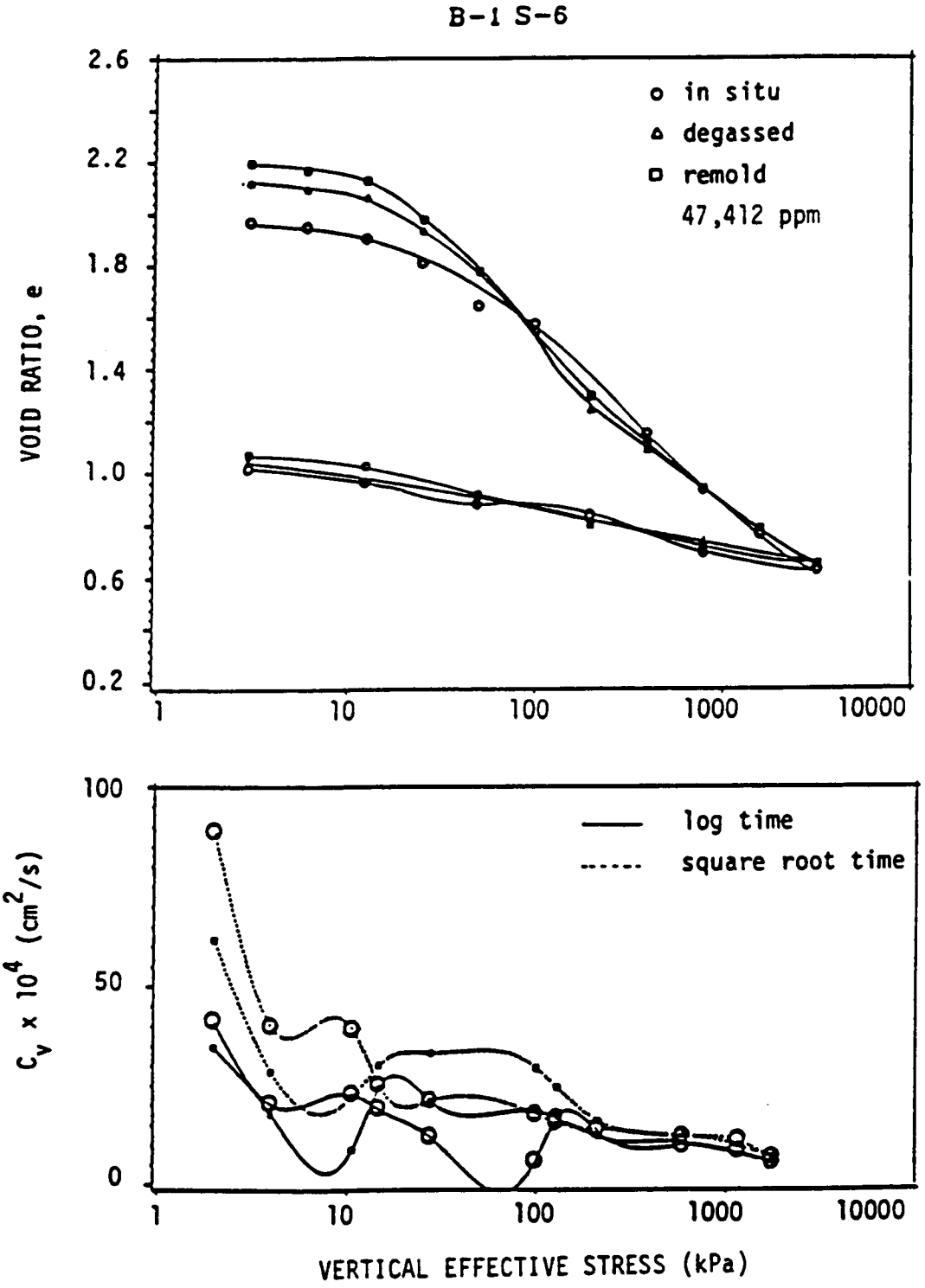

Figure 22. Comparative test results for Sample B1S6.

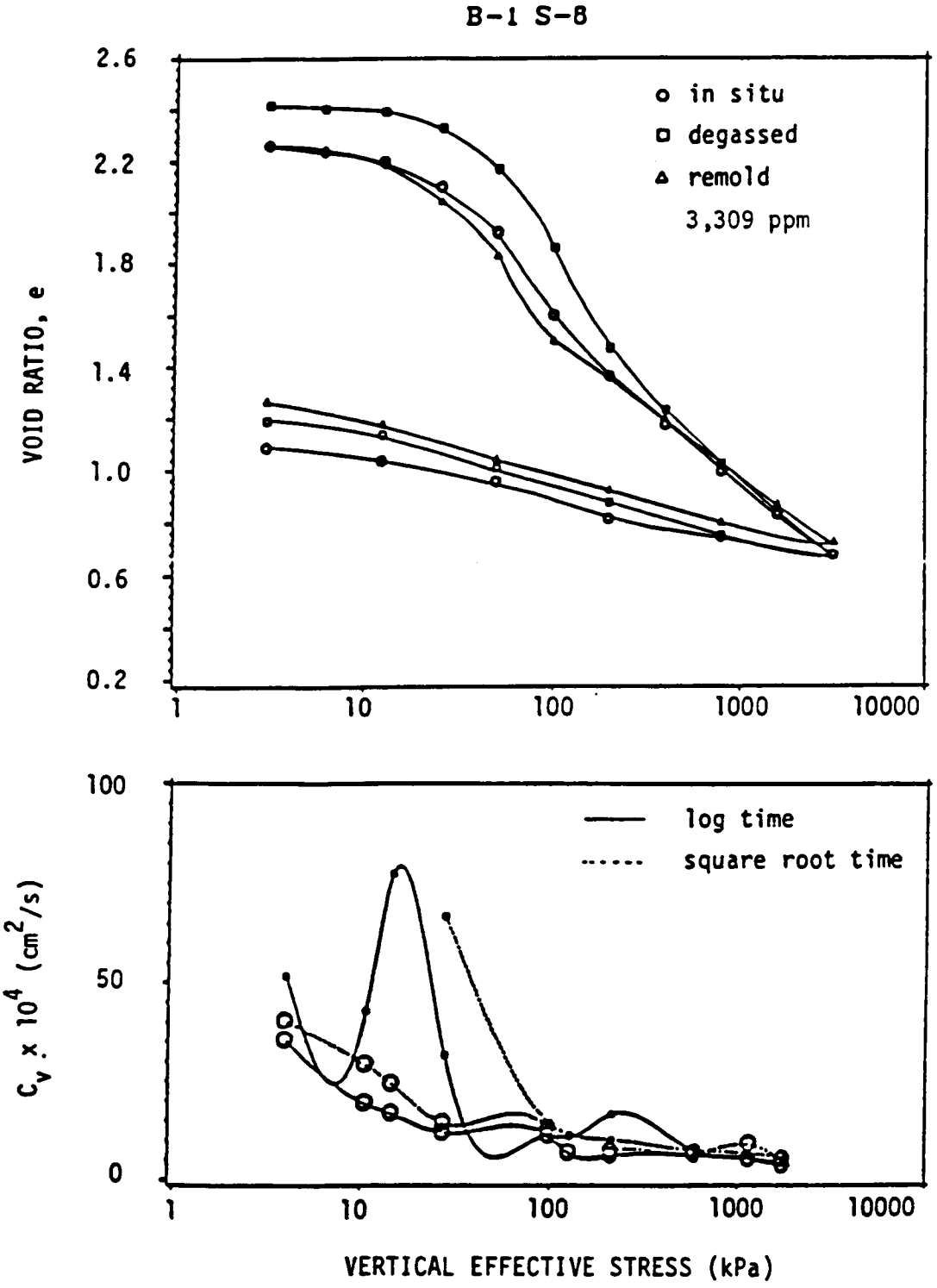

Figure 23. Comparative test results for Sample B1S8.

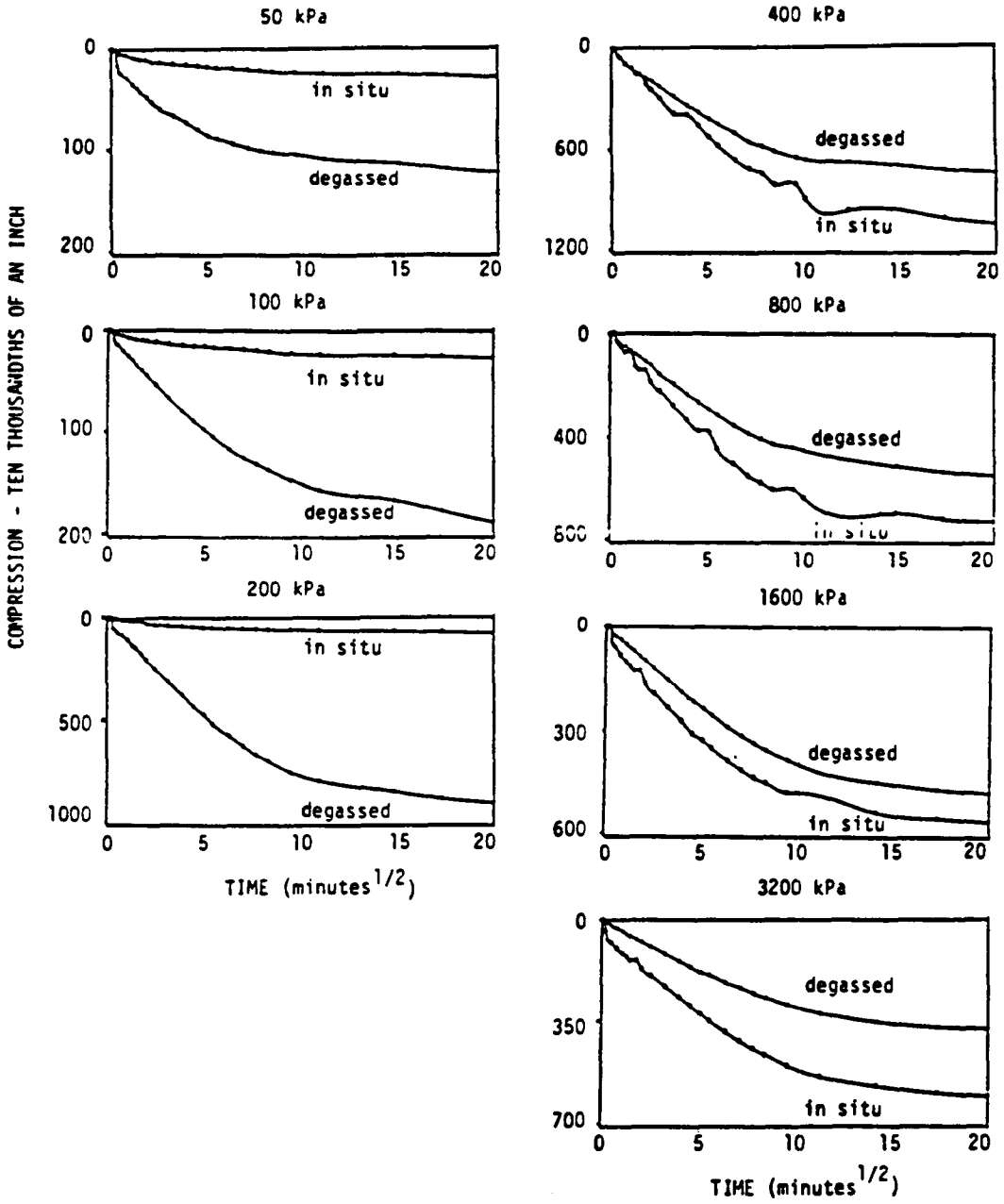

Figure 24. Comparative compression versus square root of time curves for Sample B7S9.

This figure presents the comparative square root of time curves of Sample B7S9 for the 50, 100, 200, 400, 800, 1600, and 3200 kPa loadings. For all loads, with the exception of 400 kPa, the t_{90} times are greater for the degassed consolidation curves. For loads less than 400 kPa, the time rate of compression is much larger for the degassed test results. In fact, the differences between the degassed and in situ curves increase between 50 and 200 kPa. At the 400 kPa load, the time rate of compression becomes greater for the in situ test. This trend continues throughout the remainder of the testing program. The differences in the coefficients of consolidation, C_v, result from these differences.

Compression versus log time curves for Sample B7S9 show similar results as for the square root of time curves (Figure 25). The time rate of compression is again, clearly greater for the degassed specimen at loads of 200 kPa and below. For loads of 400 kPa and greater, the time rate of compression for the in situ specimen is greater. The t_{50} times are greater for all loadings of the degassed specimen. The resultant C_v-log σ_v' curves at t_{50} are revealing (Figure 11). Initially, the degassed values are larger than the in situ values. At approximately 200 kPa, the C_v values for the degassed specimen are slightly less than for the in situ specimen. It must be noted, that at any given load the void ratio is larger for the degassed sample, however, the magnitude of the difference of the t_{50} values is markedly less (Table 4).

The instantaneous compression with loadings can best be noted by comparing the start height, d_s, of the sample with the calculated height at time zero, d_o, at any given load. Instantaneous compression, Δd can be defined as $d_s - d_o$. Initial compression of the degassed samples was

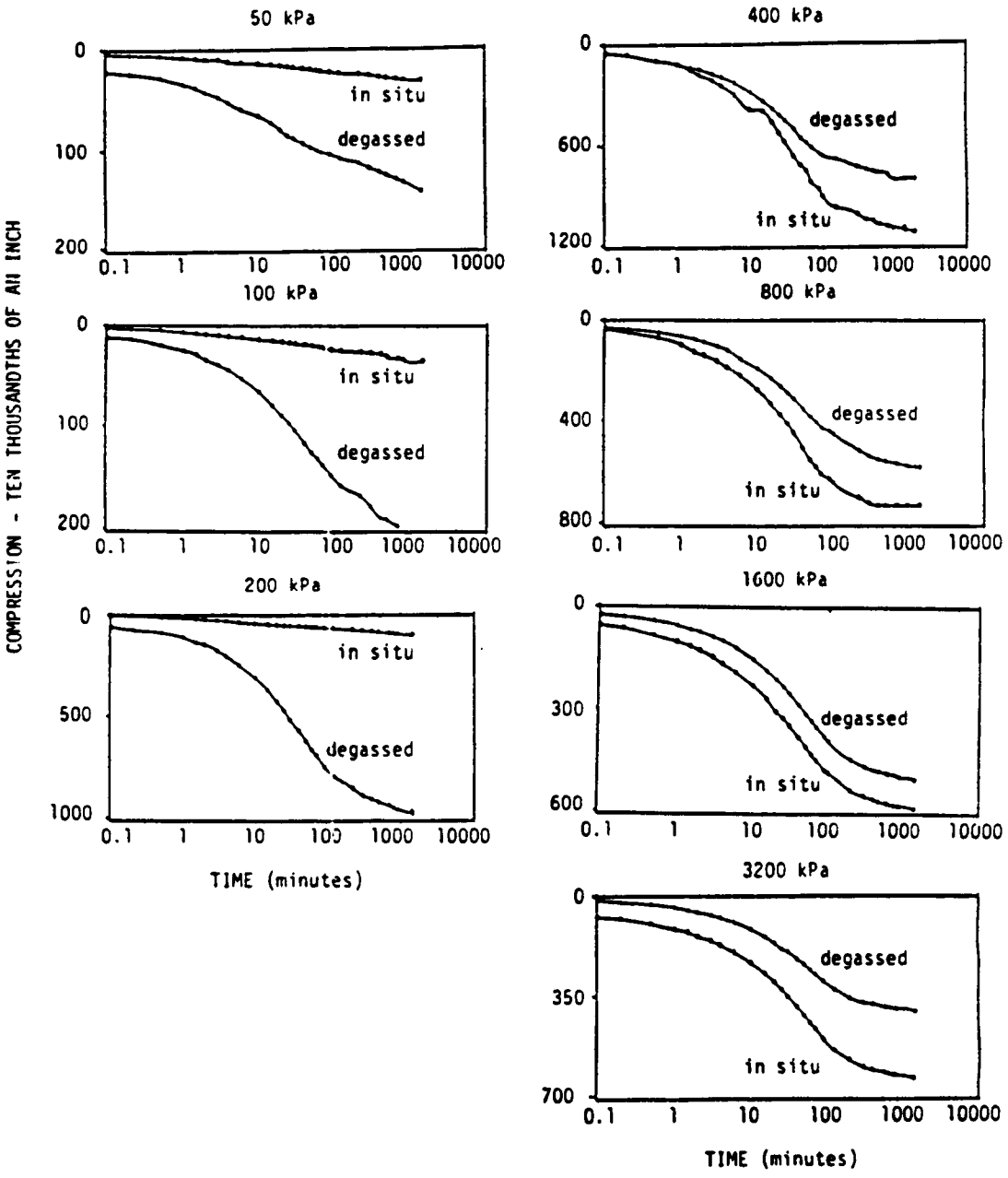

Figure 25. Comparative compression versus log time curves for Sample B759.

Table 4. Comparative log and square root of time values for sample B7S9.

Load (kPa)	t_{90} (minutes$^{1/2}$)		t_{50} (minutes)	
	in situ	degassed	in situ	degassed
50	6.25	27.04	3.0	4.1
100	17.64	60.84	2.5	16.0
200	26.01	75.69	2.2	22.0
400	112.36	73.96	21.0	23.0
800	73.96	75.69	17.5	23.0
1600	42.25	86.49	16.5	25.0
3200	72.25	81.0	25.0	27.0

found to be considerably larger than for the pressurized samples. This occurs because gas filled voids are readily compressed in the degassed, partially saturated samples. For samples with 100% pore water saturations, as in the pressurized samples, the addition of an instantaneous normal load results in an equal increase in the pore water pressure. Since permeability and pore water compressibility are low, pore water drainage, and thus time are required for significant reductions in sample height.

Figure 26 and Table 5 clearly show the greater initial compression for the degassed versus pressurized samples over the test loading range. Four points of particular interest to note are: 1) initial compression over the test loading range is greater for the degassed samples, 2) initial compression increases with increasing methane content, 3) initial compression is greatest over the load range of 25 to 400 kPa, and 4) the total compression for a given degassed specimen is greater than the comparative compression for the *in situ* specimen (Table 6).

Large differences are shown for the coefficients of consolidation, C_v, which are an averaged reflection of the time rate of consolidation. Initially, the degassed values of the coefficient of consolidation, calculated by the square root of time method, are approximately 4 times greater than the *in situ* test results. Both *in situ* and degassed log and square root of time coefficients of consolidation converge at a vertical effective stress value in excess of the effective preconsolidation stress at approximately 200 kPa. The effective preconsolidation stresses for these samples are 48 kPa and 34 kPa for the *in situ* and degassed tests, respectively.

The degassed specimen appears to be reconsolidating to its original

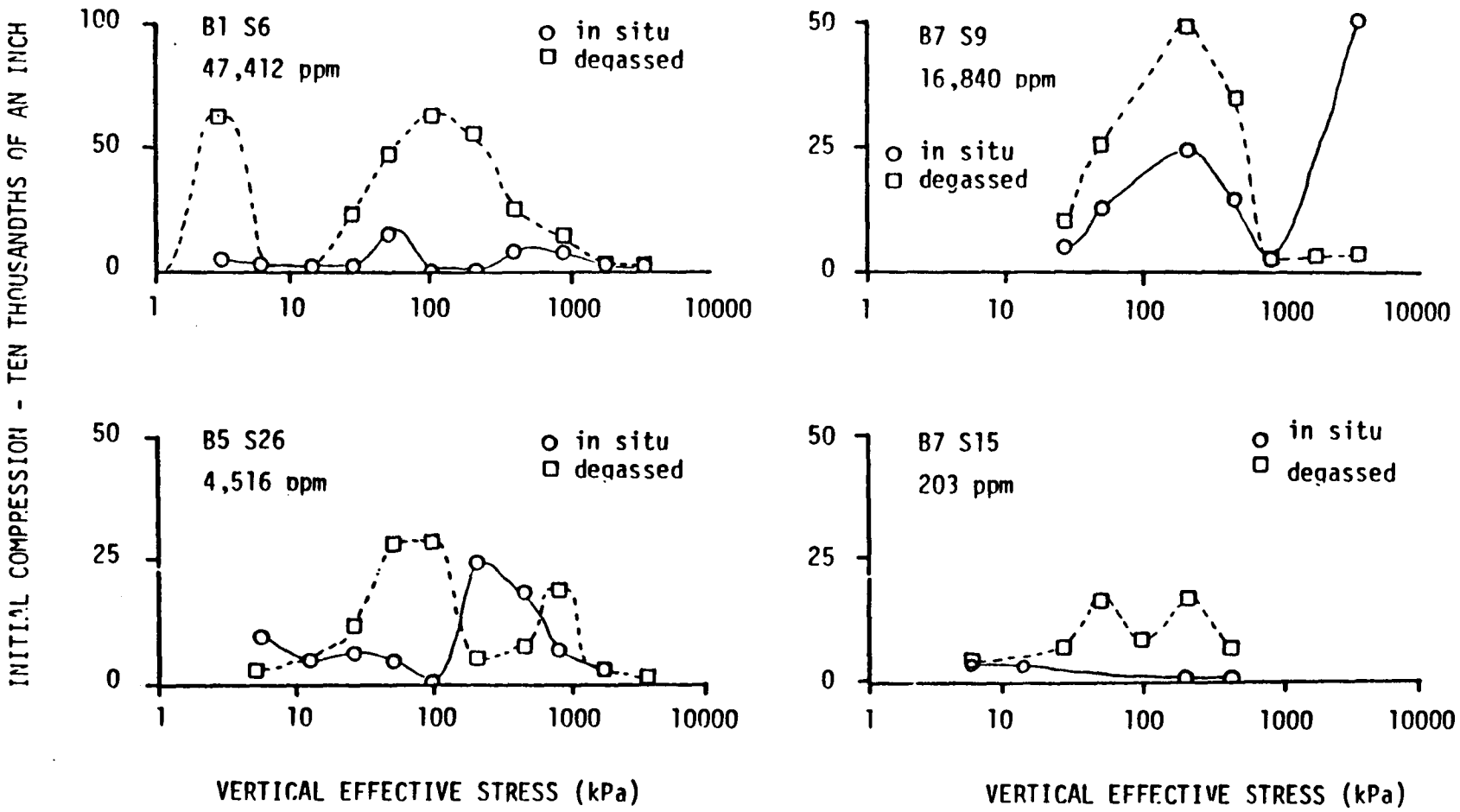

Figure 26. Initial compression ($d_s - d_o$) versus vertical effective stress for four consolidation tests of varying methane concentration.

Table 5. Total initial compression ($d_s - d_o$) for loads to 3200 kPa for *in situ* and degassed consolidation samples from PST Borings 1, 5, and 7.

Sample	Total Initial Compression (10^{-4} inches) *in situ*	degas
B1S2	63	
B1S4	49	162
B1S6	33	244
B1S8	41	97
B7S9	33	123
B7S15*	-9	50
B5S10	30	141
B5S15	67	187
B5S23	34	261
B5S26	75	114
B5S28	4	122
B5S30	-7	87
B5S32	16	133

* Values indicate the range 3 to 800 kPa.

Table 6. Total compression for loads to 3200 kPa for *in situ*, degassed, and remold consolidation samples.

Sample	Total Compression (inches)			Methane conc., (ppm)
	in situ	degassed	remold	
B1S2	0.4210		0.4038	
B1S4	0.4271	0.4522	0.4202	41,500
B1S6	0.4530	0.5144	0.5007	47,412
B1S8	0.4868	0.5139	0.4702	3,309
B7S9	0.4861	0.5064	0.4367	16,840
B7S15*	0.3306	0.3463	0.3521	203
B5S10	0.4395	0.3794	0.3756	566
B5S15	0.3323	0.3868	0.3805	485
B5S23	0.3748	0.4326	0.4315	210
B5S26	0.4674	0.4741	0.4666	4,516
B5S28	0.3940	0.4377	0.4119	120
B5S30	0.4767	0.4611	0.4098	1,370
B5S32	0.4265	0.4316	0.4356	170
B2S10	0.4469	0.4472		

* Values indicate the range 3 to 800 kPa.

state (i.e., that which the *in situ* specimen is at under a given load). But, if the inclusion of gas bubbles in the soil matrix tends to reduce effective permeability, then the time rate of consolidation and thus, the coefficients of consolidation should be less for the degassed test. However, this does not appear to be the case. Lowe et al (1964) noted a similar effect for back pressured versus non-back pressured specimens. They presented the possible explanation that the presence of gas bubbles in the soil matrix not only affects the permeability of the soil but gas bubbles also affect the rate of dissipation of pore pressure.

In this case, it appears that the effect of increased load is much greater than the effect of permeability on compressibility. The highly disturbed matrix of the degassed sample is being readily reoriented under initial load conditions. Both the coefficients of compressibility and consolidation are large for the initial loading conditions. Instantaneous compression of gas filled voids occurs in all loadings less than the effective preconsolidation stress. Taylor (1948) noted similar rapid initial compression and attributed it, in part, to small amounts of gas in the pores. For loads above the effective preconsolidation stress, compression of gas bubbles no longer constitutes the major portion of compression as the soil matrix is reoriented due to prior compression. At this point, the coefficients of consolidation calculated by the log and square root of time methods are less for the degassed versus the *in situ* test.

Similar results, as noted for the comparative tests of specimen B7S9, are noted for specimens B2S10, B5S23, B5S26, B5S28, B5S30, B5S32, B1S2, B1S4, B1S6, and B1S8. For all the above mentioned cases, both the coefficients of consolidation calculated by the log and square root of

time methods converge. This occurs in the lower portions of the e-log curves, where the vertical effective stress is greater than the effective preconsolidation stress for the respective curves.

The comparative e-log σ_v' and C_v-log σ_v' curves for sample B5S10 are quite dissimilar from the above mentioned test results (Figure 13). Both the degassed and remold results appear quite similar, the e-log σ_v' curves are parallel, indicating similar compression versus vertical effective stress. The in situ test results clearly show a distinct break in curvature and higher void ratios for a given stress. The C_v-log σ_v' curves for the in situ and degassed tests are again quite unique. The degassed results for both the log and square root of time methods are larger by a factor of 10 throughout the test. The degassed values converge at approximately 100 kPa, while the in situ values converge at approximately 60 kPa. The effective preconsolidation stresses for the degassed and in situ samples are 65 and 43 kPa, respectively.

Comparative results of samples B5S15 and B7S15 are similar in many respects. Both degassed e-log σ_v' curves show distinct breaks in curvature at higher vertical effective stresses. However, the in situ values for B7S15 have greater void ratios at a given effective stress, and show a distinct break in curvature as compared to degassed and remold test results (Figure 12). The in situ test results for sample B5S15 have lower values of void ratio for a given effective stress than the degassed test values and do not show a distinct break in curvature (Figure 14).

The comparative C_v-log σ_v' curves for both samples B7S15 and B5S15 are quite erratic and only suggest a slight decreasing trend with

increasing vertical effective stress.

Effective Preconsolidation Stress and Effective Overburden Stress

Effective overburden stress, σ_{vo}', is calculated based on the bulk density profile for the respective borings and assumes no excess pore water pressure (Figure 27). The effective preconsolidation stress, σ_{vc}', is graphically estimated from the e-log σ_v' curves by the Casagrande (1936) technique (Figure 27). The overconsolidation ratio, OCR, is defined as the effective preconsolidation stress, σ_{vc}', divided by the effective overburden stress, σ_{vo}'. The state of consolidation is determined by the evaluation of the OCR value. An OCR value equal to 1 indicates a normally consolidated sediment, while greater than 1 shows overconsolidation, and less than 1 shows underconsolidation. Values for these parameters are listed in Table 3, and graphically displayed versus depth in Figure 28. Effective preconsolidation stress values falling to the left of the effective overburden stress profile are underconsolidated.

With three exceptions, the values of effective preconsolidation stress are larger for the pressurized tests than those for the degassed tests, and in some cases they are markedly larger. Samples B1S8, B5S10, and B5S30 all exhibit reduced values of effective preconsolidation stress versus the degassed test results.

The OCR values followed the same trends as the effective preconsolidation values (Figure 28). All samples can be classified as underconsolidated, however, the OCR values for the pressurized tests are greater than for the degassed tests.

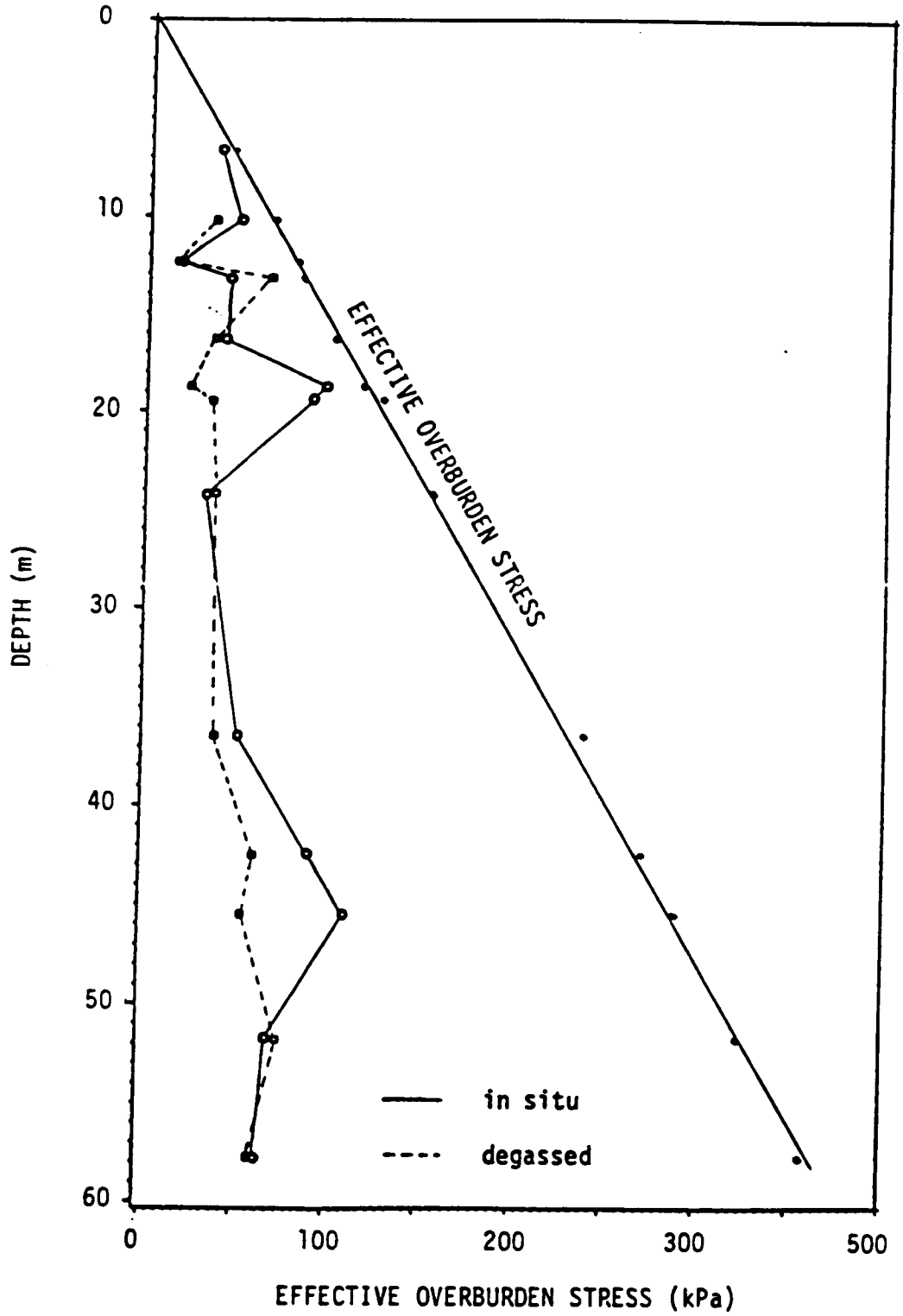

Figure 27. **Effective overburden stress versus depth with effective preconsolidation stress for <u>in situ</u> and degassed samples from PST Borings 1, 5, and 7.**

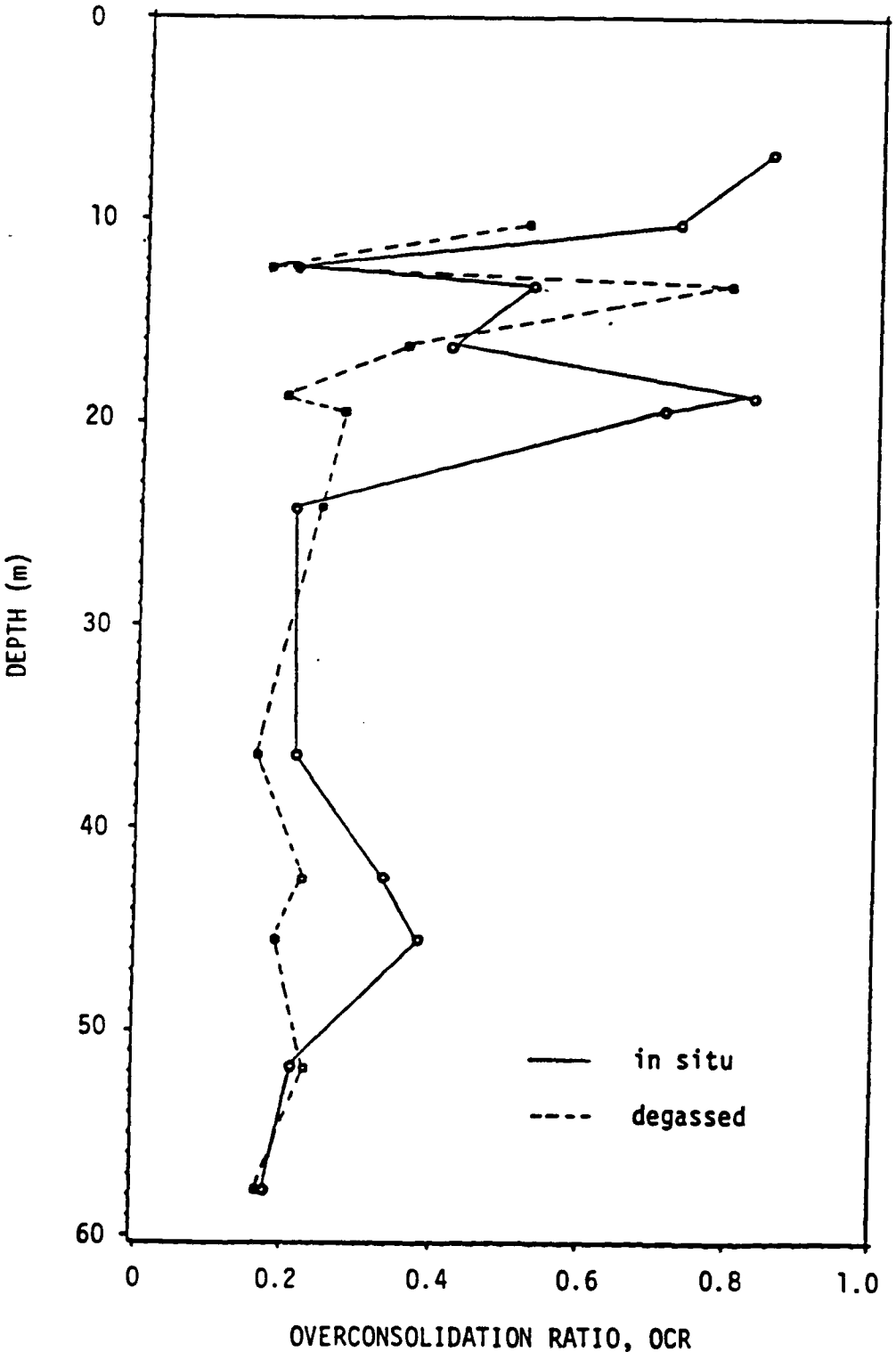

Figure 28. **Overconsolidation ratio versus depth for in situ and degassed samples from PST Borings 1, 5, and 7.**

Compression Indices

Evaluation of the e-log σ_v' curves indicates the presence of double breaks on numerous samples. Therefore, the compression indices, C_c, were calculated for both the high and low portions of these curves (Figures 29 and 30). In 75% of the cases studied, both the high and low compression indices are greater for the degassed versus *in situ* test results. For two samples that have double curves, B1S6 and B7S15, both C_c values are less for the degassed samples. Additionally, samples B5S15 and B5S28 (both with double curves) have one C_c value less for the pressurized sample. The consolidation curves of the degassed Mississippi delta sediments resemble those of highly sensitive clays, where compressibility is relatively low until the consolidation stress exceeds the preconsolidation stress. It then increases sharply as shown in Figure 11 for sample B7S9. As the void ratio reduces under higher consolidation stresses, the compressibility eventually assumes a lower value.

Pore Water Saturation

Pore water saturation values for the consolidation samples provide an interesting insight into the effects of degassing. Pore water saturation values derived by two different methods are shown in Table 7. The calculated values are indicative of theoretical pore water saturation based on the volume of pore water and gas present in the sediment. These values are calculated from:

$$S\ (\%) = \frac{V_w}{V_w + V_g}$$

where S is the degree of saturation, V_w is the volume of water, and V_g

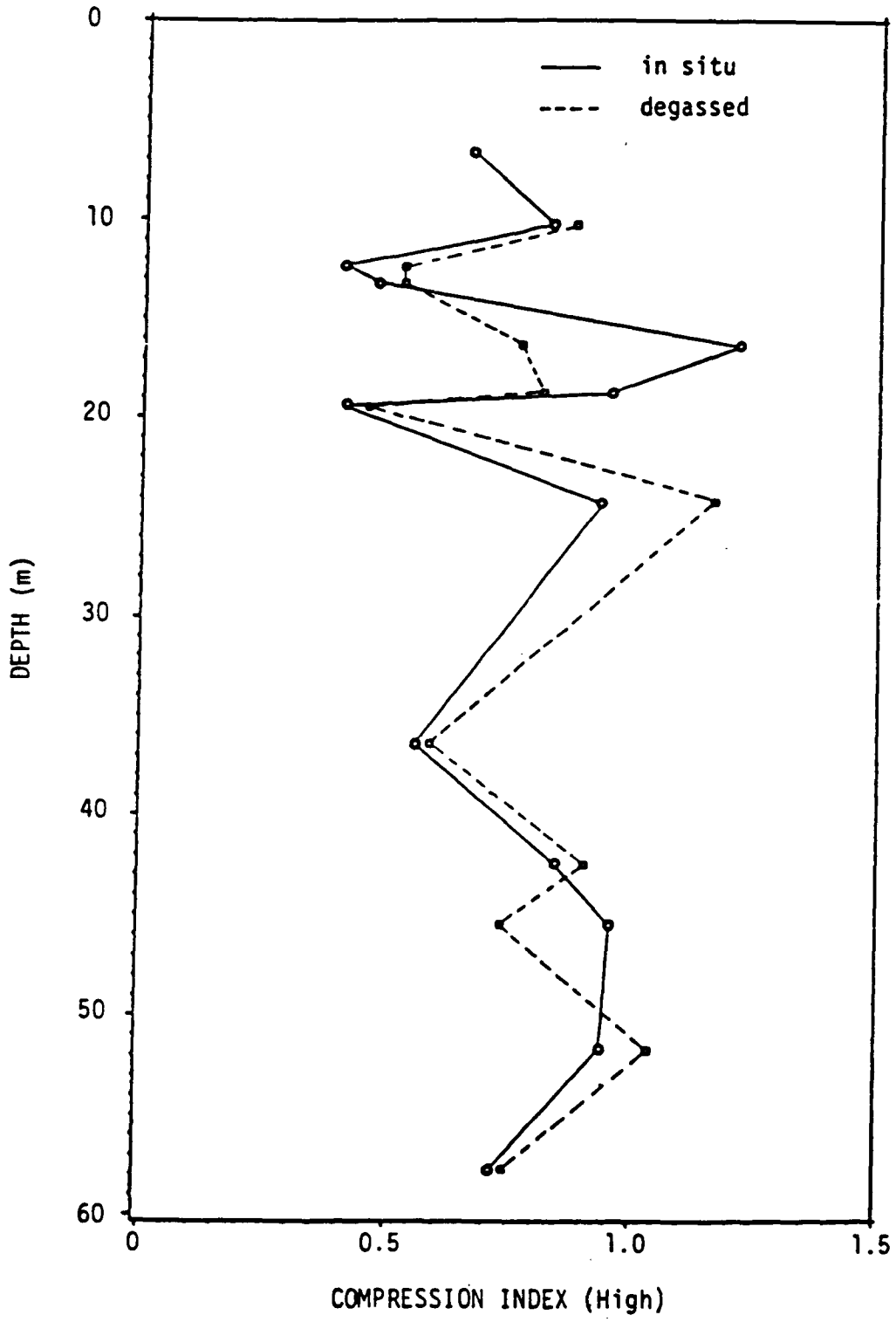

Figure 29. **High compression indices versus depth for <u>in situ</u> and degassed samples from PST Borings 1, 5, and 7.**

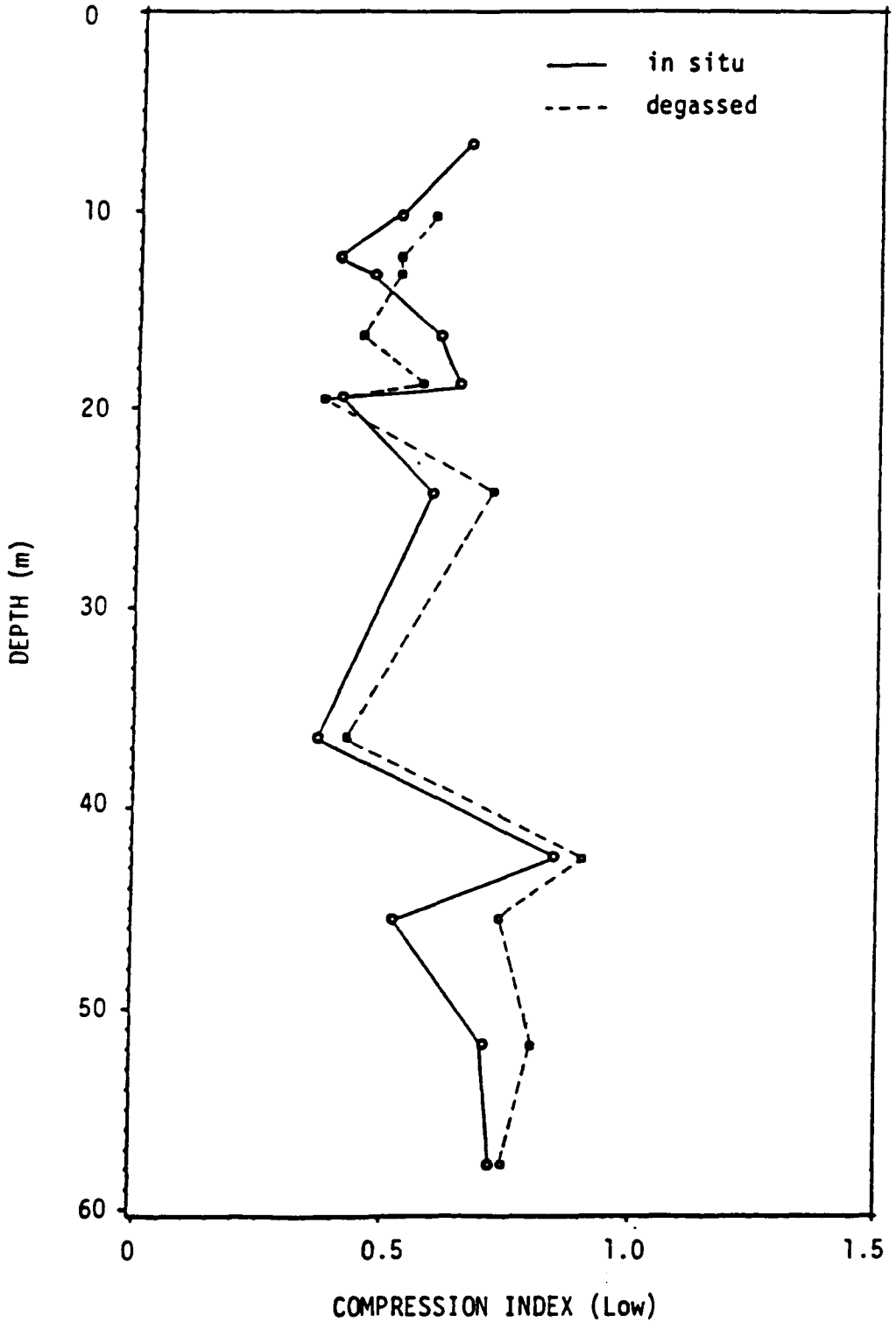

Figure 30. *Low* compression indices versus depth for in situ and degassed samples from PST Borings 1, 5, and 7.

Table 7. Pore water saturation values for consolidation test samples of PST Borings 1, 5, and 7 (all values calculated at STP).

Sample	Saturation, % Calculated		Measured	
	in situ	degas	in situ	degas
B1S2				
B1S4	93.88	93.81	100+	93.01
B1S6	93.52	93.57	100+	90.61
B1S8	99.54	99.55	100+	100+
B7S9	97.46	97.70	97.89	97.41
B7S15	99.97	99.97	100+	94.86
B5S10	99.91	99.91	100+	100+
B5S15	99.92	99.92	100+	94.46
B5S23	99.97	99.97	100+	96.11
B5S26	99.37	99.34	100+	89.14
B5S28	99.98	99.98	100+	99.38
B5S30	99.81	99.80	98.50	90.51
B5S32	99.98	99.98	97.60	95.36

is the volume of gas present in a given volume of wet sediment (see GAS CONCENTRATIONS, this chapter). These values indicate theoretical pore water saturation at standard temperature and pressure (STP) and therefore, cannot be related to in situ conditions. The presence of gasses in the pore water results in pore water saturation values below 100 percent at STP for all samples.

Measured pore water saturation values are based on consolidation test results for the initial conditions and can be calculated from:

$$Gw = Se_o \qquad (25)$$

where G is the specific gravity of solids, w is the water content, e_o is the initial void ratio, and S is pore water saturation. Nearly all the consolidation samples tested at in situ pressures have measured saturation values in excess of 100%. However, there are three exceptions, samples B7S9I, B5S30I, and B5S32I. These samples exhibit saturation values only slightly less than 100%, being undersaturated by a maximum of 2.5%. These low values, in all probability, are within sampling variability.

In marked contrast to the samples tested under in situ pressure, the degassed consolidation samples exhibit high degrees of undersaturation. The degree of saturation for the degassed samples ranges between 89% and 99%. The measured pore water saturation values are lower than the calculated theoretical values. A possible explanation is that gas expansion due to a decrease in confining stress results in an increase in pore water pressure and thus, drainage. Two samples do show measured saturation values of 100%: B1S8D and B5S10D.

Void Ratio and Porosity

The effects of porewater degassing are clearly shown as an increase in the initial void ratio or porosity (Figure 31, Table 3). Release of porewater gasses and the relative increase in initial void ratio or porosity is a function of the gas concentration. Three comparative samples exhibit the opposite of this trend, that being a decrease in initial void ratio or porosity upon release of *in situ* pressure. These samples, B7S15, B5S10, and B5S32, all had very low pore water gas concentrations.

Additionally, void ratio was calculated at the effective preconsolidation stress (Table 8). The degassed values of void ratio at the preconsolidation stress, e_o, are larger than the comparative *in situ* values (Figure 32). Again, samples B7S15, B5S10, and B5S32 do not follow this trend.

Permeability

No direct permeability measurements were performed during consolidation testing, however permeability was calculated after each load increment. The presence of gas bubbles in a partially saturated soil should act to impede the flow of water in the pores of the soil and thereby, reduce the effective permeability of the soil (Bjerrum and Huder, 1957).

Calculated permeability is graphically estimated at the preconsolidation stress for both the *in situ* and degassed test results (Table 8). Figure 33 clearly shows that the calculated permeabilities of the degassed tests are greater than the *in situ* tests. Three samples do not follow this trend: B1S4, B5S30, and B5S32.

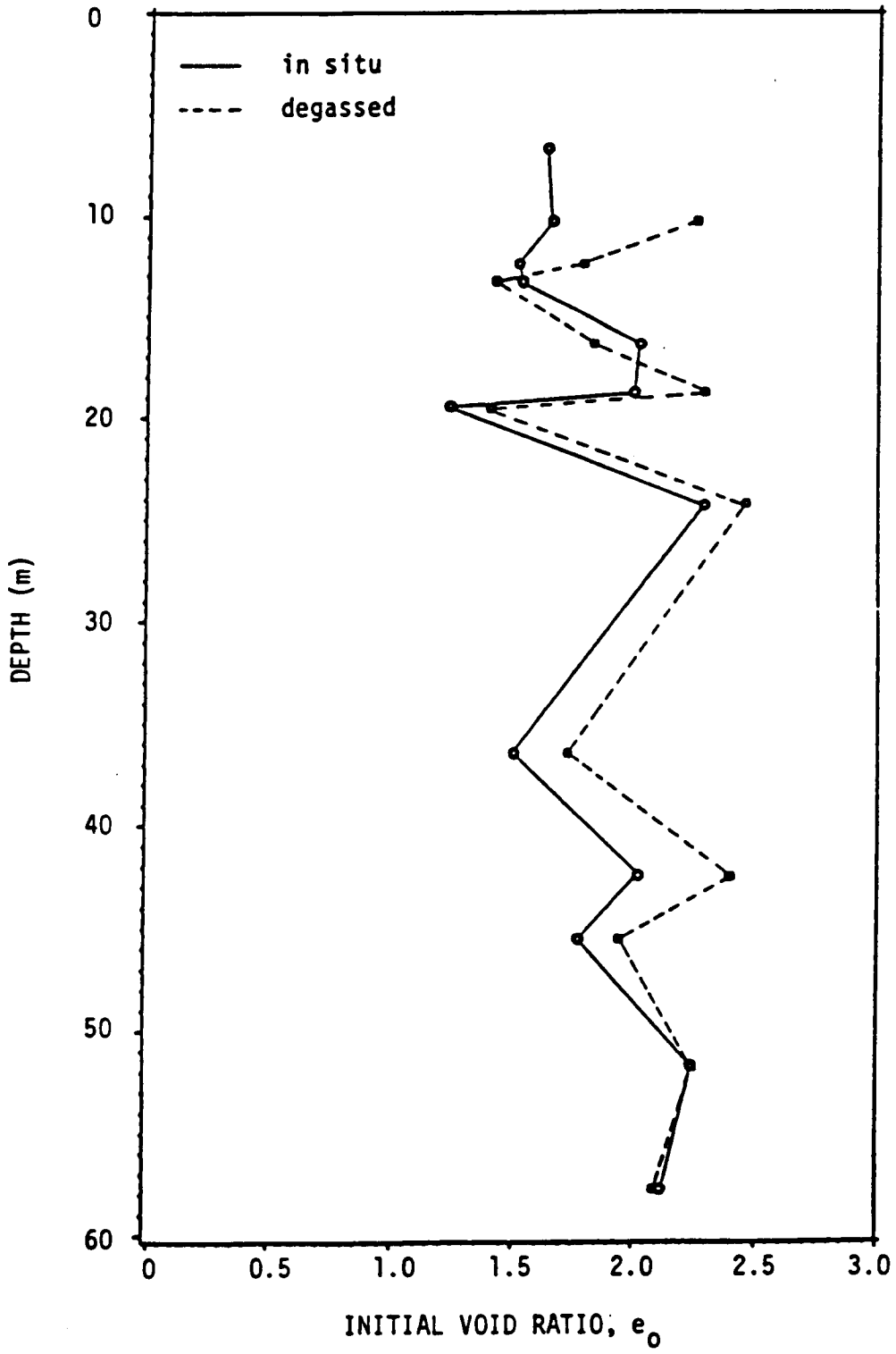

Figure 31. **Initial void ratio versus depth for in situ and degassed samples from PST Borings 1, 5, and 7.**

Table 8. Consolidation characteristics calculated at the effective preconsolidation stress for all samples.

Sample	Depth (m)		Void Ratio, e_c		Permeability, k_c (cm/s)	
	in situ	degas	*in situ*	degas	*in situ*	degas
B1S2	6.72		1.4641		2.515×10^{-8}	
B1S4	12.41	12.37	1.3790	1.5840	7.312×10^{-8}	4.269×10^{-8}
B1S6	18.78	18.72	1.5776	2.0170	2.386×10^{-9}	8.129×10^{-8}
B1S8	24.32	24.18	2.0509	2.2540	4.969×10^{-8}	1.615×10^{-7}
B7S9	10.24	10.20	1.5354	1.8868	2.078×10^{-9}	5.630×10^{-8}
B7S15	16.37	16.31	1.8137	1.6676	7.149×10^{-8}	1.572×10^{-7}
B5S10	13.29	13.21	1.4324	1.2555	2.612×10^{-8}	6.121×10^{-8}
B5S15	19.42	19.47	1.1157	1.2461	2.316×10^{-8}	2.013×10^{-7}
B5S23	36.49	36.44	1.3852	1.5337	3.985×10^{-8}	6.716×10^{-8}
B5S26	42.47	42.50	1.6980	2.1464	9.720×10^{-9}	1.047×10^{-7}
B5S28	45.54	45.49	1.6753	1.8053	1.796×10^{-8}	2.817×10^{-7}
B5S30	51.76	51.80	1.9633	2.0927	2.474×10^{-7}	7.459×10^{-8}
B5S32	57.80	57.74	2.0916	1.9479	5.425×10^{-8}	3.489×10^{-8}
B2S10	11.76	11.76	1.2589	1.4011	4.915×10^{-8}	3.645×10^{-7}

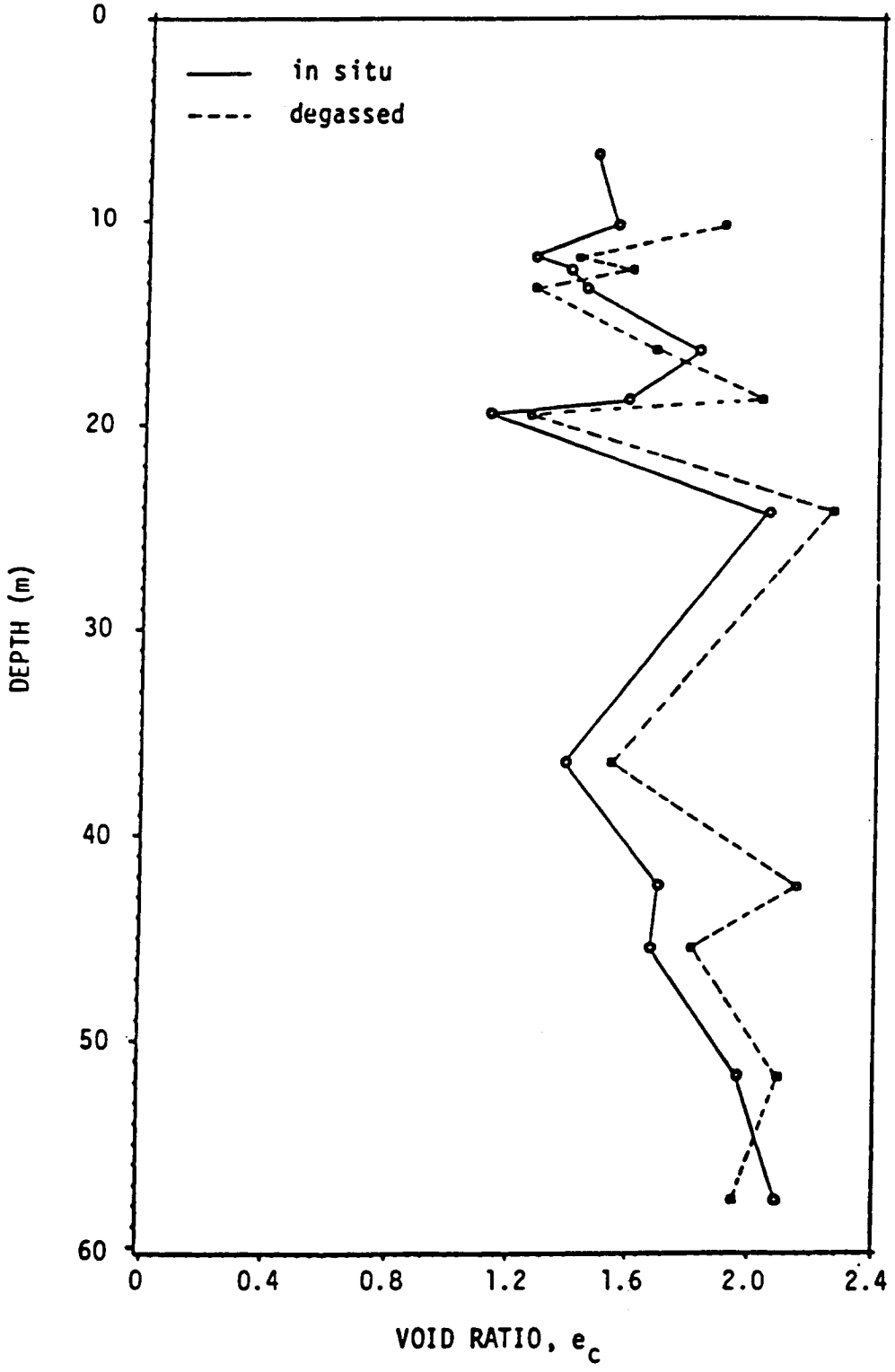

Figure 32. Void ratio calculated at the effective preconsolidation stress versus depth for in situ and degassed samples from Borings 1,2,5, and 7.

Recalling from EXPERIMENTAL PROGRAM, the theoretical coefficient of permeability can be calculated from:

$$k = C_v \, m_v \, \gamma_w \qquad (26)$$

Thus, the coefficients of consolidation and volume change control the value of the theoretical permeability. An increase in either value will result in an increase in calculated permeability, holding γ_w constant.

Shear Strength

The basic factor responsible for the strength of a soil is the frictional resistance between soil particles in contact (Mitchell, 1976). As pore water gasses evolve from solution, displacement of soil particles occurs, thereby reducing the intergranular contacts. A reduction of soil shear strength upon removal of *in situ* pressure would be expected for soils that have high porewater gas contents.

Shear strength measurements for Boring 2, sampled with the pressure core barrel, confirm this hypothesis. Figure 34 shows the reduction in undrained shear strength upon decompression of six pressure core barrel samples from Boring 2 versus their methane contents. Reductions of up to 40% were measured at Boring 2. Whelan et al (1975) measured similar shear strength reductions of up to 92% in South Pass Block 70, where a documented slide occurred. These profiles were obtained from *in situ* remote vane and ship board degassed measurements (Whelan et al, 1975).

Results of pressure Shelby tube samples tested for strength are not as conclusive as the above mentioned pressure core barrel tests, nor the remote vane measurements. It must be noted that the pressure Shelby tube results were performed using a hand held Torvane device (Table 1).

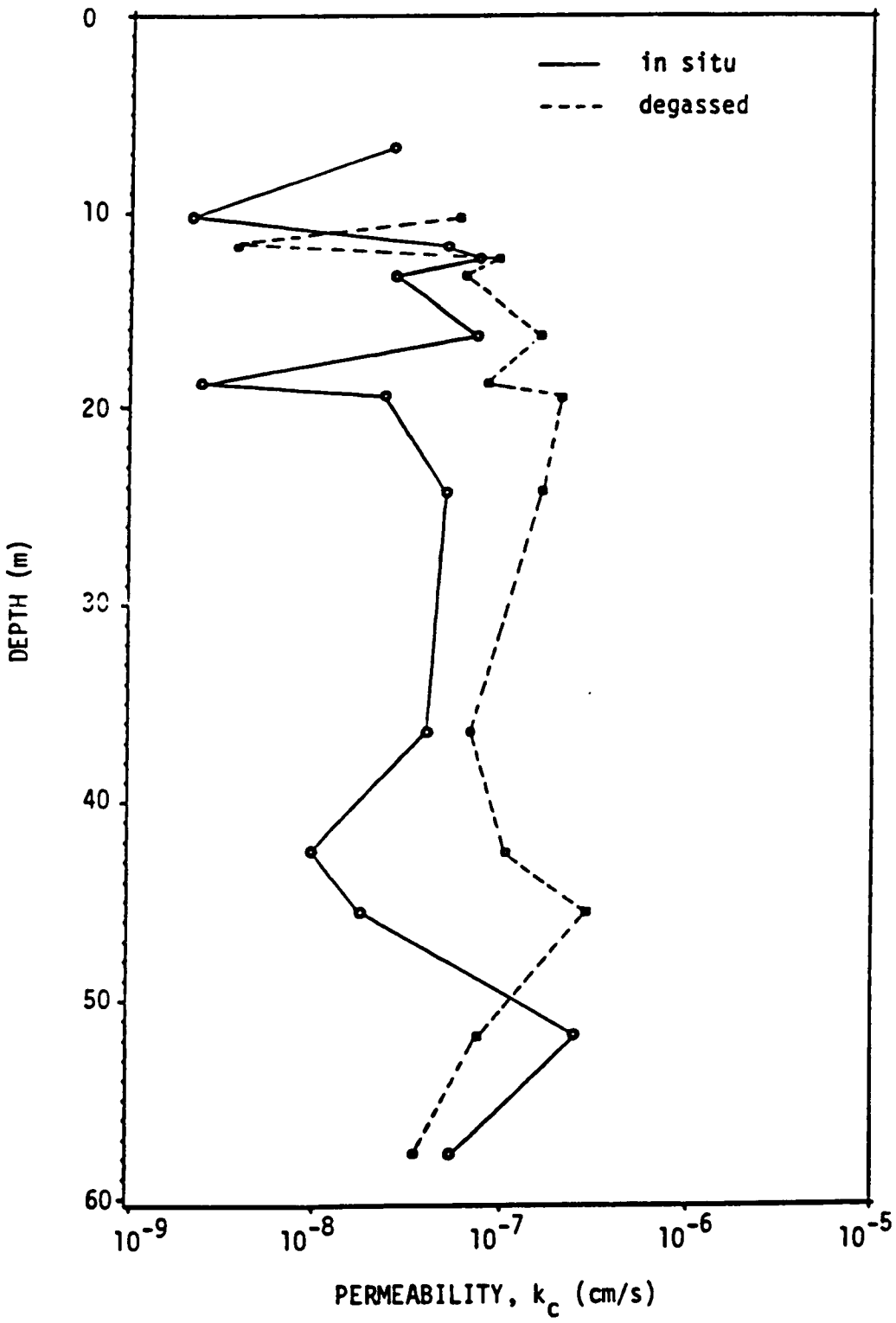

Figure 33. **Permeability calculated at the effective preconsolidation stress versus depth for in situ and degassed samples from Borings 1, 2, 5, and 7.**

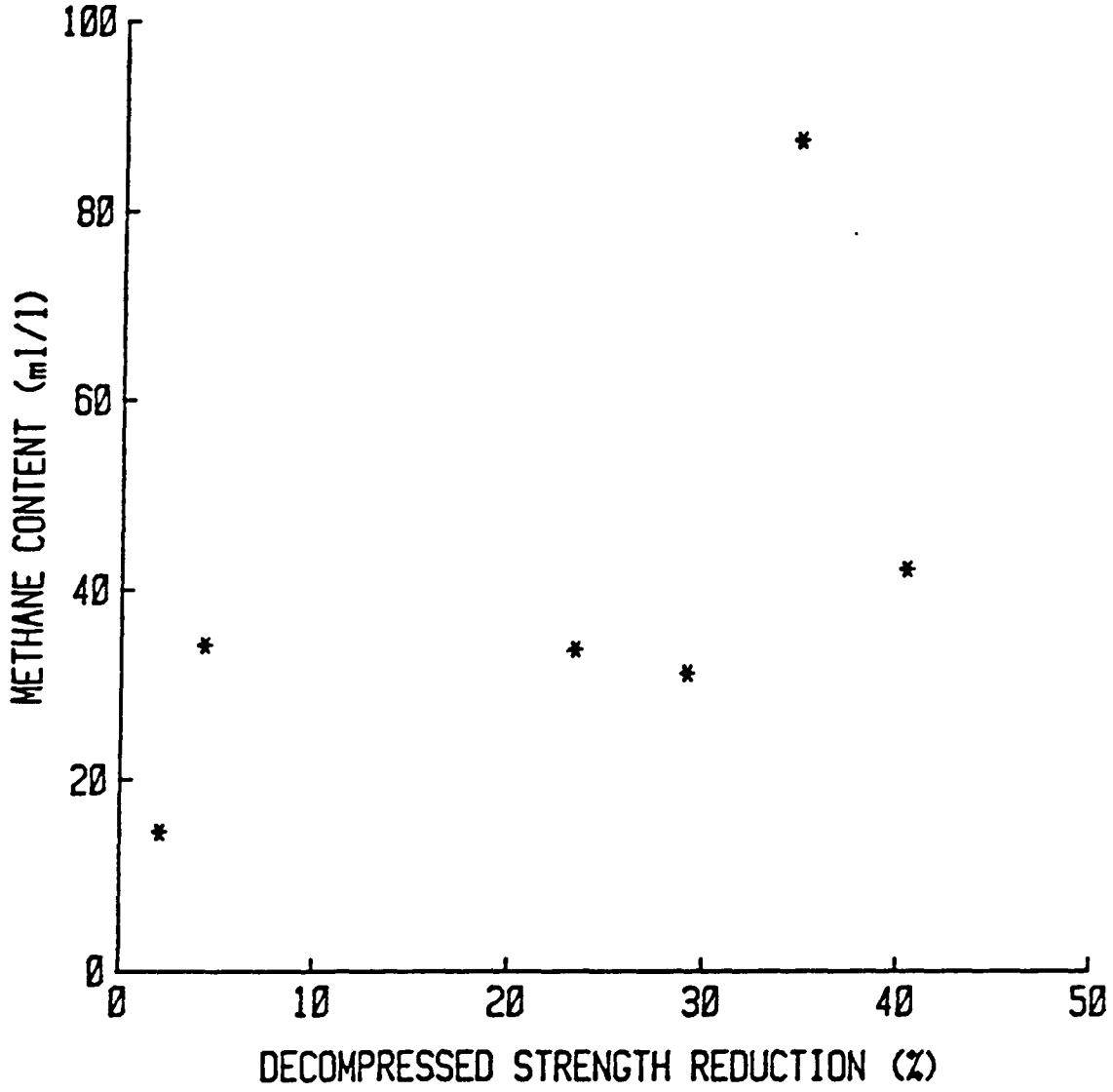

Figure 34. Methane content versus decompressed strength reduction for PCB Boring 2.

The effects of sampling error are more prevalent with the hand held device because of possible non-uniform rotation rates and improper insertion of the device. However, shear strength test results for the pressure Shelby tube samples show six of nine tests exhibit a reduction of shear strength upon decompression (Figure 35). Samples B7S15, B5S10, and B5S28 show greater values of shear strength for pressurized versus degassed samples.

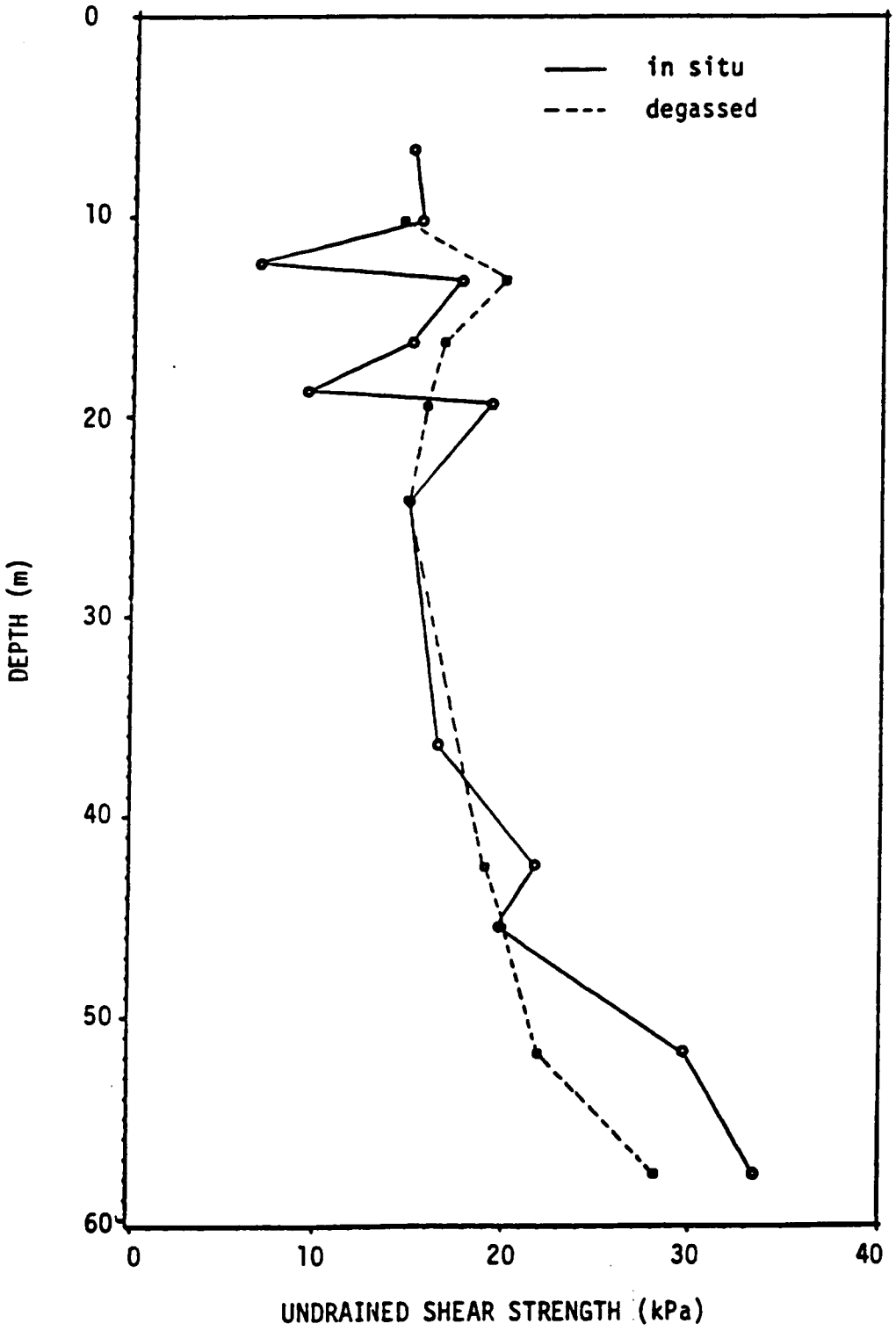

Figure 35. **Undrained shear strength versus depth for in situ and degassed samples from PST Borings 1, 5, and 7.**

DISCUSSION

The conventional theory of consolidation was solved by Terzaghi (1925) for saturated soils. Much work has been carried out to investigate cases which account for the effects of variations of permeability and compressibility during consolidation (Richart, 1957; Lo, 1960; Davis and Raymond, 1965; Janbu, 1965; Barden and Berry, 1965). These factors become important only if the void ratio changes and strains are significant, however, these studies are based on small strain theory. Additional studies have evaluated the limitation placed on finite strain theory, non-linear stress-strain relationships, and the effects of self weight of the soil particles (Gibson et al, 1967; Schiffman, 1982; Znidarcic and Schiffman, 1982).

The more advanced of these studies even evaluate the effects of non-constant permeability on soil compressibility (Schiffman, 1982). One of the basic assumptions of consolidation theory which has been largely left alone is that of complete saturation of the soil matrix. Lowe et al (1964) investigated the effects of back pressure consolidation testing on soils. Test results clearly showed that the time rate of consolidation of partially saturated soils under load is significantly different from the time rate of consolidation of a fully saturated soil under the same load. Lowe et al (1964) cited two basic reasons for this phenomena: 1) The air bubbles in a partially saturated soil are highly compressible, compared to the relatively incompressible water occupying the corresponding pore space in a saturated soil, and 2) the gas bubbles in a partially saturated soil impede the flow of water in the pores of the soil and thereby reduce the effective permeability

of the soil (Bjerrum and Huder, 1957).

All of the above mentioned studies have significantly increased our knowledge of the various aspects of consolidation theory, yet, a significant factor has remained unstudied. The effects of disturbance due to ebullition of saturated pore water gasses and its relationship to soil saturation is intuitively quite easy to understand, however, no studies have attempted to tackle this difficult problem. As sample pressure is released to ambient when a core is recovered, significant stress release can occur. The relative amount of stress release is a function of water depth, effective overburden stress, and the presence of excess pore water pressures at depth.

When no significant levels of pore water gas exist, the soil skeleton will respond to the release of overburden stress, producing negative pore pressures resulting from elastic expansion (Skempton and Sowa, 1963). If mechanical disturbance and moisture loss are prevented, this type of disturbance will be minimized, although a strength reduction would be expected.

With the presence of pore water gasses, release of in situ stresses results in significant expansion due to the high compressibility of gas as compared with pore water or the soil structure. Expansion to the bubble phase will result in the development of shear stresses within the soil structure. Shear deformations break down particle and aggregate assemblages, resulting in rupture of the interparticle bonds which inhibit swelling (Mitchell, 1976). Gas expansion acts immediately to increase the void ratio and reduce the value of pore water saturation. This is a result of the realignment of clay particles to an altered condition caused by forces exerted by gas expansion (Chiou, 1981).

Consolidation characteristics are greatly affected by the expansion of pore water gasses. Compressibility of a degassed sediment during consolidation testing is initially controlled by the rapid collapse of gas-filled voids resulting in large coefficients of consolidation and compressibility. At a stress in excess of the effective preconsolidation stress, the coefficients of consolidation and compressibility become essentially identical to the results of a comparative specimen tested under pressurized conditions. So, for the initial consolidation loads, soil permeability does not affect compressibility, rather, compressibility is controlled by the presence of macro-voids.

The volume change that occurs during consolidation is due to the reduction of the volume of voids (laterally constrained sample). For saturated soils the rate of consolidation is governed by the rate at which pore water can escape from the soil. During the consolidation test instantaneous loads are applied to the specimen. Immediately after application of a normal load, $\Delta\sigma_v$, the entire load is resisted by an increase in pore water pressure equal to $\Delta\sigma_v$ in a saturated soil. With the passage of time, volume changes occur as pore water drains from the soil and the effective stress increases. Eventually, pore water pressure returns to hydrostatic and the applied load and the effective stress are in equilibrium.

For partially saturated soils the instantaneous application of a load results in instantaneous compression of gas filled voids. This is evident upon comparison of the initial specimen heights on either the compression versus square root of time or compression versus logarithm of time curves. Initial and total compression for a given normal load

was shown to be considerably larger for the degassed samples versus the pressurized samples. Furthermore, compression is a function of methane concentration.

Based on the grain size, calcium carbonate content, Atterberg limits, and mineralogy the constituents of the comparative consolidation samples tested here are basically identical throughout the three cored sections. Variable gas concentrations, pore water saturation, undrained shear strength, and initial void ratios clearly indicate the effects of degassing between comparative *in situ* and degassed consolidation samples. The resultant effects of degassing on the soil microstructure drastically altered the consolidation characteristics of a given set of samples.

Samples B7S15, B5S10, and B5S32 exhibit consolidation characteristics which can be accounted for by sample variability. Although methane gas concentration was measured for all pressure Shelby tube samples, the exact localization of methane in the sediment matrix cannot be clearly delineated. Methane gas concentration analyses were performed on samples collected as close as possible to the consolidation sample. Although these values may more closely represent those of the consolidation sample, gas concentration measurements were not performed on the actual consolidation sample. The initial void ratio was found to be greater for the *in situ* tests, however, these samples contained low methane concentrations.

The pressure core barrel and pressure Shelby tube sampling techniques discussed previously, are a significant advancement to promote the acquisition of relatively undisturbed samples. However, significant problems exist with both techniques.

Developmental problems with the pressure core barrel have led to the acquisition of only a single set of comparative consolidation test results (B2S10). Difficulties with maintaining sample pressures during post sampling periods resulted in the loss of numerous samples. Yet, prior to this, sample acquisition was a serious problem due to mechanical difficulties with the pressure core barrel.

The pressurized Shelby tube method of sample acquisition does allow the sample to reach ambient pressures momentarily. This period is minimized to reduce the possibility of gas expansion, however, in a few cases it is felt that disturbance due to gas expansion did occur. It must be noted that disturbance was minimized, yet minor amounts of gas expansion can produce dramatically different consolidation test results.

In addition to sampling problems, the use of a manned hyperbaric chamber is extremely limiting. Space and time limitations are rigid. Ideally, when loading an oedometer, careful sample trimming and loading practices are exercised. Yet, in the limited environment of the hyperbaric chamber it becomes necessary to trim and load the oedometer within a time limit of 55 minutes. As can be expected, sample disturbances may occur.

To alleviate the problems associated with a manned hyperbaric chamber, an unmanned mini-hyperbaric chamber is being developed and tested as discussed in EXPERIMENTAL PROGRAM. This tool has been tested during a cruise in August of 1983, at which time the pressure core barrel performed flawlessly. However, mechanical problems associated with the internal mechanisms of the mini-hyperbaric chamber resulted in no sample data.

The consolidation test data acquired during this study are the

first of their kind. Actual *in situ* consolidation testing is at present physically impossible, therefore, the simulated pressure maintenance has resulted in a unique set of test data. The results of the consolidation testing program, although not 100 percent positive for all cases clearly indicates unique relationships between the consolidation characteristics and the method of sample acquisition.

CONCLUSIONS

As a result of this research the following conclusions can be drawn:

1) Degassed samples exhibit sharper breaks in the consolidation e-log σ_v' curves. The compressibility of these specimens is relatively low until the consolidation stress exceeds the preconsolidation stress. It then increases sharply as the void ratio reduces under higher consolidation stresses. The compressibility eventually assumes a lower value acting much like a sensitive clay. At stress values less than the preconsolidation stress the corresponding coefficients of compressibility are shown to be greater.

2) Degassing of pore water gasses alters the soil microstructure thus resulting in:

A) reduced undrained shear strength,

B) increased void ratio,

C) increased compression index,

D) decreased preconsolidation pressure,

E) decreased overconsolidation ratio,

F) decreased porewater saturation, and

G) micro fabric disruption.

3) An increase in calculated permeability results from sediment degassing when relative permeability should decrease due to the presence of gas filled void space. Large values of calculated permeability result from large values of the coefficients of volume change and consolidation for the degassed test results.

4) The coefficients of consolidation calculated by log time and

square root of time methods converge for the *in situ* and degassed tests at a stress beyond the preconsolidation stress for the given curves. The lower portion of the virgin curve is a region in which the soil compressibility decreases and the degassed and *in situ* values converge.

5) Due to the variability of methane gas concentrations a more accurate measurement of the actual sample gas content must be made for a more precise evaluation of test results.

6) Instantaneous compression of gas filled voids during initial loading of consolidation testing was found to be significantly larger for the degassed, partially saturated samples. Similarly, total compression for a given load was greater for degassed versus *in situ* specimens. In addition, compression is a function of methane gas concentration.

REFERENCES

Anderson, A.L., 1974, Acoustics of gas bearing sediments: National Technical Information Service, U.S. Department of Commerce, Springfield, Virginia, 162 p.

Barden, L., and P.L. Berry, 1965, Consolidation of normally consolidated clay: Proceedings of the American Society of Civil Engineers, SM5, No. 4881, p. 15-35.

Bea, R.G., 1971, How sea floor slides affect offshore structures: Oil and Gas Journal, v. 69, p. 88-92.

——— and P. Arnold, 1973, Movements and forces developed by wave induced slides in soft clays: Eighth Offshore Technology Conference, v. 1, p. 731-742.

Bjerrum, L., and J. Huder, 1957, Measurement of the permeability of compacted clays: Proceedings, 4th International Conference on Soil Mechanics and Foundations, London, v. I, p. 6-8.

Bryant, W.R., P. Cernock, and J. Morelock, 1967, Shear strength and consolidation characteristics of marine sediments, Gulf of Mexico: Marine Geotechnology, v. 1, p. 1-14.

Casagrande, A., 1936, The determination of the preconsolidation load and its practical significance: Proceedings, 1st International Conference on Soil Mechanics and Foundation Engineers, Cambridge, Mass., p. 60.

Cernock, P.J., 1967, Consolidation characteristics and related physical properties of selected sediments from the Gulf of Mexico: Master's thesis, Texas A&M University, 137 p.

Chiou, W.-A., 1980, A new technique for preparing in situ marine sediments for clay fabric study, in G.W. Bailey, ed., 38th Annual Proceedings of the Electron Microscopy Society of America, San Francisco, CA.

———, 1981, Clay fabric of gassy submarine sediments: PhD. dissertation, Texas A&M University, 248 p.

Coleman, J.M., 1976, Deltas: processes of deposition and models for exploration: Champaign, Illinois Continuing Education Publication Company, 101 p.

——— 1981, Deltas: processes of deposition and models for exploration: Champaign, Illinois Continuing Education Publication Company 101 p.

——— J.C. Ferm, and R.S. Saxena, 1972, Deltas Recent and Ancient: New Orleans Geological Society, Continuing Education Seminar, November 28-30, 1972, 169 p.

——— and S.M. Gagliano, 1964, Cyclic sedimentation in Mississippi River deltaic plain deposits: Gulf Coast Association Geological Society Transactions, v. 14, p. 67-80.

——— J.N. Suhayda, T. Whelan, and L.D. Wright, 1974, Mass movement of Mississippi River delta sediments: Transactions of the Gulf Coast Association Geological Society, v. 24, p. 49-68.

——— and L.D. Wright, 1974, Formative Mechanisms in a Modern Depocenter, in Stratigraphy and Petroleum Potential of the Northern Gulf of Mexico, Part II, New Orleans, Geological Society Seminar, January 22-24, 1974, p. 90-139.

Davis, E.H., and G.P. Raymond, 1965, A non-linear theory of consolidation: Geotechnique, v. 15, p. 161-173.

Denk, E.W., W.A. Dunlap, W.R. Bryant, L.J. Milberger, and T.J. Whelan III, 1981, A pressurized core barrel for sampling gas-charged marine sediments: Proceedings, 13th Offshore Technology Conference, v. 4, p. 43-52.

Doyle, E.H., B. McClelland, and G.H. Ferguson, 1971, Wire-line vane probe for deep penetration measurements of ocean sediments: Presented at April 19-21, 1971, Third Annual Offshore Technology Conference, held in Houston, Texas (preprint OTC 1327).

Fisk, H.N., and B. McClelland, 1959, Geology of continental shelf off Louisiana: Its influence on offshore foundation design: Bulletin of the Geological Society of America, v. 70, p. 1369-1394.

——— and E. McFarlan, Jr., 1955, Late Quaternary deltaic deposits of the Mississippi River, in The Crust of the Earth, Geological Society of America Special Paper 62, p. 279-302.

——— E. McFarlan, Jr., C.R. Kolb, and L.J. Wilbert, Jr., 1954, Sedimentary framework of the modern Mississippi delta: Journal of Sedimentary Petrology, v. 24, p. 76-99.

Folk, R.L., 1974, Petrology of sedimentary rocks: Austin, Texas, Hemphills, 159 p.

Garrison, L.E., 1974, The instability of surface sediments on parts of the Mississippi delta front: U.S. Geological Survey Open File Report, Corpus Christi, Texas, v. 18, p. 661-673.

Gibson, R.E., G.L. England, and M.J.L. Hussey, 1967, The theory of one-dimensional consolidation of saturated clays: Geotechnique, v. 17, p. 261-273.

Gould, H.R., 1965, The Mississippi delta complex, in J.P. Morgan, ed., Deltaic sedimentation, Modern and Ancient: Special Publ. Soc. Econ. Paleont. Miner., 15, p. 3-30.

Hamilton, E.L., 1971, Prediction of in situ acoustic and elastic

properties of marine sediments: Geophysics, v. 36, p. 266-284.

Hampton, L.D., 1966, Acoustic properties of sediments: Defense Research Laboratory, University of Texas, Acoustic Report 254 (DRL-A-254).

Helwick, S.J., Jr., 1977, Engineering properties of shallow sediments in West Delta and South Pass, Outer Continental Shelf lease areas, offshore Louisiana: Master's thesis, Texas A&M University, 82 p.

Henkel, D.J., 1970, The role of waves causing submarine landslides: Geotechnique, v. 20, p. 75-80.

Horslev, M.J., 1948, Subsurface Exploration and Sampling of Soils for Civil Engineering Purposes, Waterways, Experiment Station, Vicksburg, Miss.

Hottman, W.E., 1975, Areal distribution of clay minerals and their relationship to physical properties, Gulf of Mexico; Master's thesis, Texas A&M University, 53 p.

Jackson, M.L., 1956, Soil chemical analysis - advanced course, fifth printing, 1966: Published by the author, Department of Soil Science, University of Wisconsin, Madison, 991 p.

Janbu, N., 1965, Consolidation of clay layers based on non-linear stress-strain: Proceedings, 6th International Conference on Soil Mechanics, v. 2, p. 83-87.

Johns, M.W., E. Taylor, and W.R. Bryant, 1982, Geotechnical sampling and testing of gas-charged marine sediments at in situ pressures: Geo-Marine Letters, v. 2, p. 231-236.

Johns, W.D., and R.E. Grim, 1958, Clay mineral composition of Recent sediments from the Mississippi River delta: Journal of Sedimentary Petrology, v. 48, p. 186-199.

Jones, J.L., C.B. Leslie, and L.E. Barton, 1958, Acoustic characteristics of a lake bottom: Journal of the Acoustic Society of America, v. 30, p. 142.

——— C.B. Leslie, and L.E. Barton, 1964, Acoustic characteristics of underwater bottoms: Journal of the Acoustic Society of America, v. 36, p. 154.

Kolb, C.R., and R.I. Kaufman, 1967, Prodelta clays of southeast Louisiana, in A.F. Richards, ed., Marine Geotechnique: Chicago, University of Illinois Press, p. 3-21.

——— and J.R. Van Lopik, 1958, Geology of the Mississippi River deltaic plain: U.S. Corps of Engineers, Waterways Experiment Station, Technical Reports 3-483 and 3-484.

——— ——— 1966, Depositional environments of the Mississippi River deltaic plain, southeastern Louisiana, in M.L. Shirley, ed., Deltas

in Their Geologic Framework: Houston Geological Society, p. 17-61.

Krumbein, W.C., and F.J. Pettijohn, 1938, Manual of Sedimentary Petrography: New York, Appleton-Century-Crofts, 549 p.

Lambe, T.W., 1951, Soil Testing for Engineers: New York, John Wiley and Sons, 165 p.

——— and R.V. Whitman, 1969, Soil Mechanics: New York, John Wiley and Sons, 553 p.

Lo, K.Y., 1960, Discussion on Rowe, measurement of the coefficient of consolidation of lacustrine clay: Geotechnique, v. 10, p. 36-39.

Lowe III, J., P.F. Zaccheo, and H.S. Feldman, 1964, Consolidation testing with back pressure: Journal of the Soil Mechanics and Foundations Division, Proceedings ASCE, v. 90, p. 69-86.

Mitchell, J.K., 1976, Fundamentals of Soil Behavior: New York, John Wiley and Sons, Inc., 422 p.

Moore, D.G., 1961, Submarine slumps: Journal of Sedimentary Petrology, v. 31, p. 343-357.

Morgan, J.P., 1965, Depositional processes and products in the deltaic environments, in J.P. Morgan, ed., Deltaic Sedimentation, Modern and Ancient: Special Publ. Soc. econ. Paneont. Miner., 15, p. 31-47.

——— J.M. Coleman, and S.M. Gagliano, 1963, Mudlumps at the mouth of South Pass, Mississippi River: Sedimentology, paleontology, structure, origin and relation to deltaic processes: Louisiana State University, Baton Rouge, Coastal Studies Series 10, 190 p.

Nissenbaum, A., B.J. Presley, and I.R. Kaplan, 1972, Early diagenesis in a reducing fjord, Saanich Inlet, British Columbia. I. Chemical and isotopic changes in major components of interstitial water: Geochimica et Cosmochimica Acta, v. 36, p. 1007-1027.

Prior, D.B., and J.M. Coleman, 1981, High-resolution deep-tow survey imagery, Gulf of Mexico: Geo-Marine Letters, v. 1, p. 261-266.

Richart, F.E., 1957, A review of theories for sand drains: J. Soil Mech. and Found. Div., Am. Soc. Civil Engrs., 83, SM3.

Roberts, H.H., D.W. Cratsley, and T. Whelan III, 1976, Stability of Mississippi delta sediment as evaluated by analysis of structural features in sediment borings: Proceedings, 8th Offshore Technology Conference, v. 1, p. 9-28.

Russell, R.J., and R.D. Russell, 1939, Mississippi River delta sedimentation, in P.D. Trask, ed., Recent Marine Sediments: AAPG, p.153-157.

Scafe, D.W., and G.W. Kunze, 1971, A clay mineral investigation of six cores from the Gulf of Mexico: Marine Geology, v. 10, p. 69-85.

Schiffman, R.L., 1982, The consolidation of soft marine sediments: Geo-Marine Letters, v. 2, p. 199-203.

Schink, J.C., J.H. Stockwell, and R.A. Ellis, 1979, An improved device for gasometric determination of carbonate in sediment: Journal of Sedimentary Petrology, v. 49. p. 651-653.

Schubel, J.R., 1974, Gas bubbles and the acoustically impenetrable or turbid character of some estuarine sediments, in I.R. Kaplan, ed., Natural Gases in Marine Sediments: New York, Plenum Press, p. 99-135.

Scruton, P.C., 1960, Delta building and the deltaic sequence, in F.P. Shepard, F.B. Phleger and T.H. van Andel, eds., Recent Sediments, Northwest Gulf of Mexico: AAPG, p. 82-102.

Shepard, F.P., 1955, Delta front valleys bordering the Mississippi distributions: Geological Society of America Bulletin, v. 66, p. 1489-1498.

——— 1960, Mississippi delta: marginal environments, sediments, and growth, in, F.P. Shepard, F.B. Phleger and T.H. van Andel, eds., Recent Sediments, Northwest Gulf of Mexico: AAPG Bulletin, p. 56-81.

Shephard, L.E., W.R. Bryant, and W.A. Dunlap, 1979, Geotechnical properties and their relation to geological processes in South Pass Outer Continental Lease area Blocks 28, 47 and 48, offshore Louisiana: Technical Report 79-5-T, Texas A&M University College of Geosciences, 125 p.

Skempton, A.W. and V.A. Sowa, 1963, The behavior of saturated clays during sampling and testing, Geotechnique, v. 13, p. 269-290.

Taylor, D.W., 1948, Fundamental of Soil Mechanics: New York, John Wiley and Sons, Inc., 700 p.

Terzaghi, K., 1925, Principles of soil mechanics. III. Determination of permeability of clay: Engineering News Record, v. 95, p. 832.

——— 1943, Thoeretical Soil Mechanics: London, Chapman and Hall, Ltd., 510 p.

Waples, D., 1980, Organic Geochemistry for Exploration Geologists: Minneapolis, Burgess Publishing Company, CEPCO Division, 151 p.

Whelan III, T., W.R. Bryant, and W.A. Dunlap, 1981, Methane concentration and distribution in pressure core samples from Mississippi delta sediments (abstract): American Association of Petroleum Geologists, v. 65, 1007 p.

——— J.M. Coleman, H.H. Roberts, and J.N. Suhayda, 1976, The occurrence of methane in Recent deltaic sediments and its effect on soil stability: International Association of Engineers, Geology Bulletin, v. 14, p. 55–64.

——— ——— J.N. Suhayda, and L.E. Garrison, 1975, The geochemistry of Recent Mississippi River delta sediments: Gas concentration and sediment stability: Proceedings, 8th Offshore Technology Conference, v. 3, p. 71–84.

Yamamoto, T., 1982, Experiments of wave-driven soil transport in clay beds: Geo-Marine Letters, v. 2, p. 205–208.

Znidarcic, D., and R.L. Schiffman, 1982, On Terzaghi's concept of consolidation: Geotechnique, v. 32, p. 387–389.

The Department of the Interior Mission

As the Nation's principal conservation agency, the Department of the Interior has responsibility for most of our nationally owned public lands and natural resources. This includes fostering sound use of our land and water resources; protecting our fish, wildlife, and biological diversity; preserving the environmental and cultural values of our national parks and historical places; and providing for the enjoyment of life through outdoor recreation. The Department assesses our energy and mineral resources and works to ensure that their development is in the best interests of all our people by encouraging stewardship and citizen participation in their care. The Department also has a major responsibility for American Indian reservation communities and for people who live in island territories under U.S. administration.

The Minerals Management Service Mission

As a bureau of the Department of the Interior, the Minerals Management Service's (MMS) primary responsibilities are to manage the mineral resources located on the Nation's Outer Continental Shelf (OCS), collect revenue from the Federal OCS and onshore Federal and Indian lands, and distribute those revenues.

Moreover, in working to meet its responsibilities, the **Offshore Minerals Management Program** administers the OCS competitive leasing program and oversees the safe and environmentally sound exploration and production of our Nation's offshore natural gas, oil and other mineral resources. The MMS **Minerals Revenue Management** meets its responsibilities by ensuring the efficient, timely and accurate collection and disbursement of revenue from mineral leasing and production due to Indian tribes and allottees, States and the U.S. Treasury.

The MMS strives to fulfill its responsibilities through the general guiding principles of: (1) being responsive to the public's concerns and interests by maintaining a dialogue with all potentially affected parties and (2) carrying out its programs with an emphasis on working to enhance the quality of life for all Americans by lending MMS assistance and expertise to economic development and environmental protection.